

**FIXED-ABRASIVE POLISHING OF GLASS WITH
THE ASSISTANCE OF ULTRASONIC VIBRATION**

光学ガラスの超音波援用固定砥粒研磨に関する研究

This page intentionally left blank.

CONTENTS

Abstract	- 1 -
Chapter I Overview of Glass Machining	- 3 -
1.1 Fused Silica.....	- 3 -
1.2 Glass Processing.....	- 6 -
1.3 Ultrasonic Machining	- 9 -
1.4 Thesis Organization.....	- 12 -
References.....	- 15 -
Chapter II Experiment Apparatus and Details	- 19 -
2.1 Design of PZT.....	- 19 -
2.2 Vibration of the designed PZT vibrator	- 24 -
2.3 Experimental details	- 29 -
2.4 Summary	- 32 -
References.....	- 34 -
Chapter III Material Removal and Machined Surface in Fixed-Abrasive Polishing	- 37 -
3.1 Material removal	- 37 -
3.2 Surface morphology.....	- 50 -
3.3 Chemistry in polishing process	- 54 -
3.4 Machining force in polishing process	- 59 -
3.5 Other factors affecting machining process in fixed polishing	- 62 -
3.6 Wear of pellet in fixed-abrasive polishing	- 68 -
3.7 Summary	- 70 -
References.....	- 71 -
Chapter IV Sub-/Surface Damage of Fixed-Abrasive Polishing	- 73 -
4.1 Sub-/Surface characteristics of workpiece undergone varied polishing processes.....	- 73 -
4.2 Quantifying subsurface defects.....	- 87 -
4.3 Summary	- 89 -
References.....	- 90 -
Chapter V Thermal Aespects in Fixed-Abrasive Polishing	- 93 -

5.1 Temperature measuring system	- 93 -
5.2 The temperature in machining silicon and glass.....	- 94 -
5.3 Mathematical model for temperature in dry polishing of fused silica.	- 100 -
5.4 Summary	- 112 -
References.....	- 113 -
Chapter VI Determinism of Fixed-Abrasive Polishing	- 115 -
6.1 Profile of material removal of polishing tool.....	- 115 -
6.2 Summary	- 122 -
References.....	- 123 -
Chapter VII Conclusions and Future Suggestions	- 125 -
Acknowledgements	- 129 -
Accomplishments.....	- 131 -

ABSTRACT

Ultrasonics that dates back to 1940s has been utilized in numerous fields, inclusive of ultrasonic cleaning, ultrasonic detection, ultrasonic welding as well as ultrasonic machining. In manufacturing community, ultrasonics has been identified as a practical and vital technique, especially in the high efficiency and precision machining of difficult-to-machine materials, which, in some cases, is otherwise considerably difficult to be accomplished without ultrasonics. Traditional machining in the presence of ultrasonics can be categorized into ultrasonic machining and ultrasonic assisted machining.

The work presented focuses on fixed abrasive polishing of fused silica with the assistance of ultrasonics. The theoretical basis on which 2-D vibration is created is introduced first. Following the design, the manufacture and evaluation of the designed PZT was made. With the designed PZT, experiments on material removal and micro-surface roughness follow. The results on the two major issues evidence that applying vibration noticeably elevates material removal while the surface roughness was not degraded significantly.

Another issue in machining refers to subsurface nature of machined workpiece. More often than not, although the surface appears plausibly smooth, the subsurface is damaged severely after a chemical processing. In our experiments, the subsurface defect is experimentally related to chips incurred in the course of polishing. In some cases for which the chips were dispelled timely, the subsurface damage is reduced remarkably. Otherwise, on the machined surface plenty of cracks and/or scratches are characteristic of the subsurface.

The thermal aspect in dry polishing, especially chemistry-involved processes, is of paramount importance. Without exception, the temperature was examined in the polishing. The temperature lies in the range of $\sim 20^{\circ}\text{C} \sim 60^{\circ}\text{C}$, far lower than as imagined. The temperature is comparable to that in chemical mechanical polishing

where slurry is generally circulated in the course of polishing. Inferring from the experimented temperature, the mechanism of dry fixed abrasive polishing differs from CMP.

The last part of the work is to extend the method so as to open a door to potential industrial applications. To that end, the first and foremost thing is to ascertain if the polishing process is stable and repeatable. Thus, influence function was tested tentatively. We are pleased that the influence function exhibits excellent linearity with time and external controllable factors, implying that the fixed abrasive polishing is a technology well suitable for being automated.

All in all, the developed fixed abrasive polishing with the assistance of ultrasonic vibration is a promising technology from the viewpoint of material removal and subsurface properties. The technology has the potential to being further extended to other materials.

CHAPTER I

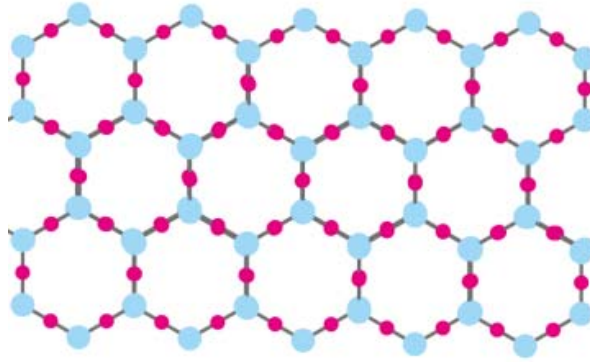
OVERVIEW OF GLASS MACHINING

Let there be light.

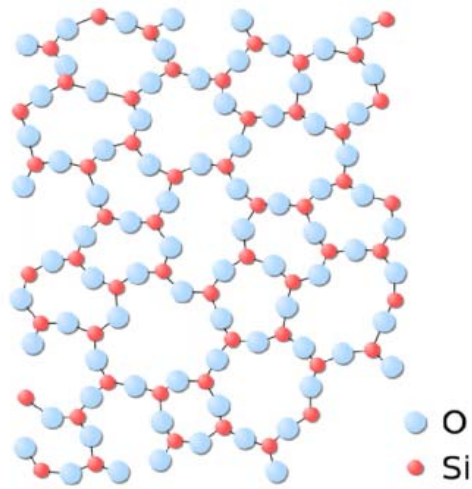
Chapter 1 starts from the introduction of fused silica and then reviews chiefly the grinding and polishing of conventional process, following which ultrasonic-oriented machining techniques are introduced. Lastly, the organized structure of the thesis was presented in the ending of the chapter.

1.1 Fused Silica

There are numerous glasses for various applications, among which fused silica is simply composed of silicon dioxide in the form of amorphous or non-crystalline state that differentiates fused silica from crystal quartz. The crystal quartz is characteristic of periodic network while the fused silica exhibits irregular links between silicon and oxygen atoms (Fig1.1). Attributing to its excellent mechanical, chemical and physical properties, fused silica can find a wide spectrum of applications in scientific and industrial fields, including luminescence, semiconductor industry, optical communication, laser systems, astronomical telescopes, etc. (Fig. 1.2). Fused silica possesses low thermal expansion coefficient and huge thermal inertia, which makes fused silica one of materials ideal for astronomical and space telescopes. Fused silica allows optical fabricators to put a very smooth polish onto the surface and produce the desired surface figure with less testing-polishing iterations. The blank material of the primary mirror of the Hubble Space Telescope finished by the Eastman Kodak was ultra-low expansion glass ULE7971 fused silica fabricated by Corning Company.

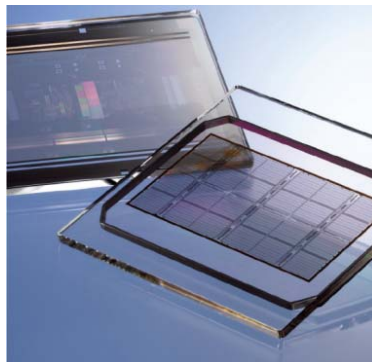


(a) Quartz Crystal

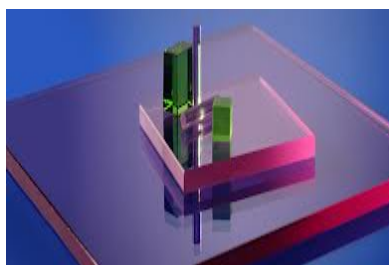


(b) Fused silica

Fig.1.1 The structure of (a) crystalline quartz and (b) fused silica



(a) Photomask in lithography



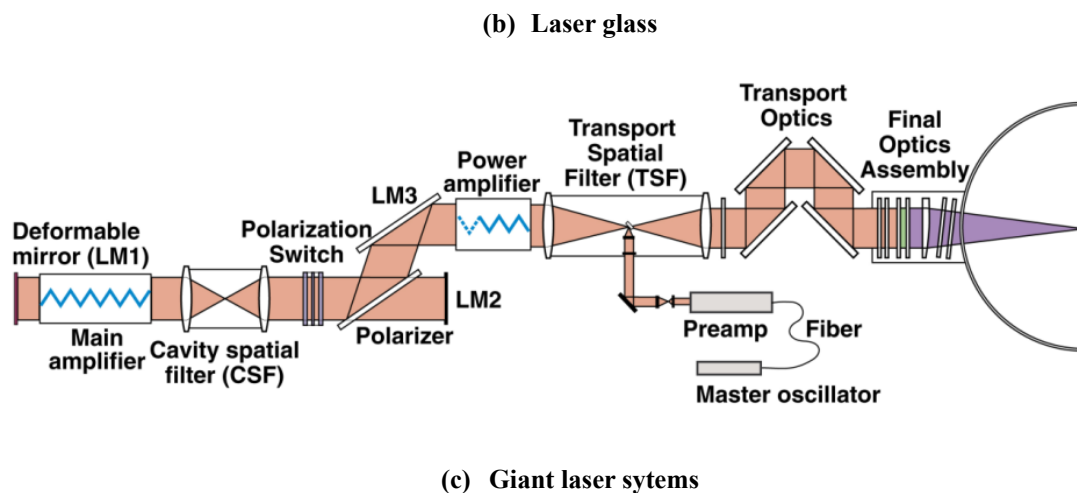


Fig.1.2 Glass in industries. Various glass used in different systems.

Fused silica offers great resistance to thermal shock and high allowable working temperature (900°C for extended periods, to 1,200°C for short periods) in the situations when the borosilicate glass cannot withstand high temperature. The aerospace-vehicle windows consist of three separate glass panes, among which the outermost and innermost ones are made of fused silica glass. In addition, the lenses of space camera are also fused silica with superior chemical and thermal stability and outstanding optical properties.

Owing to its transparency from ultraviolet to infrared light, highly pure fused silica comprises the majority of lenses, windows and gratings (~2100 large aperture optics) in high power laser systems for inertial confinement fusion, where 3ω (351 nm or 355 nm) laser light is employed. The wide forbidden band constitutes the other reason why the fused silica is used in laser systems. Because of wide band of fused silica, the intensity of the laser light (351nm or 355 nm) that causes physical damage in fused silica, theoretically speaking, are in great excess of the intensity of incident laser light. The demanding prerequisites for completing the laser facility dictate strict surface and subsurface quality as well as batch-production efficiency.

In light of the excellence in strength, thermal stability and UV transparency, ultra high-purity fused silica is suitable for photo masks substrate in UV photolithography, especially in deep ultra violet lithography when the line-width is down to 22nm.

Furthermore, fused silica lenses in present lithography have high internal transmission and homogeneity, low induced absorption and birefringence, which provide fused silica with significant potentials in refractive micro-lenses of lithography systems.

1.2 Glass Processing

Each coin has two sides. It is the very properties of fused silica that render fused silica as difficult-to-machine brittle materials. High quality surface and subsurface are required in most above mentioned applications. For instance, optical components must be extreme smooth and flat of the finished surface; specifically speaking, the surface micro-roughness should be no more than 0.4 nm and surface figure of $1/3\lambda$ ($\lambda=632.8\text{nm}$) over a $430\text{mm}\times 430\text{mm}$ area is essential to reduce the scattering-induced loss of energy. The requirements for surface roughness in UV lithographic processing are more stringent, approximating to atomic level. As to the astronomic telescopes, surface figure deviates from the desired specifications no more than 25nm in Giant Magellan Telescope (GMT) located in Hawaii, USA. Besides surface figure and micro-roughness, residual mechanical damage to surface and near surface should not be allowed in these systems. The residual stress in the optics may deform the focal image in UV lithography. The subsurface damage in fused silica optics of high power laser systems can serve as reservoirs for contaminants strongly absorbing incident laser light and therefore inducing physical damage to optics. In the meantime, fused silica is hard brittle material to which usual processing techniques inevitably generate considerable damage. The damage will be reduced using polishing process to guarantee the manufactured optics usable.

Conventional machining process, basically speaking, consists of grinding and polishing. Grinding may be fulfilled both by loose and fixed abrasive grinding. Loose abrasive grinding generally involves the use of emery and corundum that are much stiffer than fused silica (Fig. 1.3). On some occasions, synthetic diamond and alumina are employed for further grinding, which can drastically decrease surface roughness

and subsurface fractures that remains in the topmost surface of ground glass without incurring any other scratches. By contrast, it is of much difficulty to use much finer emery to diminish surface roughness and therefore subsurface fractures since finer emery is inclined to suffering the generation of scratches probably deeper than subsurface fractures.

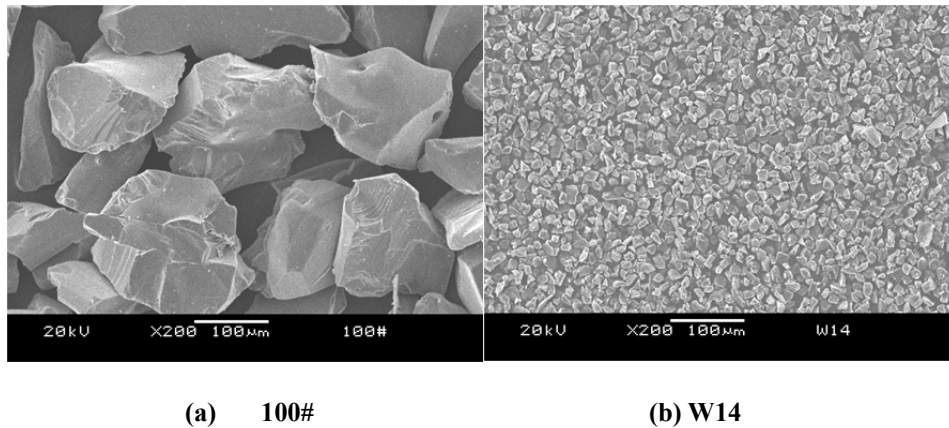


Fig. 1.3 Emery with different size which is used widespread in grinding

Fixed-abrasive grinding for glass in general takes advantage of diamond to grind glass. The diamond grits are dispersed in metal, ceramics, or resin matrix. The diamond-containing layer can be shaped in the shapes as desired, for instance, cup wheel, plate grinding, arc grinding wheel, and even pellets.

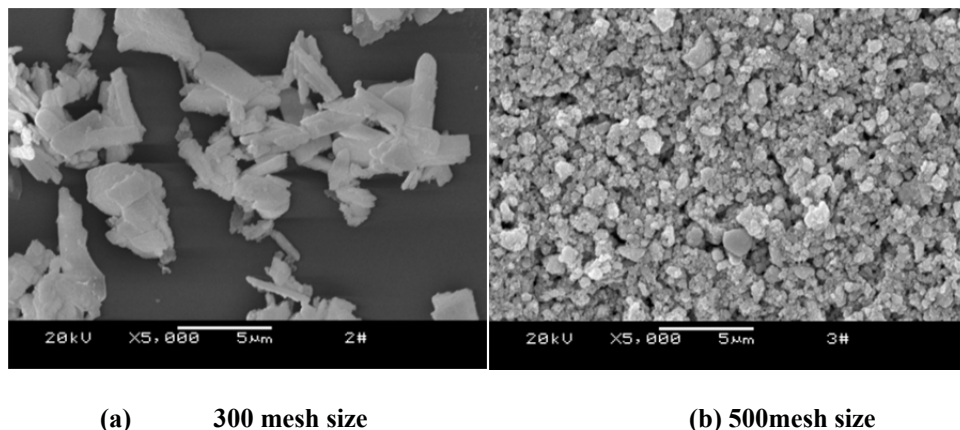


Fig. 1.4 Cerium oxide with different size which is used widespread in polishing shopfloor

Polishing is an indispensable process in precision glass manufacturing. Likewise, polishing can be categorized into fixed-abrasive and loose (or free) abrasive polishing in terms of whether the polishing abrasives are bound with bonding

materials or freely move in the course of polishing. Speaking generally, loose abrasive polishing refers to the use of oxide compounds (usually rare earth & metal compounds) with lower hardness than glass as abrasives mixed with deionized water and chemical additives to chemically-mechanically remove material from glass surface (Fig. 1.4). It is considered to be a rather complicated process among abrasives, polishing materials and polished glass as well as aqueous chemical additives. The commonly used appropriate polishing materials encompass pitch, polyurethane, non-woven, Teflon, and so forth. The polishing abrasives include ceria, rouge, SnO_2 , TiO_2 , etc., most of which are less hard than or comparable to glass in hardness and as a consequence can produce a smooth surface without any mechanical damage. Notwithstanding the widespread use, loose abrasive polishing is not environment-benign. Most importantly, it is hard to precisely predict the removal of material that is subject to motion of abrasives, because the movement of abrasives is stochastic in loose abrasive polishing. In contrast, the trace of a single abrasive in fixed-abrasive polishing can be simulated and foreseen with great ease, which is instrumental in implementing computer-controlled automatic polishing. Another superiority is that a majority portion of abrasives play a role in removing glass as opposed to small fraction of abrasives in loose abrasive polishing. It is reported that merely 0.5% of abrasives take part in material removal in loose abrasive, implying that most abrasives are actually unused and a huge portion of polishing material is wasted. For the aforementioned reasons, many groups turned to fixed abrasive polishing, including those in USA, the former USSR, Ukraine, and Japan. 3M Company has succeeded in polishing STI (shallow trench isolation) with fixed abrasive polishing pad. Noritake Corp. has manufactured the prototype of a new fixed-abrasive pad that can be utilized to polish several hard materials. A group in Ukraine inherits the legacy of the former Soviet Union and continues research on fixed-abrasive polishing. The researchers in USA also developed a new type of polishing tool specialized for glass, in which the ceria abrasives and additives are

mixed in the epoxy resin matrices. The surface roughness of glass polished with the tools approaches $R_q < 1.0\text{nm}$. Zhou *et al.* invented a cerium-containing fixed abrasive polishing process originally intended to machine silicon and later extended to glass. The surface roughness for glass and silicon can reach as low as $\sim 0.5\text{nm}(R_a)$.

1.3 Ultrasonic Machining

Ultrasonics has been recognized not only as a viable and dependable tool to prognosticate diseases in medical practices but also a prevailing technique in non-destructive detection and manufacturing. In manufacturing, ultrasonics has been extensively applied to difficult-to-machine materials. Traditional machining in the presence of ultrasonics can be delineated into ultrasonic machining (USM) and ultrasonic assisted machining (UAM).

The application of ultrasonic vibration to loose abrasive machining of hard-brittle materials dates back to as long ago as 1920s, which was proposed for the purpose of fulfilling the ever-increasing needs for machining difficult-to-machine materials productively. This machining method is well-known ultrasonic machining (USM), in which a generator transfers electric energy to magnetostrictive or piezoelectric transducer which vibrates a machining tool (Fig.1.5). The tool attached to the transducer through a mechanical amplifier, vibrates at a frequency of over 20kHz and a amplitude less than tens of μm along its own axis. The vibration, in turn, imparts a high velocity to abrasive grains by means of fluid media between the tool and the workpiece.

In typical processes of USM, the tool is separated from the workpiece surface and a gap/clearance between the tool and the workpiece surface is impregnated with fluids in which appropriate abrasives are dispersed. The material is removed by the energized abrasives, which invade the surface of workpiece. The mechanism of material removal is believed to be due to mechanical abrasion by rolling, sliding, direct hammering of the abrasives, micro-chipping. Chemical ultrasonic cavitation

erosion also contributes to material removal. The material removal rate (MRR) is elevated by, among others, static load, vibration amplitude, and vibration frequency. USM is ideally suited for drilling and holing hard-brittle materials. The USM generates no heating and induces no additional damage and is a stress-free machining method. However, the material removal rate in USM is quite low and the erosion of machining tool is a knotty problem.

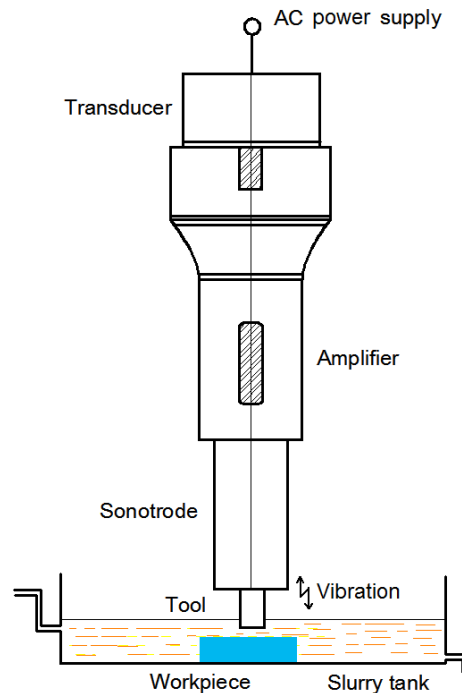


Fig. 1.5 The alternate current (AC) is converted into vibration via a transducer, which is then amplified by an amplifier. The whole vibration generating gadget is referred to as a sonotrode. The machining tool is attached to the sonotrode. The slurry can be retained in a reservoir or circulated during machining.

The other application of ultrasonics to machining is to utilize ultrasonics as an auxiliary to supplement conventional prevailing machining techniques, e.g., cutting and grinding, which is referred to as ultrasonic assisted machining (UAM). Given its universality, ultrasonics can be incorporated into most machining techniques to implement hybrid machining. The ultrasonic assisted turning, cutting, and grinding are representative of the UAM. A typical UAM process, ultrasonic assisted surface grinding, is schematically illustrated in Fig. 1.6. The material removal mechanism of

UAM differs from that of USM. The material cannot be removed without ultrasonics, that is, the ultrasonics is indispensable in USM, while in UAM ultrasonics is a supplement to facilitate conventional machining techniques. The process can be combined effectively with many conventional turning, drilling, and boring operations for both metallic and nonmetallic materials to fulfill such extraordinary manufacturing results as increased material removal rates, decreased machining forces, reduced tool wear, and improved surface finish. Recent researches confirm further that applying ultrasonic vibration can increase the critical depth of cut at which brittle-ductile transition arises. The increase in critical depth of cut may be attributed to reduction in machining forces. Moreover, wear of tools, surface roughness of machined workpiece, surface integrity and MRR are improved as well. Most of conventional UAM processes refer to the vibration of tools and/or abrasives while a method involving the vibration of workpiece in lieu of the vibration of tools/abrasives is presented by Egashira and Masuzawa to drill micro-holes. More recently, the UAM has been extended into the generation of structured surface because applying ultrasonics can alleviate the burring and smooth the edge of microstructures as well as reduce the wearing of the machining tool.

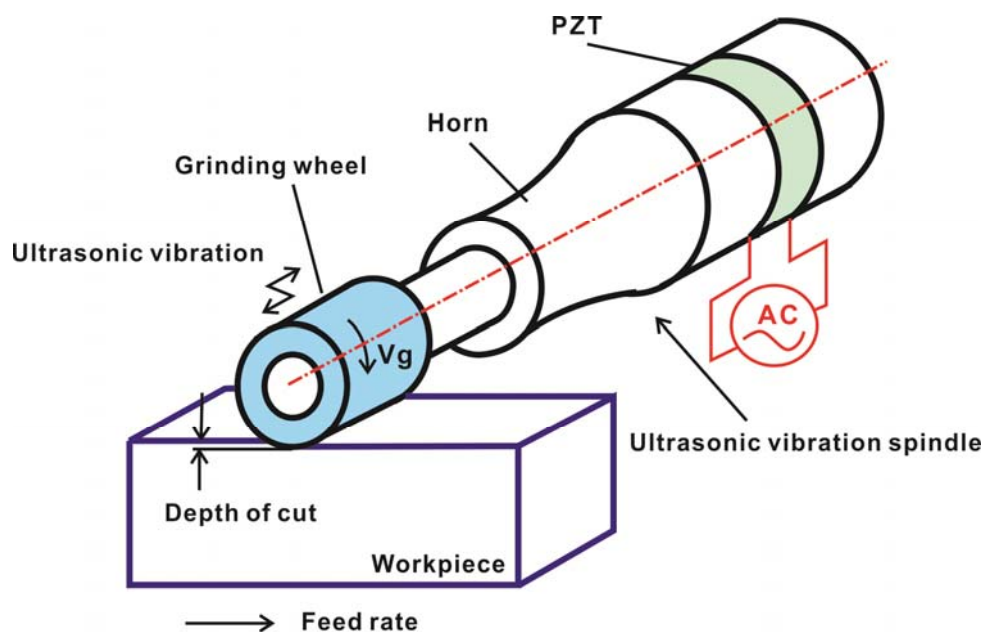


Fig. 1.6 A grinding wheel is screwed on the end face of a rotary ultrasonic

spindle composed of a hone and a bolted langevin transducer (PZT device) and rotates around its own axis. The electrical energy (AC voltage) is converted into vibration energy by the transducer and transmitted through the hone to the grinding wheel, resulting in a vibration of the grinding wheel at ultrasonic frequencies in its axial direction. Giving a depth of cut, Δ , between the workpiece and the grinding wheel, and feeding the workpiece right-forward at a feed rate of V_f results in an ultrasonic assisted surface grinding.

Most of the above-mentioned applications are limited to grinding, i.e. the use of harder abrasives. More recently, there is a sign of incipient ultrasonic assisted polishing. Ultrasonic vibration is combined with chemical mechanical polishing and satisfactory results have been demonstrated. Some researchers ultrasonically drove polishing plate onto which a pad is attached to CMP sapphire, silicon and copper. They all show that the material removal, to some extent, can be elevated and in the meantime the surface roughness be decreased. The reason is assumed to be that more abrasives will be engaged in material removal and sliding distance can be prolonged by the use of ultrasonics during the polishing process.

As it is well known, machining performance, at least material removal rate, can be improved by introducing ultrasonic vibration into manufacturing processes. The easy-to-implement adds to the universality of ultrasonics to machining processes. Inspired by the fact that machining performance can be ameliorated on the introduction of ultrasonic vibration into machining processes, we here “appropriate” this creed to amalgamate ultrasonic vibration with newly developed fixed abrasive polisher with anticipation of the improvement either in material removal rate or in surface quality. The polisher is composed of ceria abrasives, bonding materials and chemical additives.

1.4 Thesis Organization

The thesis is made up of the introductory chapter along with other 6 chapters:

Chapter I briefly reviews the glass and the machining technology of glass. Prevailing technologies and emerging ones for grinding and polishing glass is outlined.

Chapter II details the related experimental devices that were employed in the work. The theory and design of vibrating PZT is in the foremost place and followed by the test and confirmation of the designed PZT. After that, the experimental conditions under which the experiments were performed are listed.

Chapter III concentrates on phenomenological physics of the work. This chapter compares the results of ultrasonic vibration with those without vibration, verifying that material removal is improved indeed while the surface roughness is not degraded severely. The surface morphology is also presented to discriminate the effect of ultrasonic vibration on machined surface. A preliminary model is setup in order to expound the improvement in material removal of ultrasonic vibration-assisted polishing. Lastly, the wear of polishing tool differing from the wear of diamond grit in grinding process is additionally appended.

Chapter IV dedicates to the elucidation of surface scratches in “with” & “without” ultrasonic vibration assisted polishing. Some scratches may induced in polishing process that is viewed as a result of chips. The chips with intermediate “effective” hardness may damage the surface mechanically. But the results of pore-including polishing tool stand in a stark contrast to the tool without pores. The reasons are not fully understood but ascribed to the chips lodged at the interface of polishing tool and glass.

Chapter V accounts the thermal phenomena in polishing of glass and silicon. The temperature was 20~40 Celsius degree, far lower than as expected. Even if such low temperature was measured, the polishing process proceeds smoothly and the machined glass seems unaffected. The heating in polishing process was modeled and simulated analytically and numerically, respectively. It appears that the modeled temperature is slightly greater than the experimented temperature.

Chapter VI, as the extension to the industrial application, focuses on the determinism of fixed-abrasive polishing techniques. Both “with” and “without” ultrasonic vibration processes result in satisfactory determinism in material removal. The material removal rises linearly with time, that is, the material is removed time-invariantly with fixed-abrasive polishing in our experimented environments. The material removal is also linearly related to external mechanical parameters, such as velocity and downward force. Hence the steady removal of material is conducive to automation of polishing process.

Chapter VII, the last chapter summarizes and advises the work and outlines the prospects of the fixed-abrasive techniques together with utilization of ultrasonics in state-of-the-art precision machining fields.

References

- [1]. J. Cheng, *The principles of astronomical telescope design*, (Springer Science & Business LLC., New York, USA, 2009), Chap. 2.
- [2]. R. Schmit, C. McGaha, J. Tekell, J. Grove, and M. Stanek, "Performance Results for the Optical Turbulence Reduction Cavity," the 47th AIAA Aerospace Sciences Meeting Including the New Horizons Forum and Aerospace Exposition, 5~8 Jan. 2009, Orlando, FL, USA.
- [3]. J. H. Campbell, R. Hawley-Fedder, C. J. Stolz, J. A. Menapace, M. R. Borden, P. Whitman, J. Yu, M. Runkel, M. Riley, M.D. Feit and R. Hackel, "NIF optical materials and fabrication technologies:An overview," Proc. SPIE 5341, 81-101, 2004.
- [4]. R. H. French and H. V. Tran, "Immersion Lithography: Photomask and Wafer-Level Materials," *Annu. Rev. Mater. Res.* 39, 93-126, 2009.
- [5]. P. Nussbaum and H. P. Herzig, "Low numerical aperture refractive microlenses in fused silica," *Opt. Eng.* 40, 1412-1414, 2001.
- [6]. R. Voelkel, J. Duparre, F. Wippermann, P. Dannberg, A. Brauer, R. Zoberbier, M. Gabriel, M. Hornung, S. Hansen, and R. Suess, "Technology trends of microlens imprint lithography and wafer level camera (WLC)," MOC'08 Conference on Micro-Optics, 25-27 Sep. 2008, Brussels, Belgium.
- [7]. J. Xue, *In-situ, portable monitoring methods for photolithography characterization*, PhD. Dissertation, University of California at Berkeley, CA, USA, 2009.
- [8]. Matt Johns; J. Roger P. Angel; Stephen Shtetman; Rebecca Bernstein; Daniel G. Fabricant; Patrick McCarthy; Mark Phillips, "Status of the Giant Magellan Telescope (GMT) project," *Proc.* 5489, 441-453, 2004.
- [9]. L.M. Cook, "Chemical process in glass polishing," *J. Non-Crystalline Solids* 120, 152-171, 1990.
- [10]. N. N. Kachalov, *Technology of Grinding and Polishing Sheet Glass* (Acad.

- Sci., Moscow-Leningrad, U.S.S.R., 1958) (in Russian); [translated by W. Mao and Y. Yang, (China Industry Press, Peking, China, 1965), Chap. 3 (in Chinese)].
- [11]. I. D. Marinescu, E. Uhlmann, T. Doi, *Handbook of Lapping and Polishing*, CRC Press, Boca Raton, 2007.
- [12]. Bulsara, V., H., Ahn, Y., Chandrasekar, S., and Farris, T., N., “Mechanics of polishing,” *Trans. ASME: J. Appl. Mech.*, Vol. 65, No. 2, 410-416, 1998.
- [13]. K. Ochiai, Y. Nanbu, F. Tanaka, T. Sasaki, and Y. Utsunomiya, “Study on high-removal-rate mirror grinding of optical glass,” *Research Report of Saitama Industrial Technology Center*, Vol. 8, 78-83, 2009. (in Japanese)
- [14]. J. Gagliardi, A. Zagrebelny, B. Joseph, and L. Zazzera, “Advancements for sub 45nm fixed abrasive STI CMP,” *NCCAUS CMP Users Group at Semicon West Moscone Center*, San Francisco, C.A., USA, 2007.
- [15]. V. Rogov, Y. Filatov, W. Kottler, and V. Sobol, “New technology of precision polishing of glass optics,” *Opt. Eng.*, Vol. 40, No. 8, 1641–1645, 2001.
- [16]. Y. Filatov, O. Filatov, G. Monteil, U. Heisel, and M. Storchak, “Bound-abrasive grinding and polishing of surfaces of optical materials,” *Opt. Eng.*, Vol. 50, No. 6, 063401, 2011.
- [17]. L. Zhou, H. Eda, J. Shimizu, S. Kamiya, H. Iwase, S. Kimura, and H. Sato, “Defect-free fabrication for single crystal silicon substrate by chemo-mechanical grinding,” *Ann. CIRP*, Vol. 55, No. 1, 313–316, 2006.
- [18]. L. Zhou, T. Shiina, Z. Qiu, J. Shimizu, T. Yamamoto, and T. Tashiro, “Research on chemo-mechanical grinding of large size quartz glass substrate,” *Prec. Eng.*, Vol. 33, No. 4, 499–504, 2009.
- [19]. <http://www.noritake.co.jp>
- [20]. B. E. Gillman and S. D. Jacobs, “Bound-abrasive polishers for optical glass,” *Appl. Opt.* 37, 3498-3505, 1998.
- [21]. I. Markov, *Ultrasonic Machining of Intractable Materials*, (Mashgiz, Moscow, U.S.S.R.,) 1962 (in Russian) [translated by Scripta Technica Ltd., edited

- by E. A. Neppiras, (Iliffe Books Ltd., London, UK), Chap. 2, 1966].
- [22]. P. L. Guzzo, A. H. Shinohara, and A. A. Raslan, "A comparative study on ultrasonic machining of hard and brittle materials," *J. Braz. Soc. Mech. Sci. Eng.* 26, 56-61, 2004.
- [23]. T. B. Thoe, D. K. Aspinwall, and M. L. H. Wise, "Review on ultrasonic machining," *Int. J. Mach. Tool. Manuf.* 38, 239-255, 1998.
- [24]. Y. Ichida, R. Sato, Y. Morimoto, K. Kobayashi, "Material removal mechanisms in non-contact ultrasonic abrasive machining," *Wear* 258, 2005, 107-114, 2005.
- [25]. D. E. Brehl and T. A. Dow, "Review of vibration-assisted machining," *Prec. Eng.* 32, 153-172, 2008.
- [26]. T. Moriwaki, E. Shamoto, and K. Inoue, "Ultraprecision ductile cutting of glass by applying ultrasonic vibration," *Ann. CIRP* 41, 141-144, 1992.
- [27]. M. Zhou, X. J. Wang, B. K. A. Ngoi, and J. G. K. Gan, "Brittle-ductile transition in the diamond cutting of glasses with the aid of ultrasonic vibration," *J. Mater. Process. Technol.* 121, 243-251, 2002.
- [28]. W. Qu, K. Wang, M. H. Miller, Y. Huang, and A. Chandra, "Using vibration-assisted grinding to reduce subsurface damage," *Prec. Eng.* 24, 329-337, 2000.
- [29]. C. Nath and M. Rahman, "Effect of machining parameters in ultrasonic vibration cutting," *Int. J. Mach. Tool. Manuf.* 48, 965-974, 2008.
- [30]. M. Zhou, B. K. A. Ngoi, M. N. Yusoff, and X. J. Wang, "Tool wear and surface finish in diamond cutting of optical glass," *J. Mater. Process. Technol.* 174, 29-33, 2006.
- [31]. K. Egashira and T. Masuzawa, "Microultrasonic machining by the application of workpiece vibration," *Ann. CIRP* 48, 131-134, 1999.
- [32]. M.-Y. Tsai, and W.-Z. Yang, "Combined ultrasonic vibration and chemical mechanical polishing of copper substrates," *Int. J. Mach. Tool. Manuf.*, Vol. 53,

No. 1, pp. 69-76, 2012.

- [33]. W. Xu, X. Lu, G. Pan, Y. Lei, and J. Luo, "Ultrasonic flexural vibration assisted chemical mechanical polishing for sapphire substrate," *Appl. Surf. Sci.*, Vol. 256, No. 12, 3936-3940, 2010.
- [34]. P.-L. Tso, and C. Tung, "Study on ultrasonic-assisted chemical mechanical polishing," *Int. J. Abra. Technol.*, Vol. 4, No. 2, 132-139, 2011.

CHAPTER II

EXPERIMENT APPARATUS AND DETAILS

One must have good tools to do a good job.

This chapter focuses mainly on the theory and design of PZT vibrator and experiments. The theory based on which vibrator was created is mechanical vibration of an isotropic beam. The transverse and longitudinal basic resonant frequency of beam is determined by the dimension. To adjusting the dimension of the vibrator can affect the frequency and therefore make both frequencies be the same. Thereby, a two dimensional vibrator will be generated using only one vibrator. The actual dimension is finalized by numerical simulation with the aid of finite element analysis software. The designed vibration was verified by virtue of experiments. The detailed experimental conditions are also listed out along with temperature measurement methods.

2.1 Design of PZT

Both low-frequency and ultrasonic vibration are being utilized in practical applications and the former is regarded as solid vibration while the latter elastic vibration. We direct our attention towards ultrasonic vibration. An ultrasonic head is one of the most vital components in ultrasonic machining, by which the alternating electrical supply is converted into mechanical vibrations. An ultrasonic head is usually comprised of a transducer and a horn & booster (i.e. sonotrode). Two types of transducers are commonly used, namely magnetostrictive and piezoelectric transducers. Magnetostrictive transducers are capable of allowing the transmittance of vibration over broad frequencies whereas possess low energy conversion efficiency and generate appreciable heat. In contrast, piezoelectric transducer can convert energy

more efficiently up to 96% and induce little thermal damage. Piezoelectric materials refer to some solids that exhibit piezoelectricity. Piezoelectricity is an effect that charges will accumulate after applying mechanical stress to certain solid matters such as quartz, ceramics, proteins and so forth. Ultrasonic vibrations are generally created by means of piezoelectric materials owing to unique physical and electrical properties of the materials. PZT piezoelectric material (lead zirconate titanate) was selected to construct transducers in our design.

Most prevailing are 1-D and 2-D machining systems according to tool vibration path with respect to workpiece being machined; the emerging 3-D machining also appeals to a growing number of researchers. The emphasis is placed on the 1-D and 2-D vibration in our investigation. Most 2-D vibrations are created with two PZT actuators, albeit Brinksmeier et al. and Li et al. off-centered one actuator to result in 2-D tool path. We devised our vibrator for the generation of 2-D tool path despite using only one actuator, which consists of a PZT ceramic plate stacked with a metallic elastic bar. The input-voltage excited PZT plate will magnify the vibration of the metallic bar.

Longitudinal and lateral vibrations of an elastic bar (henceforth termed L mode and B mode) can be expressed with two partial differential equations, respectively (Fig. 2.1).



Fig. 2.1 An elastic bar of homogeneous mass with the length of L

$$AE \frac{\partial^2 u}{\partial x^2} - \rho A \frac{\partial^2 u}{\partial t^2} = 0 \quad (1)$$

$$EI \frac{\partial^4 y}{\partial x^4} + \rho A \frac{\partial^2 y}{\partial t^2} = 0 \quad (2)$$

where, u is the longitudinal displacement, y the lateral displacement, E Young's modulus, A cross sectional area of the bar, ρ the density of the bar, I moment of inertia of cross sectional area, L the length of the bar. By separating the variables, the solutions to the above equations can be described as stationary waves:

$$u(x,t) = f(x)g(t) \quad (3)$$

$$y(x,t) = h(x)z(t) \quad (4)$$

Substituting Eq. (3) & (4) into (1) & (2) and solving Eq. (1) & (2), we obtain the solutions to spatial parts of (1) & (2) by taking into account boundary conditions:

$$f(x) = F \cos(\alpha_n x) \quad (5)$$

$$h(x) = H \{[\sinh(\kappa_n x) + \sin(\kappa_n x)] + C[\cosh(\kappa_n x) + \cos(\kappa_n x)]\} \quad (6)$$

$$\cosh(\kappa_n L) \cos(\kappa_n L) = 1 \quad (7)$$

$$C = \frac{\sin(\kappa_n L) - \sinh(\kappa_n L)}{\cosh(\kappa_n L) - \cos(\kappa_n L)} \quad (8)$$

where, F , H are the amplitudes of longitudinal and lateral vibrations, respectively. Eq. (7) can be solved numerically and the first seven values are tabulated in Table 2.1.

Table 2.1 The first seven orders of solutions to Eq. (7).

n	1	2	3	4	5	6	7	8	9
$\kappa_n L$	4.7300	7.8532	10.9956	14.1372	17.2788	20.4204	23.5619	26.7035	29.8451

Using Eq. (5) through (8), we simulated the longitudinal and lateral vibrations of a bar with the length of L (Fig. 2.2).

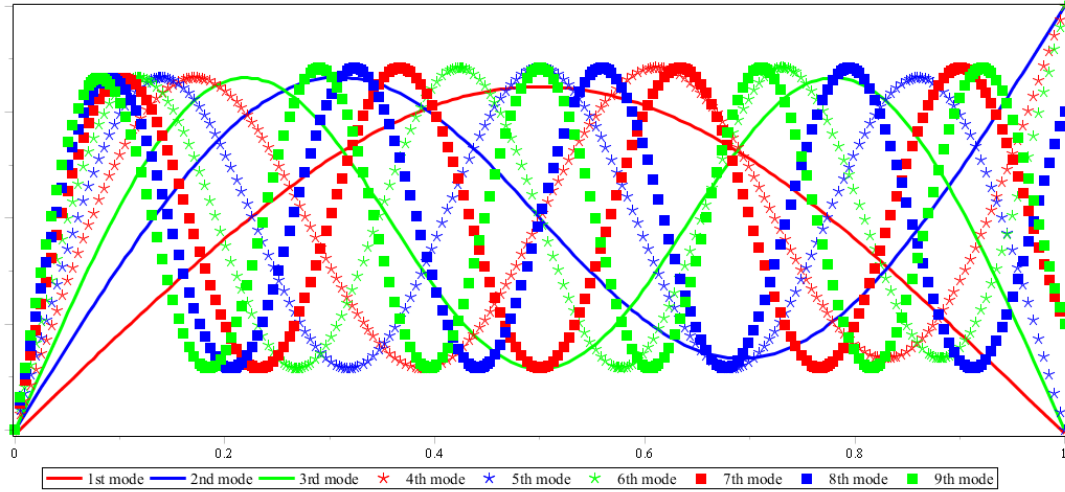


Fig. 2.2 The foremost nine vibrations of the bar in lateral (B mode) direction.

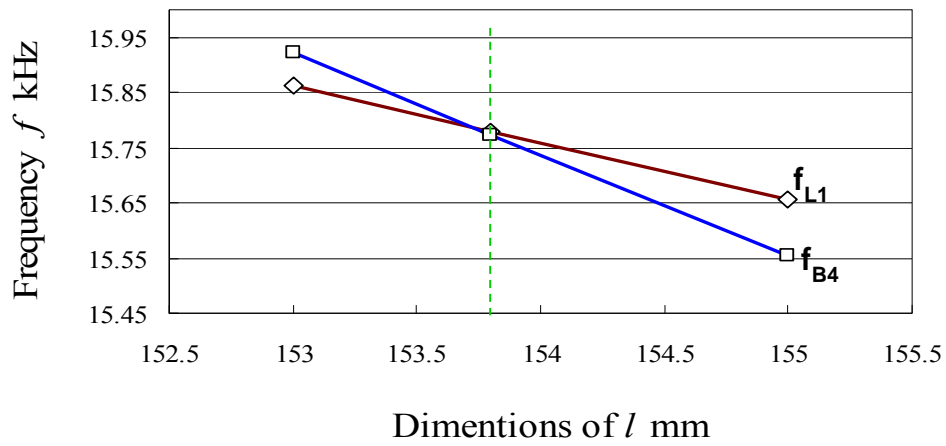
It is obvious that at the center of the bar ($x=0.5L$) the amplitude of lateral vibration is zero (relatively static) for the even orders and the maximum for the odd orders.

Speaking generally, the lower the order of vibrations, the more easily the bar vibrates. On the other hand, the longitudinal vibration must match the lateral so as to reach a stable combined vibration in two directions. In addition, a prerequisite concerning the thickness (d) and length (L) of the bar should be met:

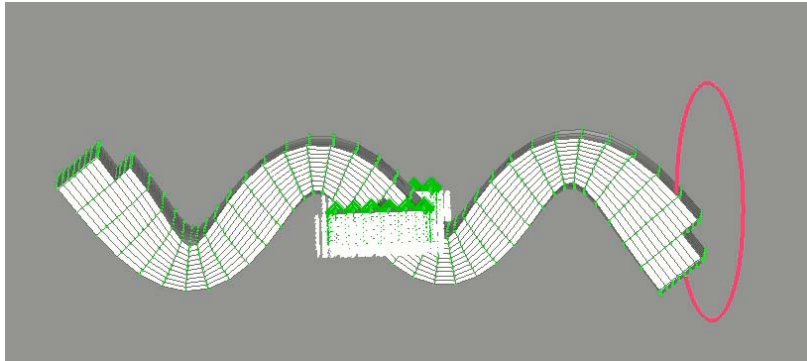
$$L = \frac{(2n+1)^2 \pi}{8\sqrt{3}m} \cdot d \quad (9)$$

where, n is the order of lateral vibrations and m the longitudinal vibration order. The equation works rather well for low order of n ($n < 8$); however, the specific dimension of PZT is determined more accurately by trial-n-error iterations with the help of FEA software.

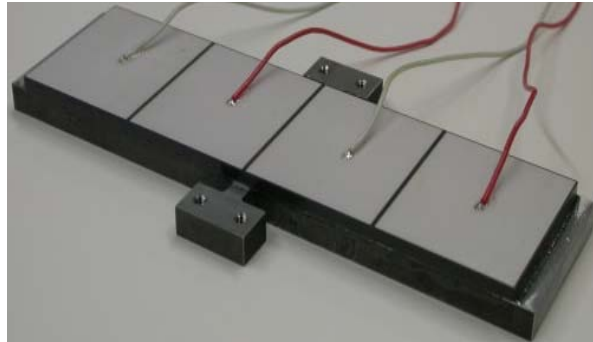
From the Eq. (9), we can understand that the combination of 1st longitudinal mode (L1) with 4th lateral mode (B4) provide reasonable dimensions of a bar, where $L = 18.4d$. Different materials of PZT and metallic elastic body dictate that the dimension of elastic body should match that of PZT, which is accomplished with FEM method and simulation software (PIEZO plus 4.0). The designed frequency of the bar is $\sim 15.8\text{kHz}$ and the vibration of the designed bar is also given (Fig. 2.3).



(a)



(b)

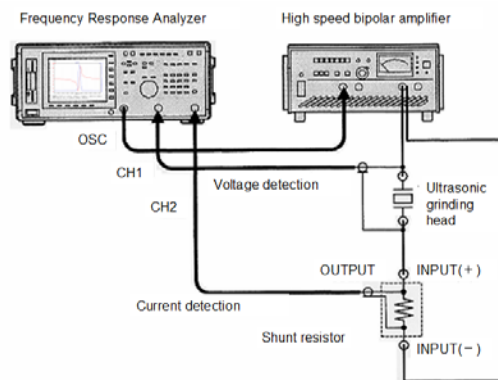


(c)

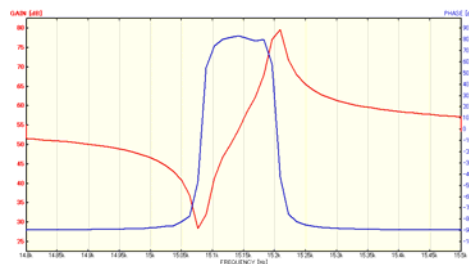
Fig. 2.3 (a) There exists a frequency at which both the L1 and B4 can be stimulated. The said frequency will be the frequency of the designed vibrator and the corresponding dimension will be the length of the bar. **(b)** The dimensions of PZT and metallic elastic body is determined with the aid of software and the vibration of the designed vibrator is demonstrated. **(c)** The designed PZT vibrator.

2.2 Vibration of the designed PZT vibrator

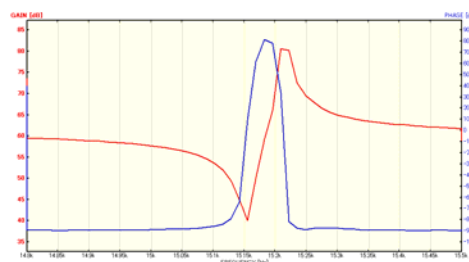
The fabricated vibrator was tested for frequency characteristics with frequency response analyzer (FRA 5090, NF Corporation, Japan). The longitudinal (L1) and lateral (B4) mode are presented in Fig. 2.4. It is apparent that both the frequencies are around 15.22kHz mildly different from the designed values, which is ascribed to manufacturing errors. A frequency of 15.3kHz slightly away from the real frequency is chosen intentionally in our experiments due mainly to the fact that operating the PZT vibrator at the resonant frequency might increase a risk of damaging the PZT vibrator.



(a) Test device for the resonant frequency of a PZT



(b) The frequency feature of L1 mode



(c) The frequency feature of B4 mode

Fig. 2.4 A small difference of 0.08 kHz in resonant frequency can be detected

owing to manufacturing errors and measuring errors.

The vibration was examined with two laser Doppler vibrometers (Ono Sokki LV-1610, Japan) equipped with an oscilloscope (LeCroy WaveJet 314, USA) (Fig. 2.5). The alternating electrical current is supplied with a wave function generator (NF W1946B, Japan), which is then amplified by two high speed amplifiers (NF HSA 4052, Japan). Changing phase difference between two inputs applied to the PZT vibrator will cause changes in tool vibrations (Fig. 2.6).

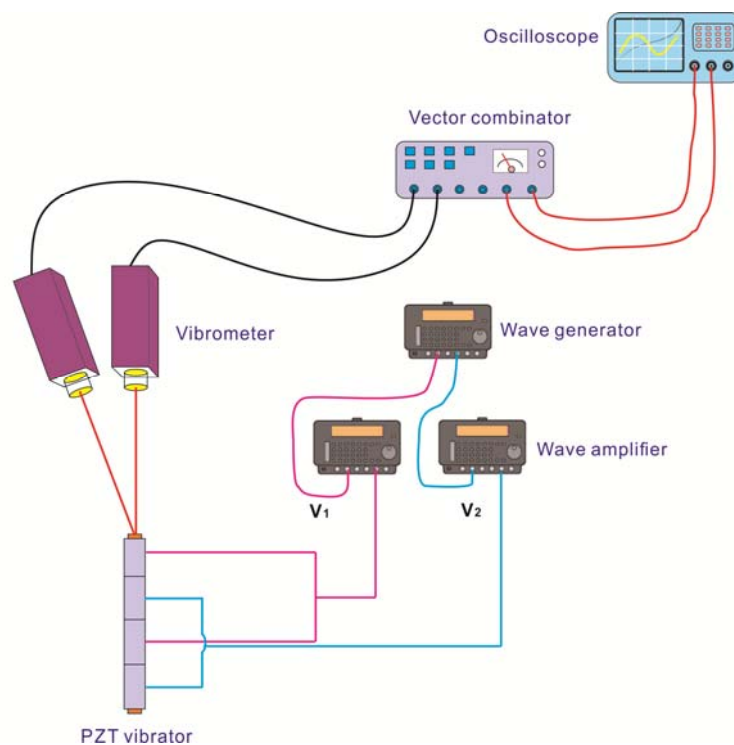


Fig. 2.5 The assembly to measure the vibration of the PZT vibrator comprises two laser Doppler vibrometers and a digital oscilloscope

Theoretically speaking, the trajectory of vibrator appears to be a line as the phase difference between two inputs equates to 0° and 180° . However, in practice the trajectory may be not a perfect line because of measuring errors. It is clear that our vibrator is capable of producing 2-D tools path as well 1-D path by tuning the phase difference.

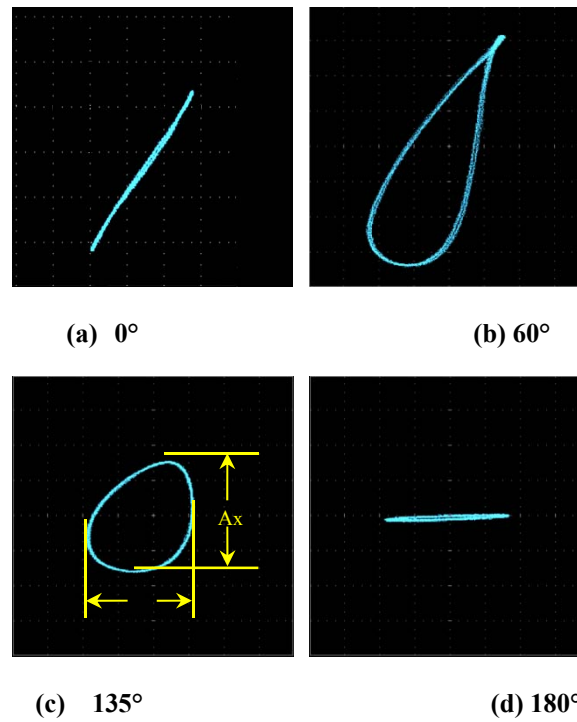


Fig. 2.6 The representative pattern of vibrations ($V_{p-p}=150V$, $f=15.3kHz$).
Adjusting phase difference will consequently lead to the alteration in vibrator trajectories

The amplitude of vibration under varied input voltages was inspected, too (Fig. 2.7). It is found that the amplitude is roughly proportional to input voltages (Fig. 2.8). We conducted all our experiments in this report under conditions of $f=15.3kHz$, $V_{p-p}=150V$, phase difference= 135° .

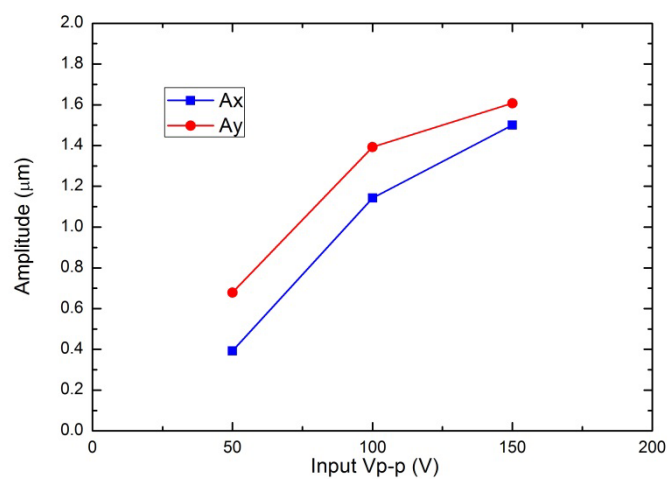


Fig. 2.7 The vibration amplitude can be boosted by increased input voltages

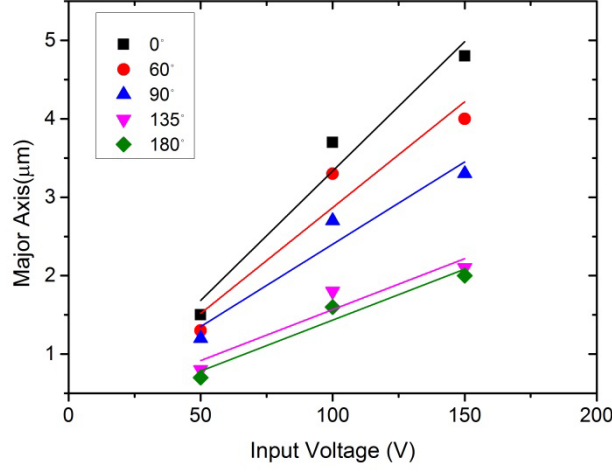


Fig. 2.8 The vibration amplitude is basically proportionate to the input voltages.

We formulate the relation of amplitudes of longitudinal (L) and bending (B) with input V_1 and V_2 :

$$L_1 = c_{L1}V_1 \cos(2\pi ft) \quad (10a)$$

$$B_1 = -c_{B1}V_1 \cos(2\pi ft) \quad (10b)$$

The L_1 and B_1 amplitudes resulting from V_2 are of the similar form:

$$L_2 = c_{L2}V_2 \cos(2\pi ft + \varphi) \quad (10c)$$

$$B_2 = c_{B2}V_2 \cos(2\pi ft + \varphi) \quad (10d)$$

where c_{L1} , c_{B1} , c_{L2} , c_{B2} are the factors relating vibration amplitude to input signals and reined by the dimensions, structure and material properties that are actually identical for V_1 & V_2 ($V_1 = V_2$ in our polishing experiments) in our present design.

This way, the combined vibrations is of the form:

$$x_{UV} = B_1 + B_2 = c_B V \cos(2\pi ft + \varphi) - c_B V \cos(2\pi ft) \quad (11a)$$

$$z_{UV} = L_1 + L_2 = c_L V \cos(2\pi ft + \varphi) + c_L V \cos(2\pi ft) \quad (11b)$$

$$c_{B1} = c_{B2} = c_B; c_{L1} = c_{L2} = c_L; V_1 = V_2 = V \quad (11c)$$

Using triangular transformation, the Eq. 11 can be converted to Eq. 12

$$\left(\frac{x_{UV}}{2c_B V \sin \frac{\varphi}{2}}\right)^2 + \left(\frac{z_{UV}}{2c_L V \cos \frac{\varphi}{2}}\right)^2 = 1 \quad (12)$$

Eq. 12 represents an elliptical as $\tan \frac{\varphi}{2} \neq \frac{c_L}{c_B}$, otherwise a straight line

($\cos \frac{\varphi}{2} \cdot \sin \frac{\varphi}{2} = 0, \varphi = n\pi, n$ is an integer) or a circle ($\tan \frac{\varphi}{2} = \frac{c_L}{c_B}$ & $\cos \frac{\varphi}{2} \cdot \sin \frac{\varphi}{2} \neq 0$).

$c_B V \sin \frac{\varphi}{2}$ is the semi-major or semi-minor axis of the ellipse, depending on φ (Table

2.2). We estimated c_B & c_L from the measurements of vibration as listed in Table 2.3.

It is clear that the c_L is a factor of 1.5 greater than c_B , indicating that longitudinal vibration is susceptible to phase difference than the lateral one.

Table 2.2 Measured and plotted vibration at various phase difference

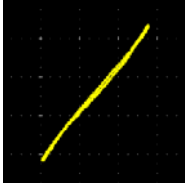
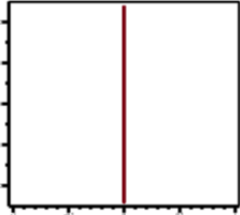
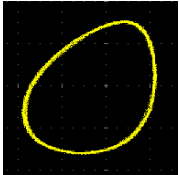
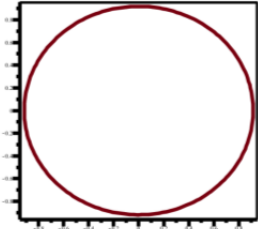
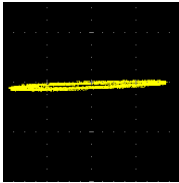

φ	Measured	Derived
0°		
135°		
180°		

Table 2.3 The estimation of c_B & c_L (@ 150V).

φ	$c_B / \mu\text{m}/\text{V}$	$c_L / \mu\text{m}/\text{V}$
0°	N/A	0.0080
60°	0.0040	0.0077
90°	0.0028	0.0077
135°	0.0027	0.0091
180°	0.0033	N/A
Avg.	0.0032	0.0081

2.3 Experimental details

A customized apparatus was constructed as schematically illustrated in Fig. 2.9. The apparatus consists of a unit composed of a PZT vibrator, a mass-spring-damper mechanism, a dynamometer and a holder, a linear motion actuator for the right or left toward cross motion of the unit, a mechanism for the vertical feed motion of the unit, a vacuum chuck for holding the workpiece, and a spindle for rotating the vacuum chuck. In the unit, the mass-spring-damper mechanism is installed in order to guarantee that the pellet attached on the lower end face of the vibrator has flexible contact with the workpiece so that a constant-pressure was maintained. The machining pressure is controlled by relative displacement of vibrator in Z-direction and determined quantitatively with a strain gauge.

The pellets are composed of ceria and binding material - phenolic resin. In addition, the pellets are full of abundant pores with diameter of tens of microns. The functionality of the pores may be to accommodate polishing debris and to dissipate the heat in polishing process, which may be beneficial to high material removal rate and surface of high quality. The external downward load is provided by a pair of compression springs and was calibrated with a dynamometer (Kistler 9257A, Switzerland) (Fig. 2.10). The load is in excellent linear relation to the vertical displacement of the grinding head along Z-axis (vertical direction). Then the downward load is determined by the relative displacement of the head. The lower

spindle is able to rotate with respect to its central axis. An octagon ring force sensor (Kyowa, Japan) was also adjusted in accord with dynamometer so as to acquire *in-situ* normal and tangent forces as well. The output voltage exhibits satisfactory linearity to input forces (Fig. 2.11). The workpiece is sucked onto the spindle by virtue of vacuum chuck. Furthermore, the head can move back and forth in X-direction (horizontal direction).

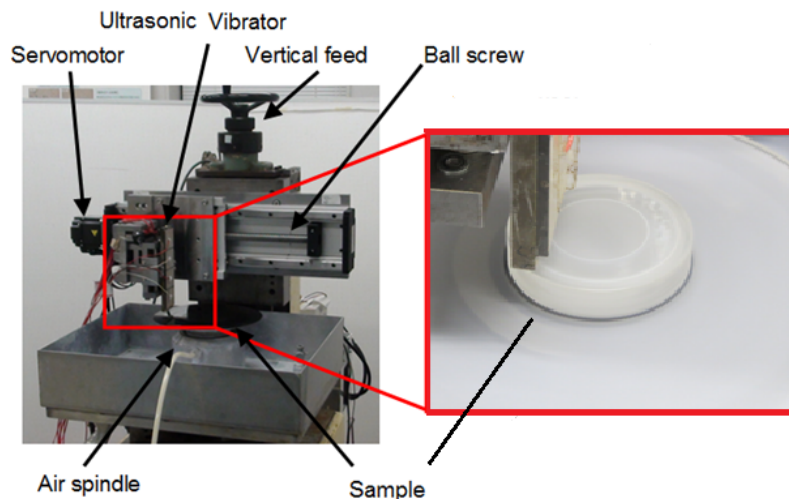


Fig. 2.9 The set-up for the experiments (a) and a close-up of machining head (b). vibrator is screwed to a connector which is able to move in both the vertical and horizontal directions. The downward force is exerted by a pair of springs. The spindle on which workpiece rests can rotate independently.

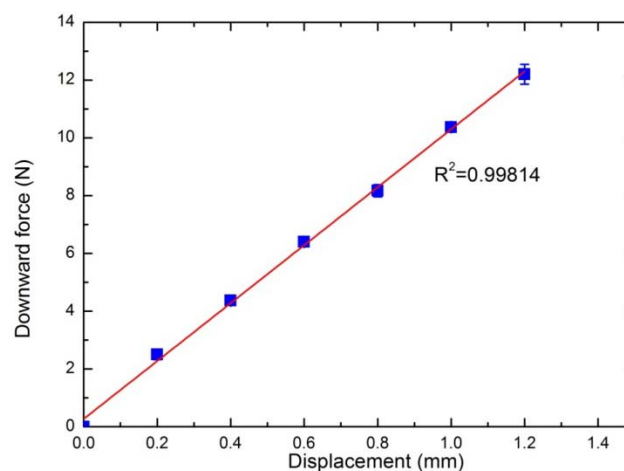


Fig. 2.10 The downward force is calibrated with a dynamometer. The force bears a quite good linear relation to the vertical displacement of the machining head.

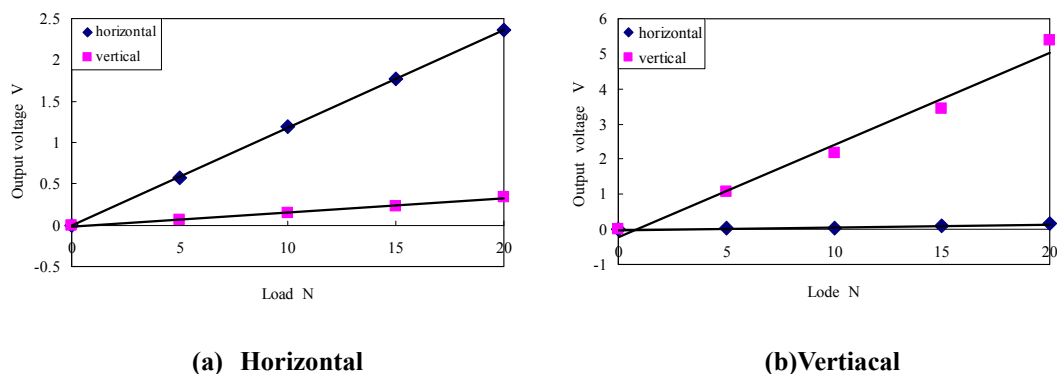


Fig. 2.11 Calibrated force for octagonal ring force sensor.

A circular fused silica sample with dimension of $\Phi 50\text{mm} \times 10\text{mm}$ and initial surface roughness of $\sim 200\text{nmRa}$ was placed on the vacuum chuck as the workpiece. The possible effects of processing parameters and specifications of ultrasonic vibration, i.e. stroke speed in X-axis, normal force, rotational speed, applied voltage and phase difference, on the MRR and surface roughness were investigated systematically in the presence (denoted “with UV”)/absence (denoted “without UV”) of ultrasonic vibration. The rotation rate in our experiments was set to be $\sim 400\text{rpm}$, $\sim 600\text{rpm}$, $\sim 800\text{rpm}$. The polishing head oscillated along the X axis at 3mm/s , 6mm/s , 9mm/s during the machining process. Table 2.4 shows the processing parameters.

Table 2.4 The experimental parameters are detailed as follows.

Sample	Fused silica	$\Phi 50\text{mm} \times 10\text{mm}$
	Initial surface roughness Ra	$\sim 200\text{nm}$
Pellets	Dimension	$\Phi 4\text{mm} \times 1\text{mm}$
	Abrasive	CeO_2
Ultrasonics	Frequency	15.3kHz
	Applied voltage	150V
	V_{p-p}	
	Phase difference	135°

Stroke in X direction	A	3mm
Velocity of oscillation	V_x	3mm/s, 6mm/s, 9mm/s
Downward load	L	4N, 8N, 12N
Rotation rate	ω	400rpm, 600rpm, 800rpm

The machined region was an annulus offset $\sim 15\text{mm}$ away from the center of the fused silica sample. Four measurements of surface roughness were taken in the middle of the annulus at 3, 6, 9, 12 o'clock positions with a non-contact optical profilometer at $10\times$ magnification (Zygo Newview 600, USA) (Fig. 2.12). The surface roughness is the average of the four measurements. The material removal was tested with a contact stylus profiler (Tokyo Seimitsu Surfcom480A, Japan). Another stylus profiler (Taylor Hobson Form Talysurf 50, UK) was utilized in the course of appreciating removal function (polishing imprint). The surface roughness and material removal were checked every 10min after cleaning the surface with ethanol. During each run, the polishing debris was not removed. Each sample was polished for 6 times, i.e. 60min in total. All the experiments were conducted without adding any fluids during the polishing process unless otherwise specified.

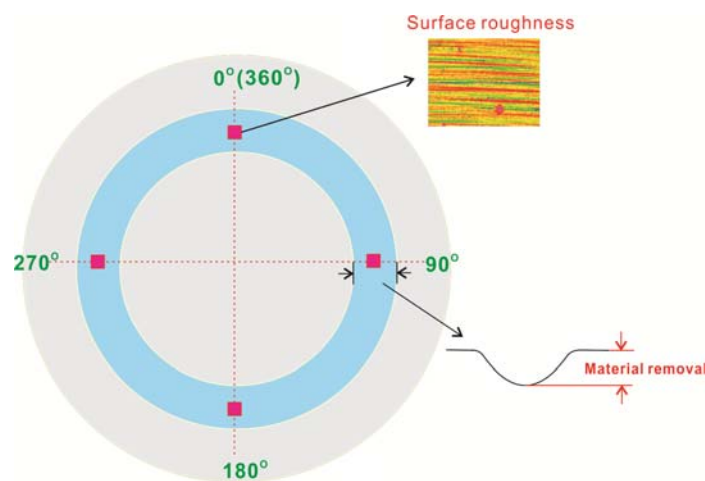


Fig. 2.12 Evaluation method for surface roughness and material removal

2.4 Summary

Firstly, the theory on which the design of vibrator is introduced. Thereafter, a PZT

vibrator to create a 2-D vibration was manufactured and appraised. The vibration resonance of the PZT with two ends free from restrictions was measured to be elliptic. The vibration is in excellent consistency with the design. The vibration amplitude basically scales with regard to exciting voltage. The necessary force sensor was calibrated in advance so that machining force can be monitored on-line. The way the material removal and surface roughness is outlined and sketched. All that is described in the chapter is preparatory but fundamental work for the following chapters.

References

- [1]. H. Suwabe, and K. Ishikawa, "Nontraditional lapping processes," in Handbook of Lapping and Polishing, edited by Marinescu, Uhlmann, and Doi, (CRC Press, Baco Raton, F.L., USA), Chap. 4.3, 2007.
- [2]. D. E. Brehl, and T. A. Dow, "Review of vibration-assisted machining," *Prec. Eng.*, Vol. 32, No. 3, 153–172, 2008.
- [3]. T. B. Thoe, D. K. Aspinwall, and M. Wise, "Review on ultrasonic machining," *Int. J. Mach. Tool. Manuf.*, Vol. 38, No. 4, 239-255, 1998.
- [4]. I. Markov, *Ultrasonic Machining of Intractable Materials*, (Mashgiz, Moscow, U.S.S.R.,) 1962 (in Russian) [translated by Scripta Technica Ltd., edited by E. A. Neppiras, (Iliffe Books Ltd., London, UK), Chap. 2, 1966].
- [5]. Shamoto, E., Suzuki, N., Tsuchiya, E., Hori, Y., Inagaki, H., and Yoshino, K., "Development of 3 DOF ultrasonic vibration tool for elliptical vibration cutting of sculptured surfaces," *Ann. CIRP*, Vol. 54, No. 1, 321-324, 2005.
- [6]. Shamoto, E., and Moriwaki, T., "Study on elliptical vibration cutting," *Ann. CIRP*, Vol. 43, No. 1, 35-38, 1994.
- [7]. Ahn, J.-H., Lim, H.-S., and Son, S.-M., "Improvement of micro-machining accuracy by 2-Dimensional vibration cutting," *Proc. ASPE*, Vol. 20, 150-153, 1999.
- [8]. Brinksmeier, E., and Glabe, R., "Elliptical vibration cutting of steel with diamond tools," *Proc. ASPE*, Vol. 20, 163-166, 1999.
- [9]. Li, X., and Zhang, D., "Ultrasonic elliptical vibration transducer driven by single actuator and its application in precision cutting," *J. Mater. Process. Technol.*, Vol. 180, No. 103, 91-95, 2006.
- [10]. Timoshenko, S., *Vibration Problems in Engineering*, Second Edition, (D. Van Nostrand Company, Inc., New York, USA), Chap. 6, 1937.
- [11]. Wu, Y., Fan, Y., Kato, M., Kuriyagawa, T., Syoji, K., and Tachibana, T., "Development of an ultrasonic elliptic-vibration shoe centerless grinding

- technique,” J. Mater. Process. Technol., Vol. 155-156, 1780-1787, 2004.
- [12]. S. Ueha, Y. Tomikawa, M. Kurosawa, N. Nakamura, Ultrasonic motors: theory and applications, Clarendon Press, Oxford, UK, 1993.

This page intentionally left blank.

CHAPTER III

MATERIAL REMOVAL AND MACHINED SURFACE IN FIXED-ABRASIVE POLISHING

Well begun is half done.

This chapter presents phenomenological results of fixed-abrasive polishing, inclusive of material removal and surface characteristics of machined glass. A physical model intended to elucidate potential mechanism of the increase in material removal was put forward. In addition, the wear of pellet in fixed abrasive polishing was also briefly discussed.

3.1 Material removal

Referring to Fig. 3.1, the material removal rate is indeed increased by introducing ultrasonic vibration regardless of the processing parameters. The Preston coefficients, reflecting the ability of a specific polishing process/device to remove material, for UV process are greater than those without UV by 125% on average in our experiments, demonstrating the efficacy of UV in the polishing efficiency (Table 3.1). Changing downward load significantly changes material removal rate, which is indicated by the drastic change in intra-group Preston coefficients (the slopes of the fitted linear lines) in the group of downward loads as compared to the other two groups (intra-groups) (Table 3.1). It is noteworthy that increasing the downward load paradoxically decreases the material removal rate for the experimented loads, which ostensibly contradicts common creeds held by polishing community that material removal rate should ascend with the elevated pressure. The reason may be that greater pressure is not conducive to the vibration of vibrator and therefore the ability to dispel chips is hampered, which in return undermines the MRR (some blackish substance was

incurred on the pellet surface, which is conjectured to be an obstacle to polishing). The nominal pressure in our experiments ranges 318kPa~955kPa owing to the capacity of the apparatus used in the experiments, far greater than typical pressure of 6.9kPa~69kPa in CMP process . The properties of resin matrix of the pellet have been burnt under the load of 12N and the surface is remarkably different from that under 4N load, as shown in Ref. 1. The decrease in material removal is ascribed to the burnt surface. On some occasions, the polishing process cannot progress under such high load and greater rotation rate. If decreasing the load and linear velocity, that is, lowering the product of load and velocity with another device of different mechanical motion, it is found that the material can be removed without any abnormalities. Thus it is reckoned that there exists a threshold for the applied load and velocity. The resin cannot stand such extreme load/velocity which will induce greater temperature rise that will modify the attributes of resin matrix. Hence the material removal is decreased under such stringent conditions. Furthermore, the vibration actually slightly changes with load and approaches a steady value when the load exceeds a certain level, which will cause material removal rate (the slope of vibration) slightly decrease, agreeing with experiments.

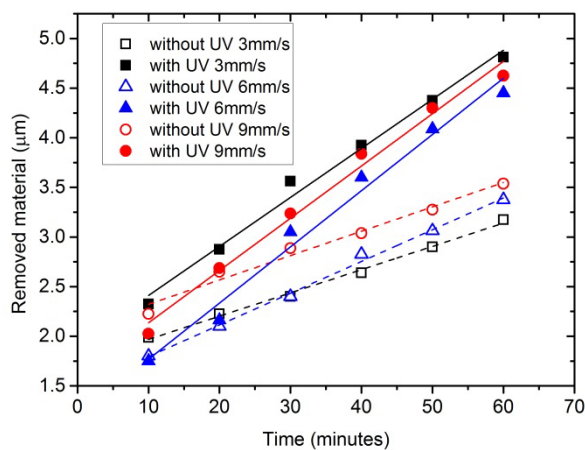
As narrated by Preston, “there is good experimental evidence to believe that the amount of polishing done in time t is proportional to pvt (By the amount of polishing done we mean, strictly, the amount of glass polished off.” Material removal rate ($d\delta/dt$) is linearly related to the product of velocity(v)and pressure(P) while the effects of other factors (k) are reflected in an all-purpose coefficient.

$$\frac{d\delta}{dt} = k(t)P(t)v(t) \quad (13a)$$

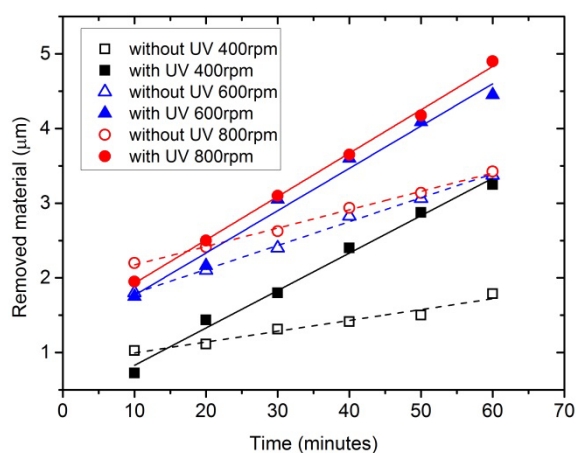
$$\delta = \int_0^T k(t)P(t)v(t)dt \quad (13b)$$

$$\delta = k \int_0^T P(t)v(t)dt \quad (13c)$$

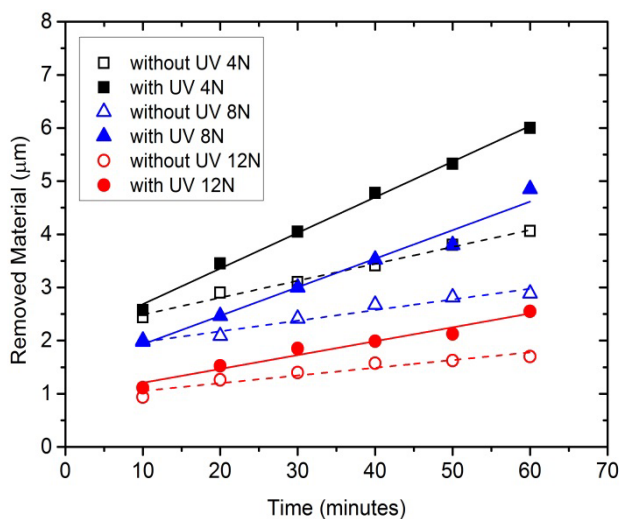
The material removal after an interval of T , in principle, will be worked out from Eq. (13b). When pressure and velocity as well as manufacturing conditions remain constant during the process, the Eq. (13b) reduces to (13c). k can be viewed as an index of the ability of a specific machine and process to polish a certain work-piece. In other words, effect of ultrasonic vibration can be evaluated in terms of k . The k 's for two processes under various conditions are tabulated in Table 3.1. The effect of stroke speed on the relative velocity of pellet to workpiece is not taken into account in the Eq. 13 since it can be rationally neglected relative to rotation rate. The average vibrational velocity of pellet is estimated $1\mu\text{m}\times 15.3\text{kHz}=15.3\text{mm/s}$ while the relative velocity between workpiece and pellet is 1256mm/s in our experiments. The Preston coefficient reflecting the capability of removing material of specific machinery and process, as expected, increases by a factor of $>77\%$. It is noteworthy that the Preston coefficients in the table are computed as the slope of fitting straight lines rather than the ones deduced from the actual material removal at the instant 60min which is far smaller than the ones in the table. Vide the Fig. 3.1, imagine drawing lines to connect the origin (material removal at $t=0$) to the points at $t=10\text{min}$ and it can be found that these lines are steeper, which is caused by the micro-cracks pre-existing in the topmost layer of ground glass. The material removal of the first 10 minutes behaves much different from the material removal of other 50 minutes and the data are singular at $t=0$. It is the slopes for the first ten minutes that make the average material removal rate over 1 hour different from the slopes of current fitted lines. Thus the material removal within first 10min. is excluded in the fitting when material removal rate is referred to.



(a)



(b)



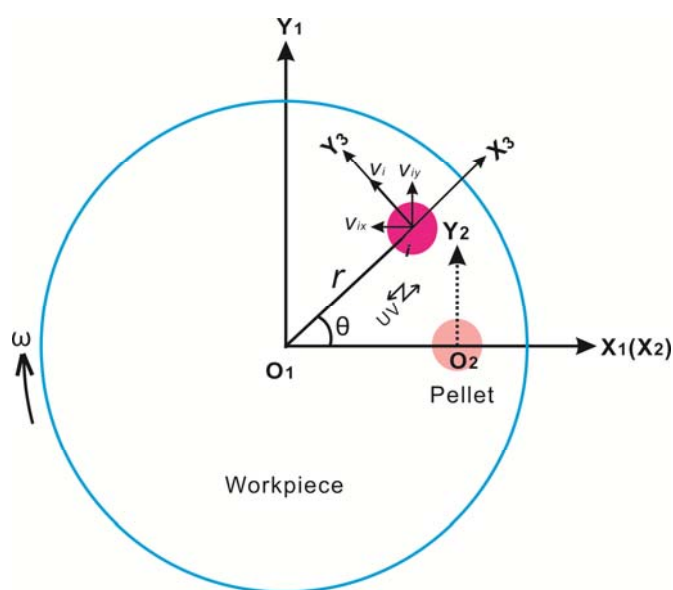
(c)

Fig. 3.1 Material removal rate versus polishing time under varied processing parameters. (a) Stroke speed, rotation rate=600rpm, load=4N, (b) rotational

rate, stroke speed=6mm/s, load=4N (c) downward load on material removal rate, stroke speed=6mm/s, rotation rate=600rpm, in “without UV” & “with UV” polishing. Each datum stands for the average of four measurements.

Table 3.1 Normalized Preston coefficients for different conditions (average of 6 measurements). UV specs: frequency=15.3kHz, $V_{p-p} = 150V$, phase difference =135°.

Processing parameters		Without UV	With UV	Percentage of Increase
Stroke	3	0.02343	0.04943	111%
speed(mm/s)	6	0.03196	0.05664	77%
	9	0.02454	0.05268	115%
Rotational rate(rpm)	400	0.02175	0.07517	246%
	600	0.03196	0.05664	77%
	800	0.01846	0.04355	136%
	Downward load(N)	4	0.0318	0.0671
	8	0.0100	0.0269	169%
	12	0.0048	0.0087	81%



(a)

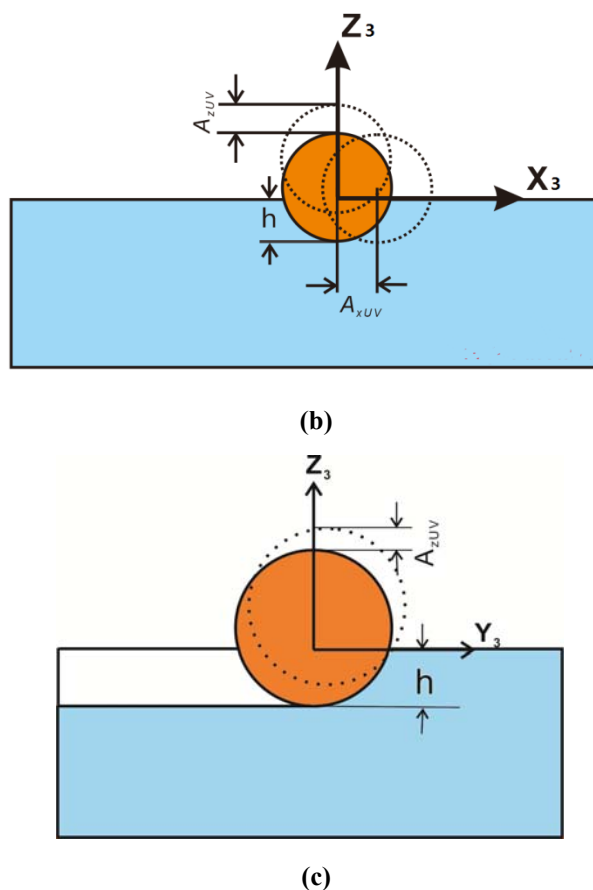


Fig. 3.2 The model for material removal in fixed abrasive polishing. (a) Top-view (not to scale) of the motion of pellet relative glass; (b) sectional view of an abrasive indenting into glass surface in $X_3O_3Z_3$ plane; (c) cross-sectional view in $Y_3O_3Z_3$. The abrasive is selected to be sphere in the model. The model works well in terms of material removal no matter the abrasive is sphere, conical, three-/four-sided pyramid or truncated conical or pyramid (not to scale).

To elucidate the potential reason why vibration can make material removal increased, the sliding distance of an abrasive was mathematically computed (Fig. 3.2). The material removal (δ_i) by a single abrasive (i) after time T is

$$\delta_i = \int A_i(t) \cdot ds_i = \int A_i(t) s_i(t) dt \quad (14)$$

where A_i is sectional area of the abrasive i penetrating into the glass and determined

by the shape and size of the abrasive and the load imposed on the abrasive and s_i is the sliding distance of the abrasive i . In our experiments, the stroke length and the velocity in X-direction are ignorably trivial compared to the distance of polishing tool away from the center of circular workpiece (r) and rotation of workpiece (ω), respectively. (The average radial velocity of pellet due to vibration is estimated $1\mu\text{m}\times 15.3\text{kHz}=15.3\text{mm/s}$, whilst the tangent velocity owing to the relative motion between workpiece and pellet is 1256mm/s .) Thus the material removal δ can be expressed as follows:

$$\delta = \int N(t)\delta_i(t)dt = \int A_i(t)N(t)s_i(t)dt \quad (15a)$$

Supposing that abrasives are identical and $N(t)$ is constant over the polishing time, Eq.(15a) can be transformed into

$$\delta = N\delta_i = N \int A_i(t)N(t)s_i(t)dt \quad (15b)$$

and the material removal is dictated by δ_i .

a) Conventional polishing

For the polishing without ultrasonic vibration, the cross-sectional area A_i is assumed to be unchanged in the entire polishing process and the position of the abrasive i relative to workpiece is written as

$$x_{i1} = r \cos(\omega t) \quad (16a)$$

$$y_{i1} = r \sin(\omega t) \quad (16b)$$

$$z_{i1} = 0 \quad (16c)$$

$$s_i = \int ds_i = \int \sqrt{(dx_{i1})^2 + (dy_{i1})^2 + (dz_{i1})^2} dt = \int r\omega dt \quad (17a)$$

$$A_i = \text{const.} \quad (17b)$$

The material removal by a single abrasive i in non-UV process at the interval T is derived, presupposing the depth at which the abrasive indents into the workpiece

is denoted by h_0 :

$$\delta_i = \int A_i ds_i = A_i \int r \omega dt = A_i r \omega t \quad (18a)$$

$$A_i \propto h_0 \quad (18b)$$

b) Ultrasonic polishing

In contrast with conventional polishing, vibration-assisted polishing possesses additional vibration velocity other than v_i . The pellet vibrates elliptically in the plane normal to X-Y plane (i.e. X-Z plane) and the projection of the trajectory of ellipse onto the X-Y plane is actually a straight line perpendicular to v_i (i.e. parallel to r) at any instant. Let the coordinate $X_3O_3Y_3$ be stationary with respect to the pellet. The motion of the abrasive i can be described with following equation derived from Eq.(11).

$$x_{i3UV} = 2c_B V \sin \frac{\varphi}{2} \sin(2\pi ft + \frac{\varphi}{2}) = A_{xUV} \sin(2\pi ft + \frac{\varphi}{2}) \quad (19a)$$

$$y_{i3UV} = 0 \quad (19b)$$

The same is applicable to the movement of the abrasive in X-Z plane but the initial phase that is prescribed by input exciting signals. Hence the Z location of the abrasive is

$$z_{i3UV} = 2c_L V \cos \frac{\varphi}{2} \cos(2\pi ft + \frac{\varphi}{2}) = A_{zUV} \cos(2\pi ft + \frac{\varphi}{2}) \quad (19c)$$

The locus of the abrasive at an instant t is acquired by virtue of geometric transformation (Eq. (20)).

$$\begin{bmatrix} x_{iUV} \\ y_{iUV} \\ z_{iUV} \\ 1 \end{bmatrix} = \begin{bmatrix} \cos \theta & -\sin \theta & 0 & 0 \\ \sin \theta & \cos \theta & 0 & 0 \\ 0 & 0 & 1 & 0 \\ 0 & 0 & 0 & 1 \end{bmatrix} \cdot \begin{bmatrix} 1 & 0 & 0 & r \\ 0 & 1 & 0 & 0 \\ 0 & 0 & 1 & 0 \\ 0 & 0 & 0 & 1 \end{bmatrix} \cdot \begin{bmatrix} x_{i3UV} \\ y_{i3UV} \\ z_{i3UV} \\ 1 \end{bmatrix} = \begin{bmatrix} x_{i3UV} \cos \theta - y_{i3UV} \sin \theta + r \cos \theta \\ x_{i3UV} \sin \theta + y_{i3UV} \cos \theta + r \sin \theta \\ z_{i3UV} \\ 1 \end{bmatrix}$$

(20)

Substituting (19a), (19b)& (19c) and $\theta = \omega t$ into (20), the coordinates of the abrasive i in the $X_1O_1Y_1$ take the form:

$$x_{iUV} = [A_{xUV} \sin(2\pi ft + \frac{\varphi}{2}) + r] \cos(\omega t) \quad (21a)$$

$$y_{iUV} = [A_{xUV} \sin(2\pi ft + \frac{\varphi}{2}) + r] \sin(\omega t) \quad (21b)$$

$$z_{iUV} = A_{zUV} \cos(2\pi ft + \frac{\varphi}{2}) \quad (21c)$$

then

$$dx_{iUV} = 2\pi f A_{xUV} \cos(\omega t) \cos(2\pi ft + \frac{\varphi}{2}) - \omega \sin(\omega t) [A_{xUV} \sin(2\pi ft + \frac{\varphi}{2}) + r] dt \quad (22a)$$

$$dy_{iUV} = 2\pi f A_{xUV} \sin(\omega t) \cos(2\pi ft + \frac{\varphi}{2}) + \omega \cos(\omega t) [A_{xUV} \sin(2\pi ft + \frac{\varphi}{2}) + r] dt \quad (22b)$$

$$dz_{iUV} = -2\pi f A_{zUV} \sin(2\pi ft + \frac{\varphi}{2}) dt \quad (22c)$$

and

$$\begin{aligned} ds_{iUV} &= \sqrt{(dx_{iUV})^2 + (dy_{iUV})^2 + (dz_{iUV})^2} dt \\ &= \sqrt{[2\pi f A_{xUV} \cos(2\pi ft + \frac{\varphi}{2})]^2 + [2\pi f A_{zUV} \sin(2\pi ft + \frac{\varphi}{2})]^2 + \omega^2 [A_{xUV} \sin(2\pi ft + \frac{\varphi}{2}) + r]^2} dt \end{aligned} \quad (22d)$$

$$\delta_{iUV} = \int A_{iUV}(t) ds_{iUV} = \int A_{iUV}(t) \sqrt{(dx_{iUV})^2 + (dy_{iUV})^2 + (dz_{iUV})^2} dt \quad (23)$$

Supposing that the initial indentation depth without ultrasonic vibration is h_0 and that

$h_0 - A_{zUV} > 0$ & $h_0 + A_{zUV} < \frac{d_g}{2}$ (the abrasive keeps contact with substrate throughout

the entire polishing process), it follows

$$\frac{A_{iUV}(t)}{A_i} = \frac{[h(t)]^2}{h_0^2} = \frac{[h_0 - A_{zUV} \cos(2\pi ft + \frac{\varphi}{2})]^2}{h_0^2} \quad (24)$$

The Eq. (23) is rewritten as follows:

$$\delta_{iUV} = A_i \int [1 - \frac{A_{zUV}}{h_0} \cos(2\pi ft + \frac{\varphi}{2})]^2 \sqrt{(dx_{iUV})^2 + (dy_{iUV})^2 + (dz_{iUV})^2} dt \quad (25)$$

For $\varphi = 180^\circ$, using the Eq. (25) the material removal can be expressed in terms of power series, discarding the higher order of t

$$\delta_{iUV180} = A_i t \sqrt{(8\pi f V \sin \frac{\phi}{2} \cos \frac{\phi}{2})^2 (c_B^2 + c_L^2) + \omega^2 (r + 2c_B V (\sin \frac{\phi}{2})^2)^2} = A_i \omega (r + 2c_B V) t \quad (26)$$

In the case of $\phi = 135^\circ$, the integrand of Eq. (25) seems fairly simple, although the integral is so complicated that it is not an easy work to solve the equation analytically since elliptical functions are included in the integral of the Eq. (25). By replacing the values for the arguments over a wide range, it is found that ds_{iUV} is negligibly different from ds_i (Fig. 3.3). For instance, the s_{iUV} is 6810.31m ($\phi = 0^\circ$), 6805.88m ($\phi = 60^\circ$), 6801.42m ($\phi = 90^\circ$), 6794.98m ($\phi = 135^\circ$), 6792.34m ($\phi = 180^\circ$), respectively, but only 0.36%, 0.30%, 0.23%, 0.13%, 0.096% increase compared to “without UV” process, justifying the replacement of the sliding distance s_{iUV} in ultrasonic vibration with s_i . This way, the Eq.(22d) is reasonably reduced to $ds_i = r\omega dt$ even if the machining process is implemented with vibration for the convenience of calculation in some cases. The Eq. (25) can be written

$$\begin{aligned} \delta_{iUV} &= \int A_{iUV}(t) ds_{iUV} = \int A_{iUV}(t) ds_i \\ &= A_i \sqrt{(8\pi f V \sin \frac{\phi}{2} \cos \frac{\phi}{2})^2 (c_B^2 + c_L^2) + \omega^2 (r + 2c_B V (\sin \frac{\phi}{2})^2)^2} \int [1 - \frac{2c_L V \cos \frac{\phi}{2}}{h_0} \cos(2\pi f t + \frac{\phi}{2})]^2 dt \end{aligned} \quad (27)$$

Using the formulae (18),(26),(27), normalized material removal was computed in the cases of four machining processes, i.e. with UV($\phi = 0^\circ$, $\phi = 135^\circ$, $\phi = 180^\circ$) in addition to without UV. Based on the Eq. (18) & (26), the material removal for $\phi = 180^\circ$ is very close to that without UV in that vibration amplitude is extremely tiny as compared to r . As $\phi = 0^\circ$ and $\phi = 135^\circ$, the material removal is time-dependent. Both modes will induced increased material removal, though theoretically speaking, the increase for $\phi = 0^\circ$ is greater than $\phi = 135^\circ$ in that the amplitude of vibration in

vertical direction is slightly greater for $\varphi = 0^\circ$ than $\varphi = 135^\circ$ as measured in our experiments (Table 2.2). The function of input voltage is also modeled. It is easily identified from Fig. 3.4(b) that augmenting the input voltage and therefore the vibration amplitude will make the material removal rise by 2.5%, 10% and 22% for the input voltage 50V, 100V, and 150V, respectively (the first term in Eq.(27) is taken to be a constant).

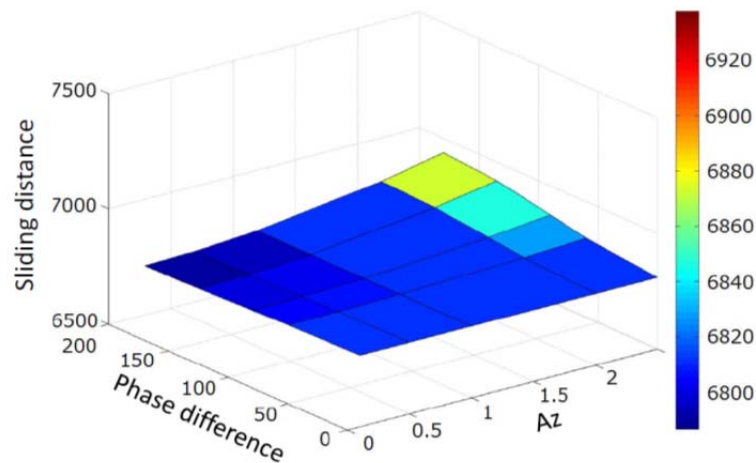
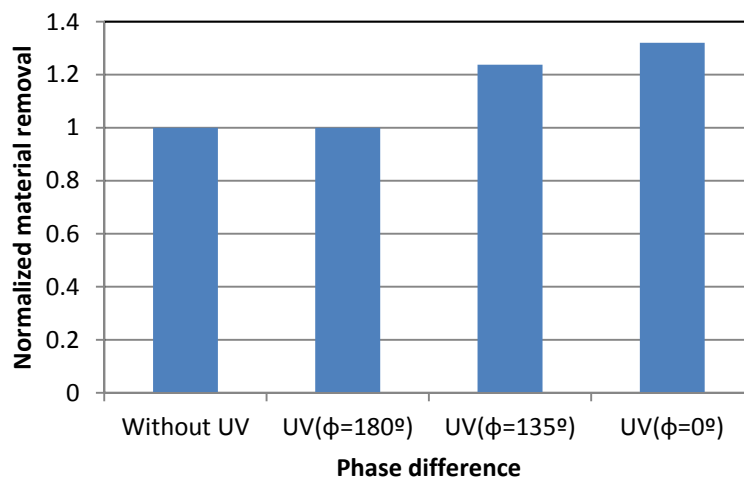
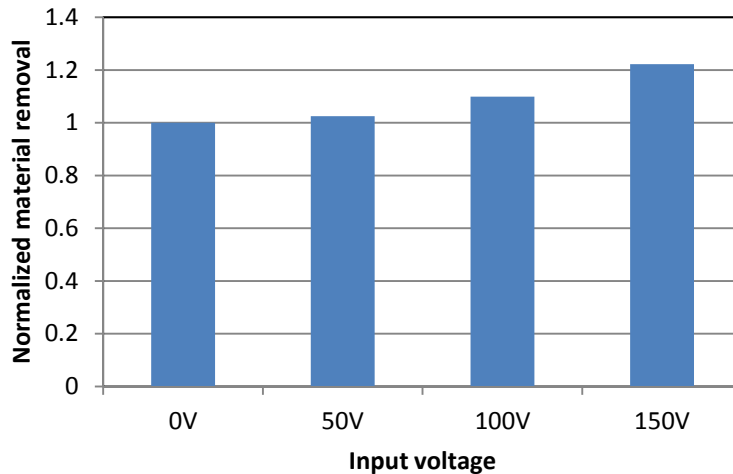


Fig. 3.3 The sliding distance for different vibrations, including those used in our experiments



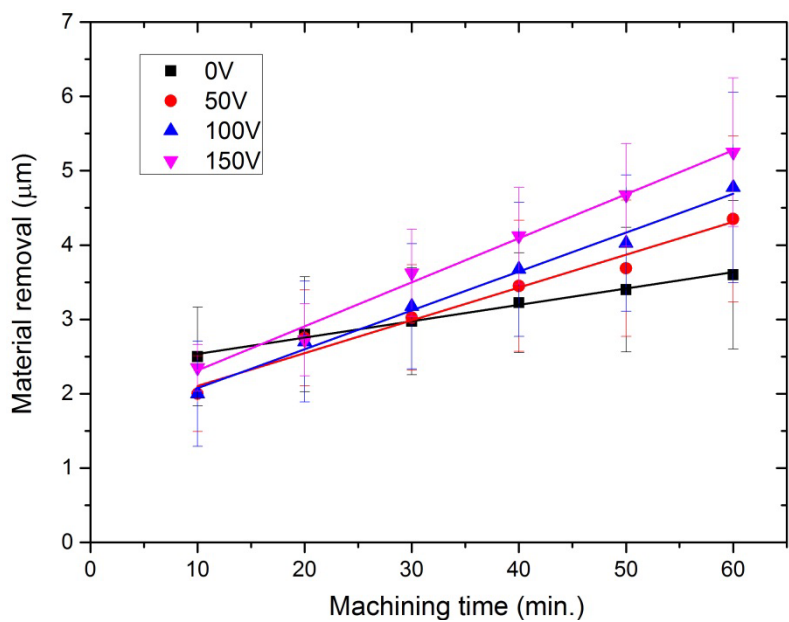
(a)



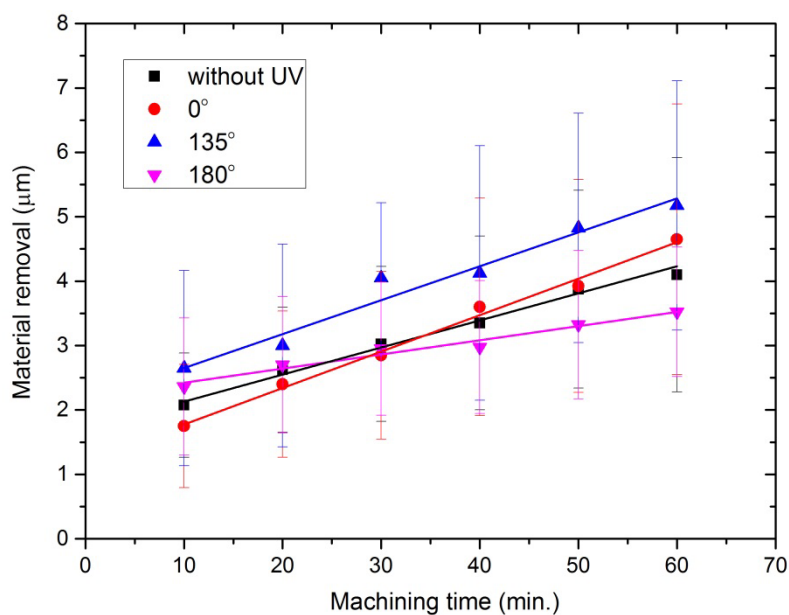
(b)

Fig. 3.4 Simulated normalized material removal for varied (a) phase difference (input voltage=150V) and (b) input voltages ($\varphi=135^\circ$). The ratio of amplitude in vertical direction to h_0 is 2/3 when $\varphi=135^\circ$ in our model.

The results on UV specifications illustrate that the MRR is the greatest when the vibration motion is elliptical (phase difference= 135°) and increases with the applied voltages under experimented conditions (Fig. 3.5). The excellent performance of elliptic vibration is attributed to the dispelling of polishing chips at the interface of abrasive and workpiece. Increasing the applied voltage and resultant vibration amplitude will also enhance the dispelling of chips. The chips are comprised of ceria and silica and the silica will be harmful to the reactions between ceria abrasives and glass workpiece.



(a)



(b)

Fig. 3.5 The material removal vs. (a) varied input voltages and (b) phase differences. The greater the input voltage is, the greater the material removal is. The greatest material removal is found under the conditions of elliptical vibration. The reason is reckoned to be due presumably to exceptional ability of elliptic vibration to dispel polishing chips that hampers the chemical actions between abrasives and glass. The error bars stand for standard deviation.

3.2 Surface morphology

The surface topography was modeled and simulated using a method that was modified based on the technique developed by other researchers. Since the surface morphology is viewed as the resultant interaction of pellet and glass, the morphology of pellet predominates final glass surface and thus regenerating the pellet surface is paramount. The abrasives in the matrix of pellet are assumed to be with the size of normal distribution (Eq. 28) (a_{ij} , the coordinates of abrasives in local coordination system of pellet).

$$p(d_g) = \frac{C_1}{\sigma_g \sqrt{2\pi}} \exp\left[-\frac{1}{8} \left(\frac{d_g - \bar{d}_g}{\sigma_g}\right)^2\right] \quad (28a)$$

C_1 is a rule-of-thumb constant, σ_g is the standard deviation of grain size expressed as the following,

$$\sigma_g = \frac{d_{g \max} - d_{g \min}}{6} \quad (28b)$$

The glass morphology is formed by the scratching of abrasives against glass surface. Supposing that the glass surface is flat at first ($g_{mn} = 0$, the coordinates of glass surface), the surface of glass will be scratched by the abrasives (a_{ij}) that protrude beyond a distance that is determined by the most protruded abrasive (a_{\max}) on the pellet along with the indentation depth (h) of that abrasive (Fig. 3.6). All the abrasives that stick out heights which exceed the difference ($a_{\max} - h$) of maximum protrusion subtracted by the indentation depth will participate in material removal, that is, the abrasives satisfying the equation ($a_{ij} > a_{\max} - h$) will remove material. After the first row of abrasives remove the material, the g_{ij} will be updated. Then abrasives in the following row (a_{ij+1}) will alter the surface of glass left by the

preceding abrasives except those the protrusion of which is less than precursor (a_{ij}) and the morphology will be represented by $\min(g_{ij}, g_{i+1j})$. In the case where vibration was applied to pellet, the abrasives will vibrate in line with the vibrator and therefore the trajectories will be imposed by additional motion. The surface morphology, as a result, will be a synergic effect of vibration and sliding. Using the similar procedure to that without vibration, the glass surface morphology can be modeled.

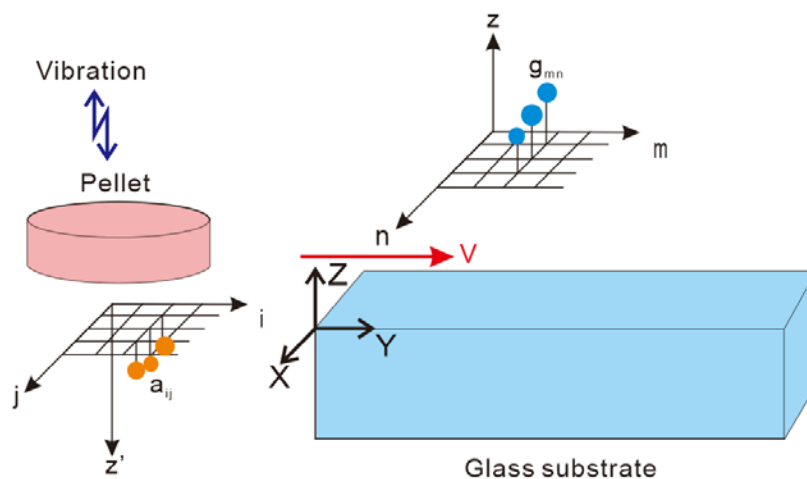
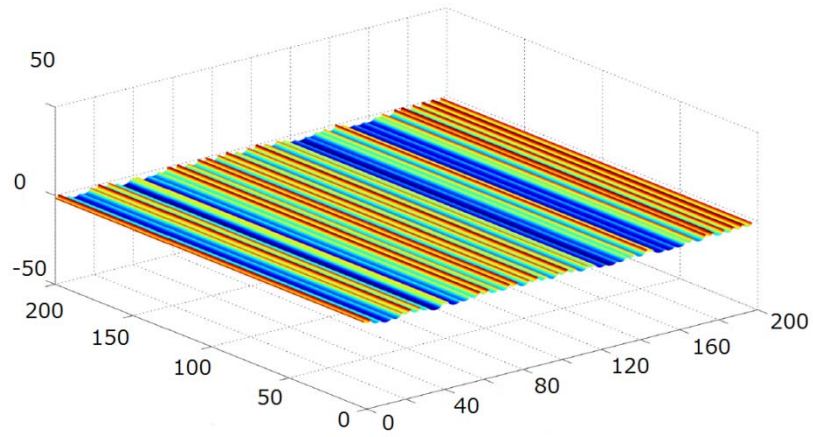
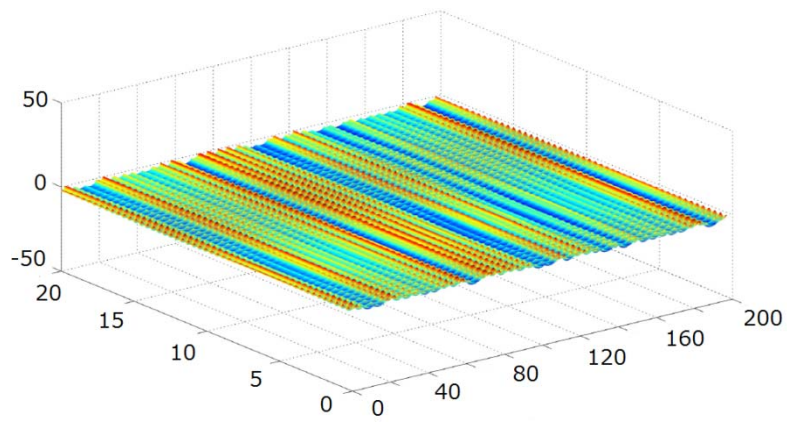


Fig. 3.6 The morphology and trajectory of pellet is mapped to glass surface

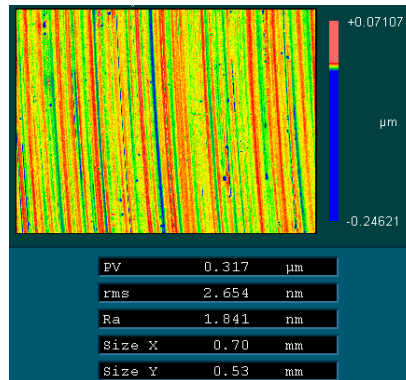
Then the surface morphology of glass with and without vibration is modeled and tested (Fig. 3.7). It is clearly from both the simulated and experimented results that on the machined surface periodic structure is formed in the presence of vibration, in which case the spatial period is regulated by the frequency of vibration and the relative velocity between glass and pellet. However, only tiny scratches are found on the surface in the process without vibration. The periodic structure on the vibration polished surface with spatial period consistent with the frequency of vibration implies that the structure was induced by vibration indeed. The structure might aggravate surface roughness on certain occasions.



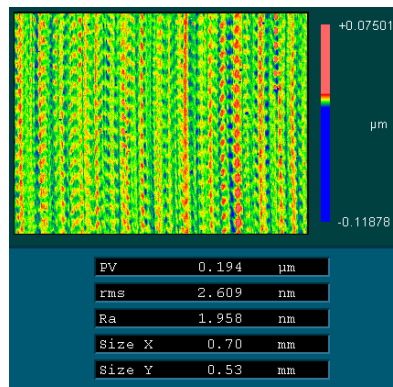
(a)



(b)



(c)



(d)



(e)



(f)

Fig. 3.7 Surface morphologies (a) simulated surface morphology “without UV”; (b) simulated surface morphology “with UV”; (c) experimented surface morphology “without UV”; (d) experimented surface morphology “with UV”; (e) the surface after polished without vibration, free of cracks; (f) the surface after polished with vibration, free of cracks. The surface contains no cracks after being polished with and without vibration if no any further post-processing was applied. From the (c)&(d), some scratches or periodic textures are present in polished surface, the depth of which are on the order of several hundred nanometers. The results support the material is removed in

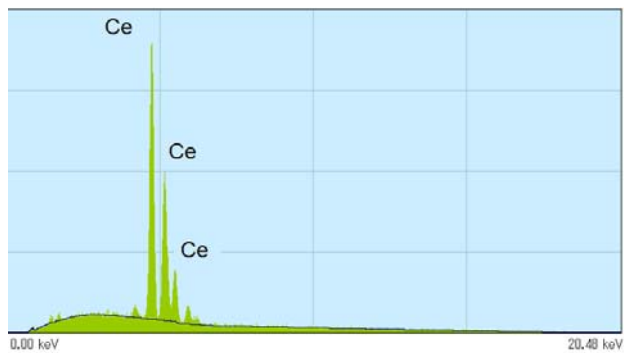
plastic regime.

3.3 Chemistry in polishing process

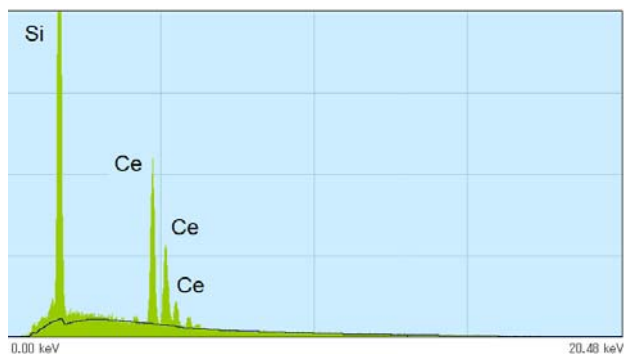
In order to find out the likely mechanism in dry polishing process, essential chemical analysis was made, EDX, FTIR and XRD included. Comparing EDX chemical analysis of polishing pellets and chips, it can be recognized without much difficulty that Si element has been transferred to chips (Fig. 3.8). Moreover, the XRD and FT-IR spectra evidence that in the chips are crystal CeO_2 and amorphous glass (Fig. 3.9 & 3.10). The FWHM of peaks in the chips has broadened, signaling that crystallite has shrunk. From the Scherrer formula (Eq. 29, D_{hkl} is mean crystallite size, λ is the wavelength of X-ray, B_{hkl} is the full-width at half maximum of diffraction peaks, hkl is the Miller indices, θ is the Bragg angle, K is closely approximate to 0.89), the grain size in the pellet is estimated to be 731.5\AA while it decreases to 142.0\AA , indicating a considerable distortion of lattices that originates from the Ce-O-Si bonding. The FI-IR spectra corroborate the inference, by which it is demonstrated that the Si-O @1099/cm has red-shifted to 1085/cm resulting from the Si-O-Ce bond.

$$D_{hkl} = \frac{K\lambda}{B_{hkl} \cos\theta} \quad (29)$$

On the basis of the above chemical testing, the material removal process is reckoned as follows (Fig. 3.13): firstly, the ceria bonds with silica in solid-state phase under the circumstances of exceedingly high pressure to form new substances with lower hardness than glass bulk and ceria on the topmost of fused silica and then the resultant softer substances are removed by ceria abrasive mechanically and plastically; alternatively, the Ce in ceria abrasives bonds with Si in glass due to extreme pressure, next silica material is torn away from glass as a lump on account of strong shear force and greater strength of Ce-O bond than Si-O bond and lastly the lump is disengaged and this way the glass material is removed. Our experiments appear to corroborate the latter mechanism.



(a)



(b)

Fig. 3.8 EDX spectra of (a) pellets and (b) chips. Si element can hardly be identified in the pellets; in contrast, abundant Si was contained in the chips.

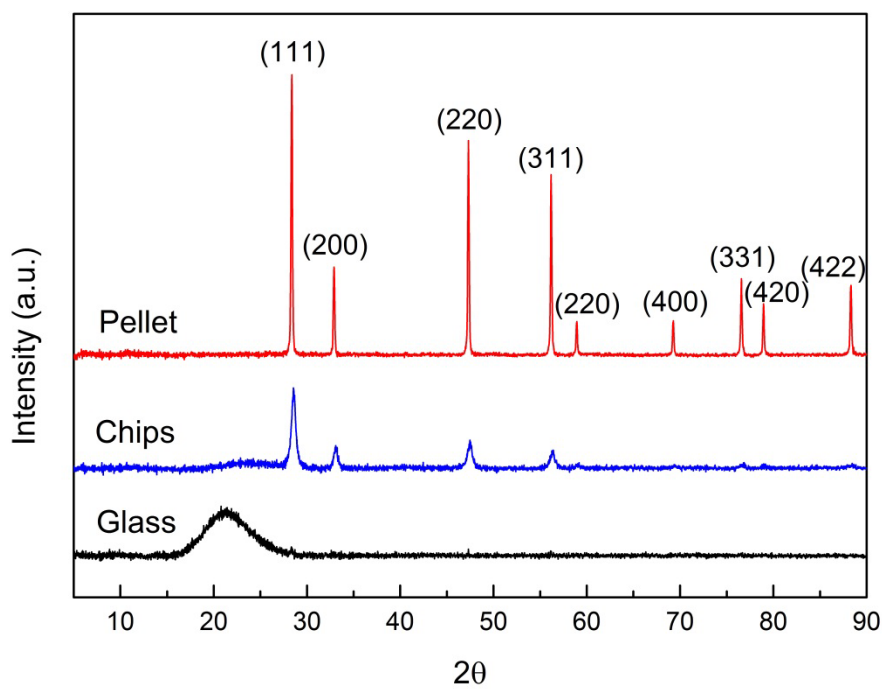


Fig. 3.9 XRD analysis of fused silica powder, pellets and chips. Slight bump

appears in the spectrum of chips and peaks corresponding to Ceria can also be found in chips spectrum.

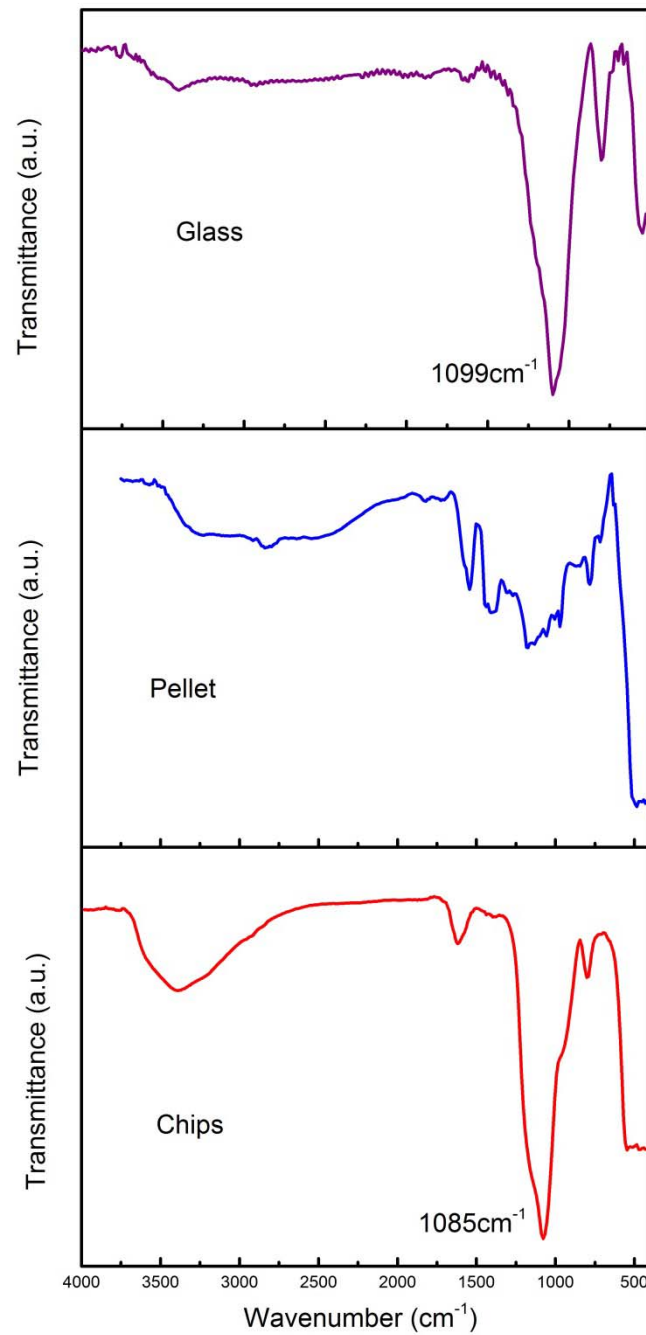


Fig. 3.10 FT-IR results of fused silica powder, pellets and chips. The redshift of $1099/\text{cm}(\text{Si-O})$ to $1085/\text{cm}$ indicates the potential formation of Si-O-Ce .

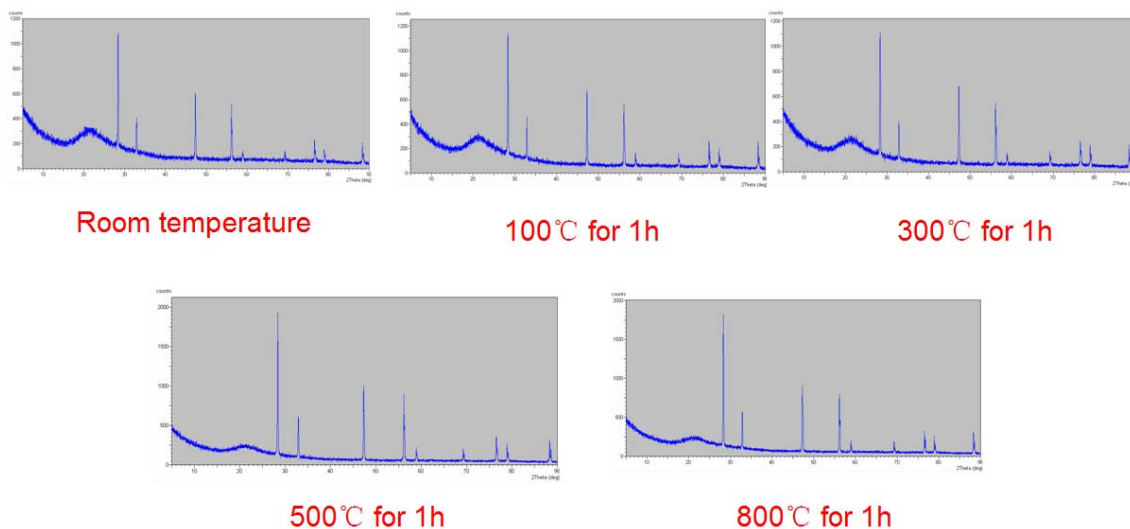


Fig. 3.11 XRD spectra of ceria-glass mixture at varied temperatures

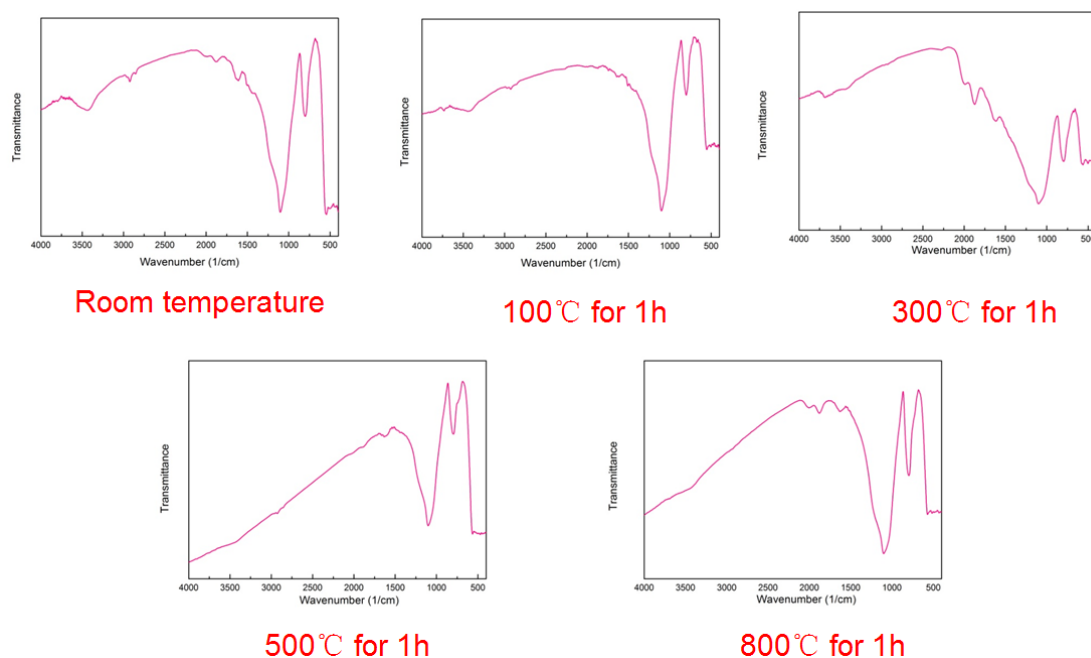


Fig. 3.12 FT-IR of ceria-glass mixture at varied temperatures: in all the plots

are the peaks located at 1100cm^{-1} and 820cm^{-1}

Comparing EDX chemical analysis of polishing pellets and debris, we can recognize without much difficulty that Si element has been transferred to debris (Fig. 3.8). The material removal process is reckoned as follows: firstly, the ceria reacts with silica in solid-state phase under the circumstances of exceedingly high pressure to form new substances with lower hardness than glass bulk and ceria on the topmost of fused silica and then the resultant softer substances are removed by ceria abrasive mechanically and plastically; alternatively, the ceria abrasives remove glass material

just like the SiC, alumina and diamond. The XRD and FT-IR of fused silica, pellets and debris has been performed in order to elucidate the potential mechanism (Fig. 3.9). The lump in the XRD spectrum of debris indicates some amorphous matter appears in the debris. However, is the amorphous matter glass itself or some new materials? We further assayed the debris and pellet together with glass by virtue of FT-IR (Fig. 3.10). The FT-IR results imply that the matter in the debris is glass not new materials (~1099/cm: Si-O; ~1085/cm: stretched vibration of Si-O bond). The heating of ceria and glass powder mixture show no evidence for new crystalline or amorphous materials (Fig. 3.11 & 3.12). Now we may come to some conclusions to the mechanism of fused silica CMG: the probable removal mechanism is the same as that in grinding and the ceria is not necessarily softer than fused silica glass as well as that no new substances are generated during CMG of fused silica. “The results clearly showed the difference in reaction mechanism between CMG process and static heating in air.” The authors postulate that the mechanism of CMG of silicon is not fully understood (note: please refer to the citation). In my opinion, the amorphous phase in the debris of Si CMG is due either to some new amorphous substances which are produced during CMG or to amorphous silicon that is generated because of extreme pressure in CMG process. Plenty of evidences show that crystalline Si can be converted to amorphous state under such great pressure as the indentation process with a sharp diamond indenter.

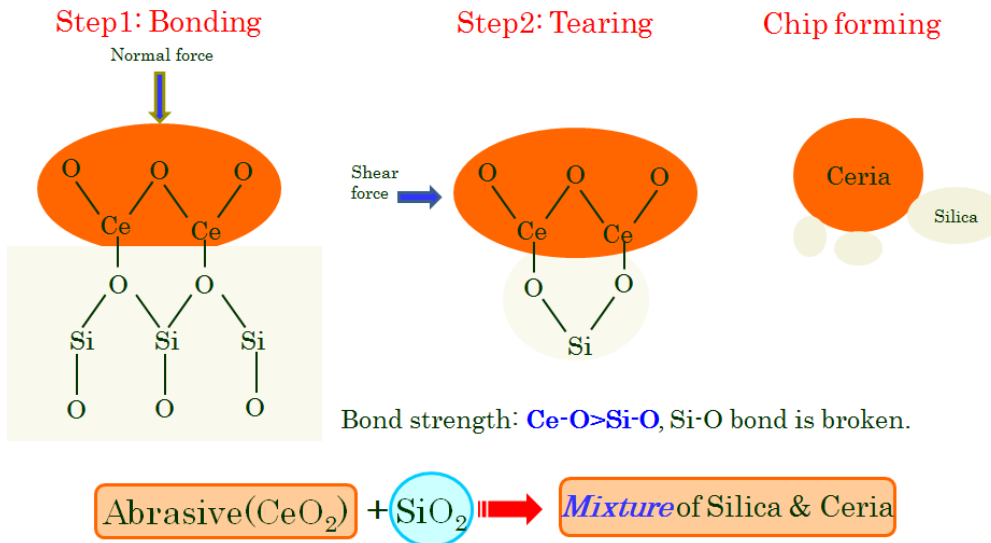


Fig. 3.13 The possible mechanism in dry polishing of glass with ceria.

3.4 Machining force in polishing process

The forces and coefficient of friction (CoF) is important in machining processes, which significantly influence the material removal and wear of tools. The forces, namely tangential force and normal force, was in-situ registered with an octagonal ring force sensor. The coefficient of friction (CoF), defined as the ratio of tangential force to normal force, is plotted as follow. It is found that the CoF decreases with machining time in both cases with and without ultrasonic vibration, which is ascribed to the reduced surface roughness with machining time. The CoF in ultrasonic polishing basically exceeds that without vibration.

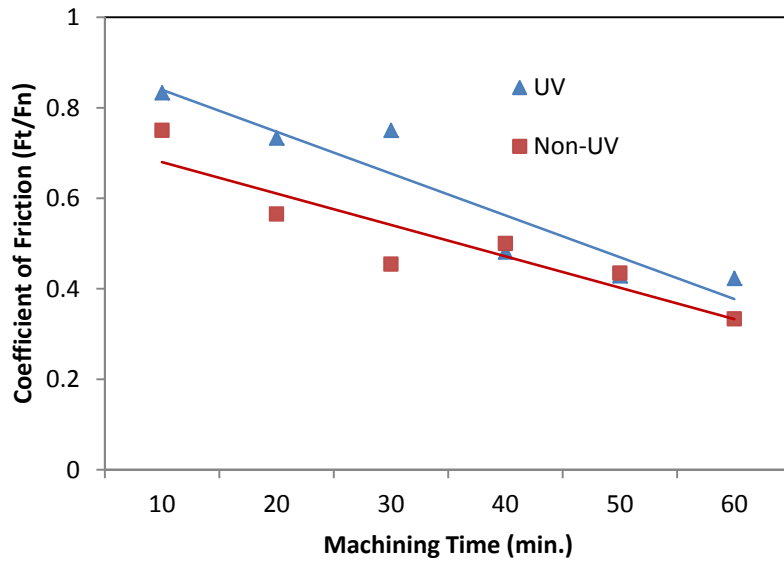


Fig. 3.14 Coefficient of friction with time for Non-UV & UV process.

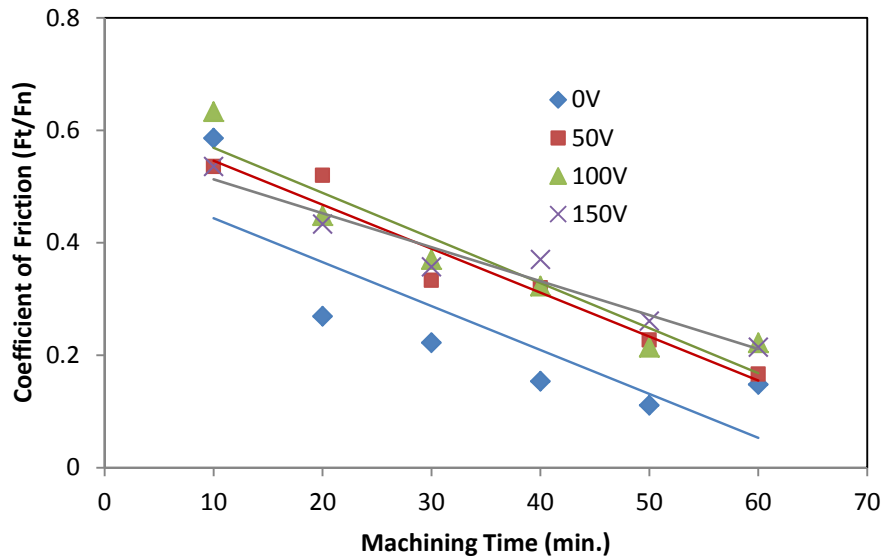


Fig. 3.15 Coefficient of friction with time for different input voltage in UV process.

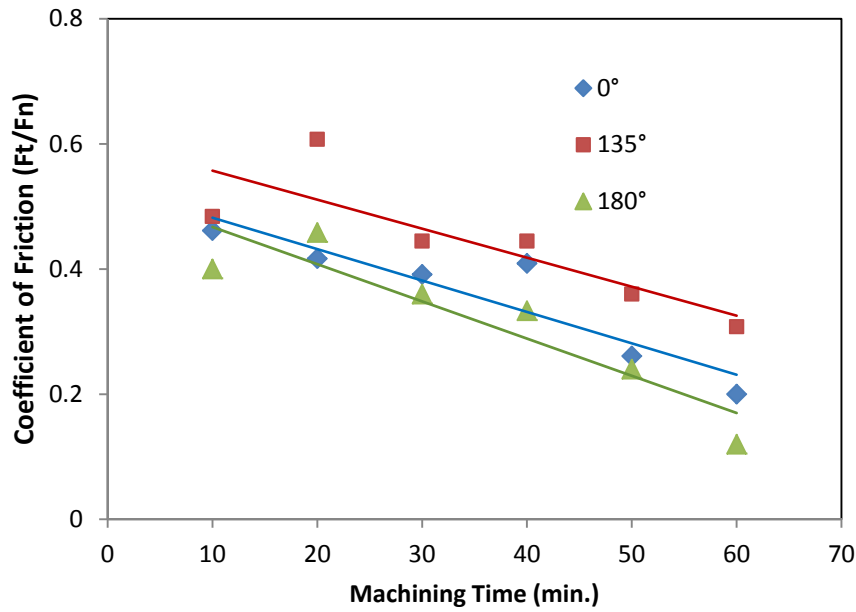


Fig. 3.16 Coefficient of friction with time for different phase difference in UV process.

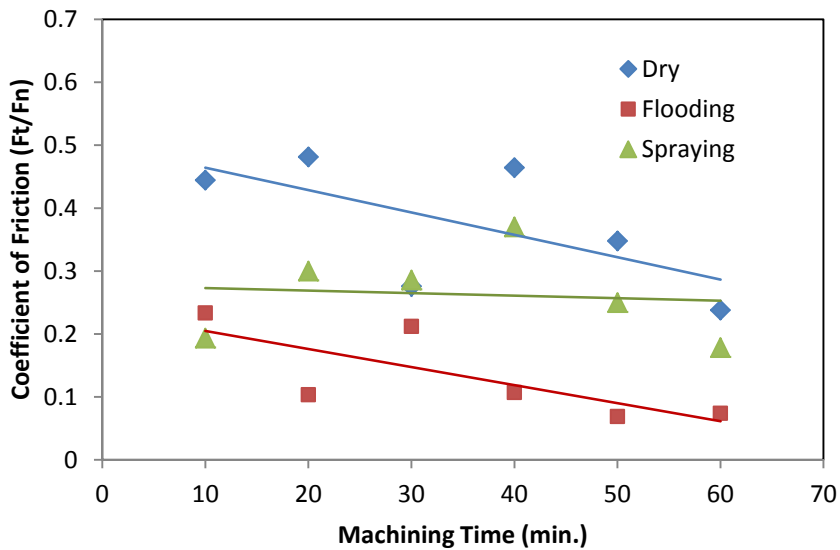
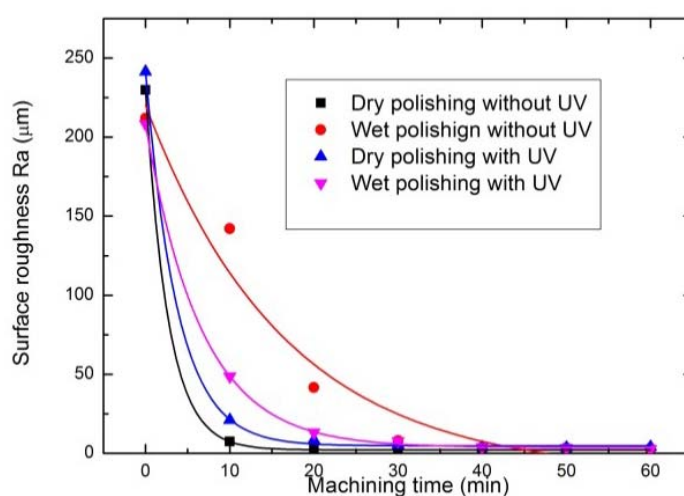


Fig. 3.17 Coefficient of friction in different polishing environments in Non-UV process.

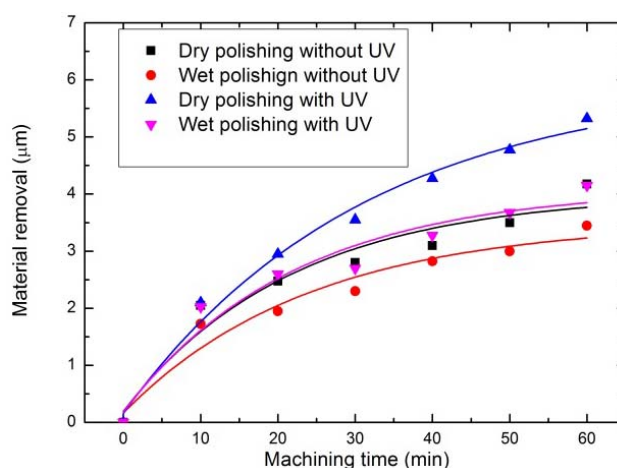
Overall, the CoF of UV polishing is far greater than Non-UV process. Recalling the material removal rate is in the same trend, we might associate the material removal rate with CoF.

3.5 Other factors affecting machining process in fixed polishing

As we all know, water is indispensable in conventional loose polishing process in that water will react chemically with polishing materials and glass to form a layer of sol-gel that is much softer than bulk glass and can be smoothed with polishing lap easily. The loose abrasive polishing can give rise to perfect surface of surface roughness $<0.5\text{nm(RMS)}$ and free of cracks and scratches in well-controlled environment. Therefore, we also examined the water as well ethanol in fixed-abrasive polishing.



(a) Material removal

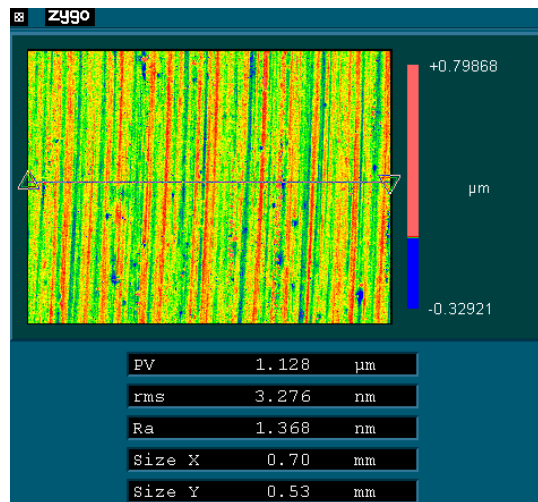


(b) Micro-surface roughness

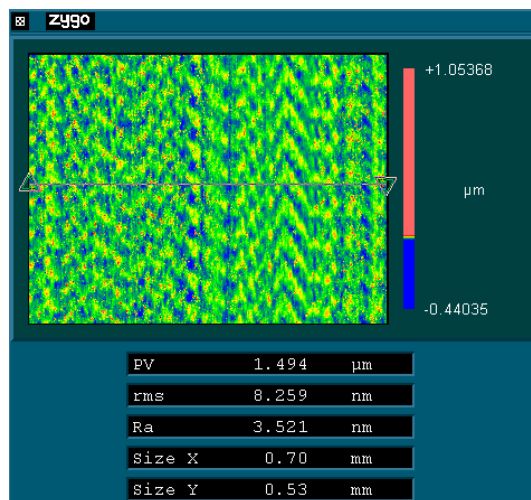
Fig. 3.18 Water function in fixed abrasive polishing

Carefully checking the above plots, we can find that using liquid can generate better final surface than dry polishing, viz. lower surface roughness. However, it

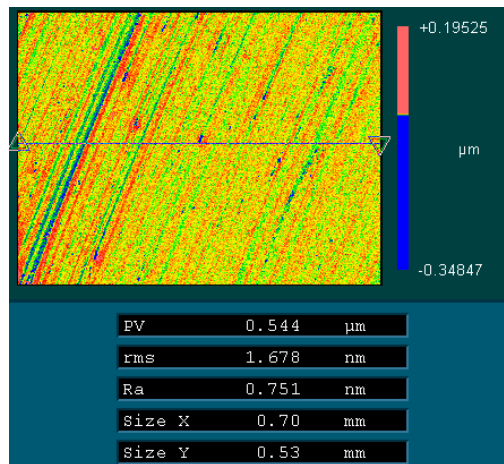
seems that the better surface is achieved at the price of material removal. The same inference applies to vibration. Applying vibration can increase material removal whereas deteriorates surface roughness. It might be paradoxical to obtain impressive material removal and surface roughness at the same time.



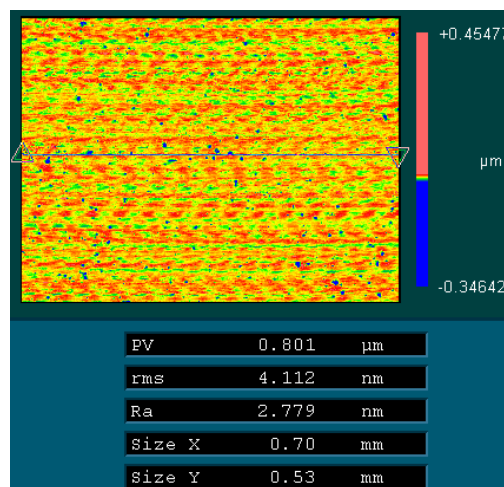
Ra=1.37nm dry grinding CM10000BP without UV



Ra=3.52nm, dry CM10000BP with UV



Ra=0.75nm wet grinding CM10000BP without UV



Ra=2.78nm wet CM10000BP with UV

Fig. 3.19 Surface topography for different processes

Note that the water volume per unit time in the above experiment is quite sufficient, i.e. flooding in the experiments. We also qualitatively evaluated the water volume effect on the material removal in polishing process. It is very surprising that material removal was maximized when we sprayed water onto workpiece surface and on the contrary further increasing water volume decreased material removal instead of increasing material removal.

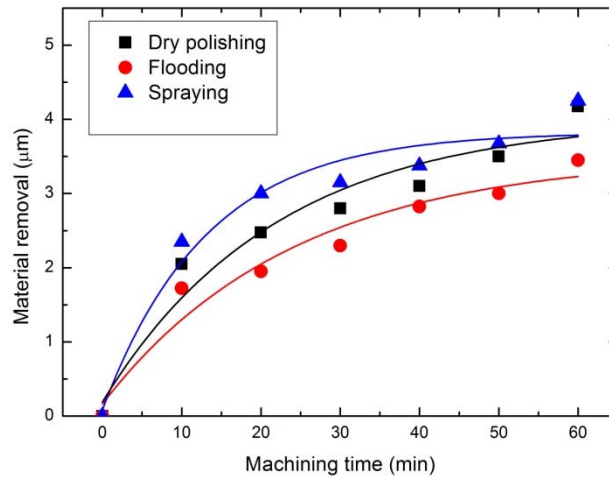


Fig. 3.20 The effect of water volume on polishing process

There are two types of pellets on hand to polish glass. The remarkable difference lies in whether pores are included in pellets. We simply compared pore function in polishing process. The preliminary results show that pore-containing pellets are superior to the other in material removal and surface roughness as no aqueous additives were used. Pellet without pores can hardly polish out glass under dry conditions. But pellets without pores excel over the other at surface roughness at the meantime not make material removal shrink significantly.

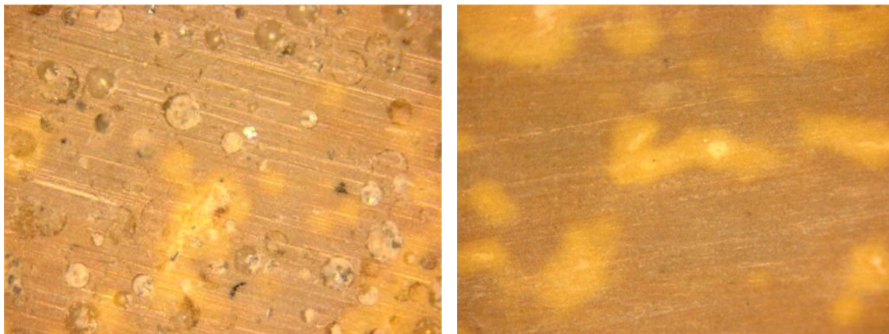
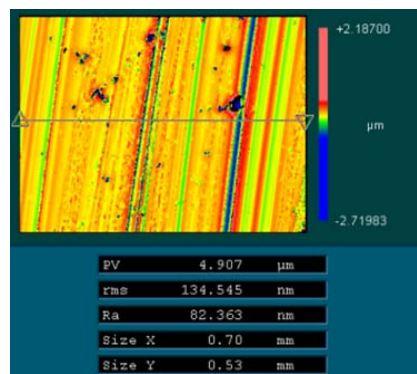
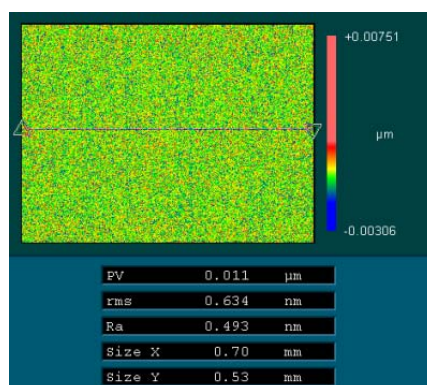
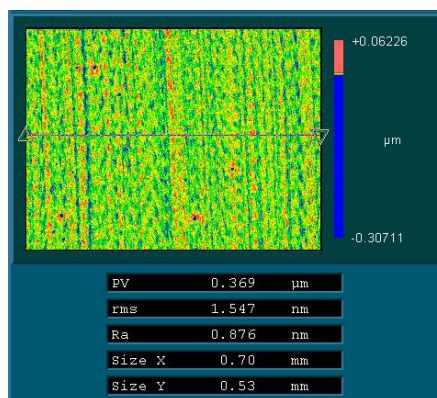


Fig. 3.21 Pellets containing pores and free of pores



Ra=82.4nm CM1000B without water

**Perfect stochastic surface machined by CM1000B+water (Ra=0.493nm,
RMS=0.634nm)**



Surface machined by CM1000B+water+UV

Fig. 3.22 Water makes a marked difference for polishing process as the pellets free of pores were used. Slightly periodic structure on UV machined surface. Actual spatial period 66microns, agreeing with UV frequency.

Besides the water, we also inspected the polishing fluid (alkaline solution pH=10.37) as well as organic liquid (ethanol) so that the mechanism was explored. Surface roughness cannot be lowered as there was not any liquid whilst surface can be as low as several nanometers once liquid was applied. Now that it is impossible for ethanol to react chemically with glass, chemical effect of liquid, in my view, is not so critical as in conventional loose abrasive polishing. Water/pH fluid: cooling the interface between glass and surface, engendering likely chemical reactions with glass, removing debris during polishing. Ethanol: cooling the interface between glass and

surface, removing debris during polishing. The pellet (CM10000B) can yield smooth surface when water, alkaline fluid and ethanol was used as polishing fluid. Nonetheless, the fused silica cannot be polished properly without any fluids for CM10000B. The experiments on pore-containing pellets tell that the glass can be polished even if no any fluids were implied. From the results, we also find out that aqueous fluids are able to decrease surface further and pH of liquids play a trivial part in surface roughness. It is inferred that the removal of chips is crucial to achieving smooth surface and the mechanism in fixed-abrasive polishing differs from that in conventional process. The cause for the inability of CM10000B is the debris, which hinders the polishing of glass, not the potential chemical actions of water. The pores serve as the similar effects to that of fluids to remove or accommodate the harmful debris.

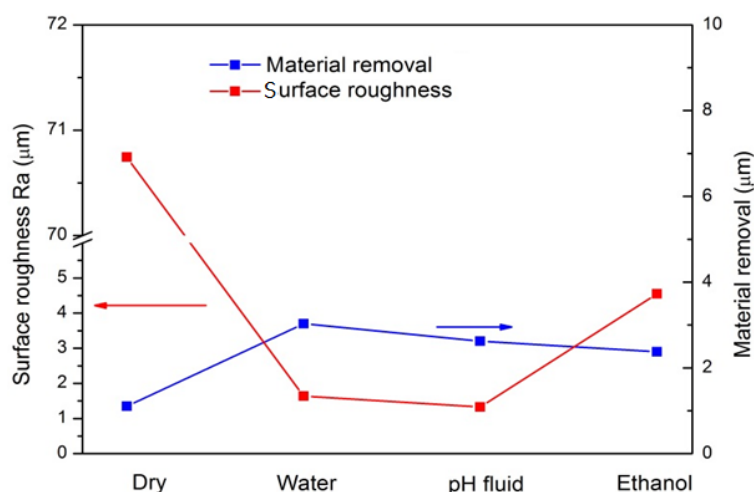


Fig. 3.23 Different liquid in polishing with pore-free pellets

To sum up, the comprehensive results are tabulated in the following table.

Table 3.2 Results for two kinds pellets

Type of Pellet	Wet or dry	Surface roughness/nm	MRR/um/h	Surface scratched (naked eye)
CM10000BP	dry	5.0	3.8	Severe
CM10000BP	water	3.7	2.8	Severe

CM10000BP	pH	3.3	2.9	Severe
CM10000B	dry	70.7	1.35	Observable
CM10000B	water	1.6	3.7	Invisible
CM10000B	pH	1.3	2.6	Invisible
CM10000B	ethanol	4.6	2.4	Invisible

3.6 Wear of pellet in fixed-abrasive polishing

In grinding where harder abrasives are made use of, wear of abrasive is an issue of much interest. The state of abrasive will contribute to material removal and much more surface roughness. Likewise, we took into account the wear of polishing tools in our polishing process. Nevertheless, the wear of tools instead of a single abrasive is considered since the abrasives are less hard, at most comparable to glass. We define “G-ratio” the ratio of the removed thickness of glass to the wear thickness of pellet. On the basis of the definition, we calculated the “G-ratio” that are greater in vibration-assisted process than in non-vibration process, indicating the UV process will somehow make the process more economical. The reason is reckoned to be due to timely dispelling of chips in UV process that may not only scratch the surface of glass but scrape the pellet surface. The “G-ratio” reflects that ability of tool to polish a glass workpiece. G-ratio less than 1 implies that the polishing tool wears actually severer than glass, unlike grinding process where G-ratio generally lies within 20~80.

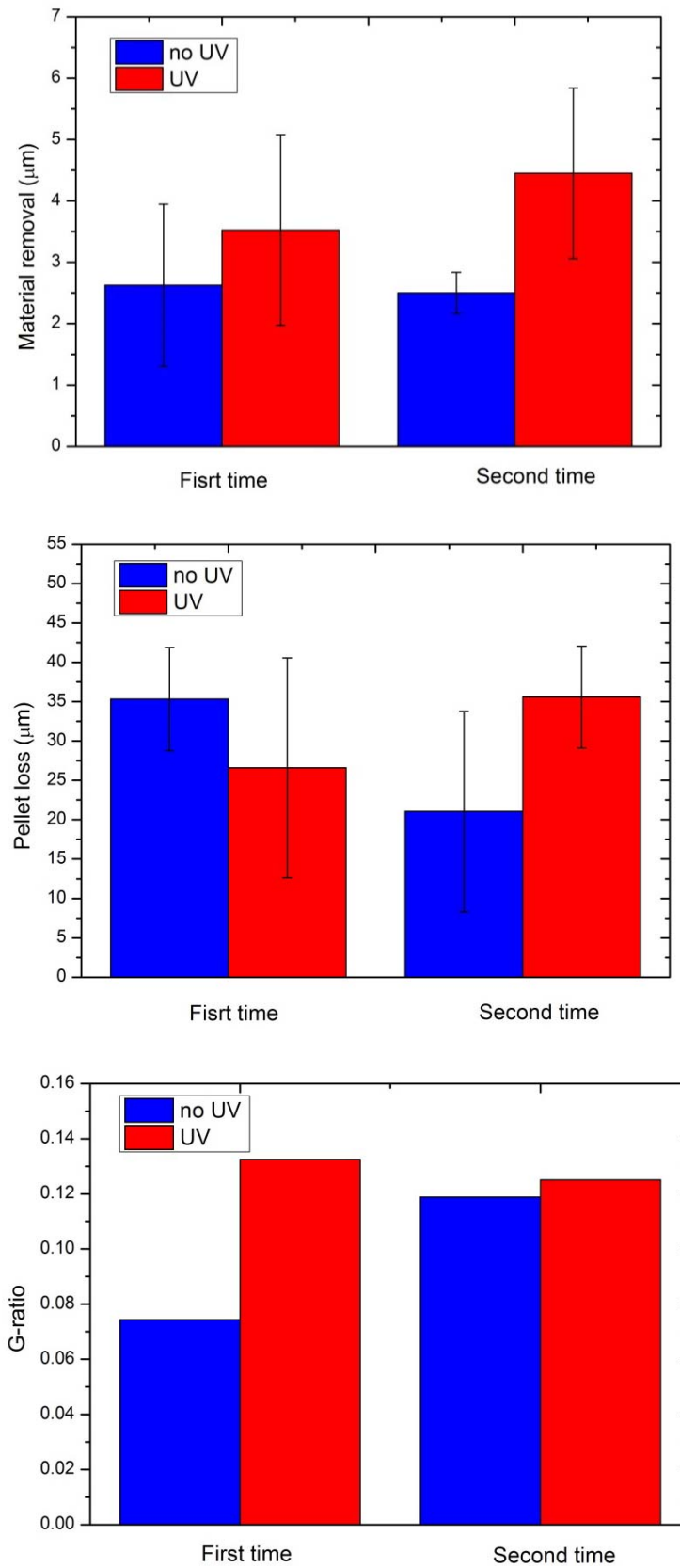


Fig. 3.24 Material removal, wear of pellet and G-ratio of UV and Non-UV processes

3.7 Summary

We applied the designed tools to fixed abrasive polishing. The results show that the material removal rate can be increased up to >50% after integrating ultrasonic vibration while surface roughness is not degraded significantly. The removing of the cracked layer left by grinding process can be expedited further by means of ultrasonic vibration assisted polishing. The reason for the efficient material removal in vibration-assisted polishing lies in that abrasive indentation volume which is significantly increased on average in vibration-assisted process. The surface morphology simulation shows that the vibration makes little difference to surface roughness, which agrees well with experiments. The surface roughness for both processes is as low as ~1nm. The relevant chemical analysis assures that the mechanism of material removal is due to the synergic effects of chemical and mechanical actions. In ultrasonic vibration assisted polishing, the great material removal rate is attributed to the exceptional ability to discharge polishing chips, which can, to a considerable extent, retard the chemical reactions between ceria in polishing pellets and silica in fused silica glass and thereby deter the machining process.

References

- [1]. Y. Li, Y. Wu, L. Zhou, M. Fujimoto, J. Wang, Q. Xu, S. Sasaki, and M. Kemmochi, "Chemo-mechanical manufacturing of fused silica by combining ultrasonic vibration with fixed-abrasive pellets," *Int. J. Prec. Eng. Manuf.* 13,2163-2172, 2012.
- [2]. T. Eusner, *Multi-Scale Scratching in Chemical-Mechanical Polishing*, PhD. Dissertation, Massachusetts Institute of Technology, 2010.
- [3]. S. K. Sinha and S. K. Biswas, "Effect of sliding speed on friction and wear of uni-directional aramid fiber-phenolic resin composite," *J. Mater. Sci.* 30, 2430-2437, 1995.
- [4]. F.W. Preston, "The theory and design of plate glass polishing machines," *J. Soc. Glass Technol.* 11, 214-256, 1927.
- [5]. N. N. Kachalov, *Technology of Grinding and Polishing Sheet Glass* (Acad. Sci., Moscow-Leningrad, U.S.S.R., 1958) (in Russian); [translated by W. Mao and Y. Yang, (China Industry Press, Peking, China, 1965), Chap. 3 (in Chinese)]
- [6]. Y. Cao, J. Guan, B. Li, X. Chen, J. Yang, C. Gan, "Modeling and simulation of grinding surface topography considering wheel vibration," *Int. J. Adv. Manuf. Technol.* 66, 937-945, 2013.
- [7]. E. J. Salisbury, K. V. Domala, K. S. Moon, M. H. Miller, J. W. Sutherland, "A three-dimensional model for the surface texture in surface grinding, part 1: surface generation model," *Trans. ASME J. Manuf. Sci. Eng.* 123, 576-581, 2001.
- [8]. X. Zhou, F. Xi, "Modeling and predicting surface roughness of the grinding process," *Int. J. Mach. Tool. Manuf.* 42, 969-977, 2002.
- [9]. P. Koshy, L. K. Ives, S. Jahanmir, "Simulation of diamond-ground surfaces," *Int. J. Mach. Tool. Manuf.* 39, 1451-1470, 1999.
- [10]. S. Malkin, C. Guo, *Grinding Technology: Theory and Application of Machining with Abrasives*, Sec. Ed., Industrial Press, 2008.

- [11]. Z. B. Hou, R. Komanduri, "On the mechanics of the grinding process – part I, stochastic nature of the grinding process," *Int. J. Mach. Tool. Manuf.* 43, 1579-1593, 2003.
- [12]. A. Guinier, *X-Ray Diffraction in Crystals, Imperfect Crystals, and Amorphous Bodies*, W. H. Freeman and Company, USA, 1963, Chap. 5.
- [13]. L.M. Cook, "Chemical process in glass polishing," *J. Non-Crystalline Solids* 120, 152-171, 1990.

CHAPTER IV

SUB-/SURFACE DAMAGE OF FIXED-ABRASIVE POLISHING

Fair skin covers a multitude of sins.

The chapter deals with surface scratches and subsurface cracks induced in polishing process. Polished surfaces were first compared by various polishing techniques following and prior to chemical etching. The UV behaves differently in different processes, depending mostly on the pellets. Based on the results, we speculate that different results originate from chips which affect surface and subsurface characteristics by means of accumulation between glass and pellet surface.

4.1 Sub-/Surface characteristics of workpiece undergone varied polishing processes

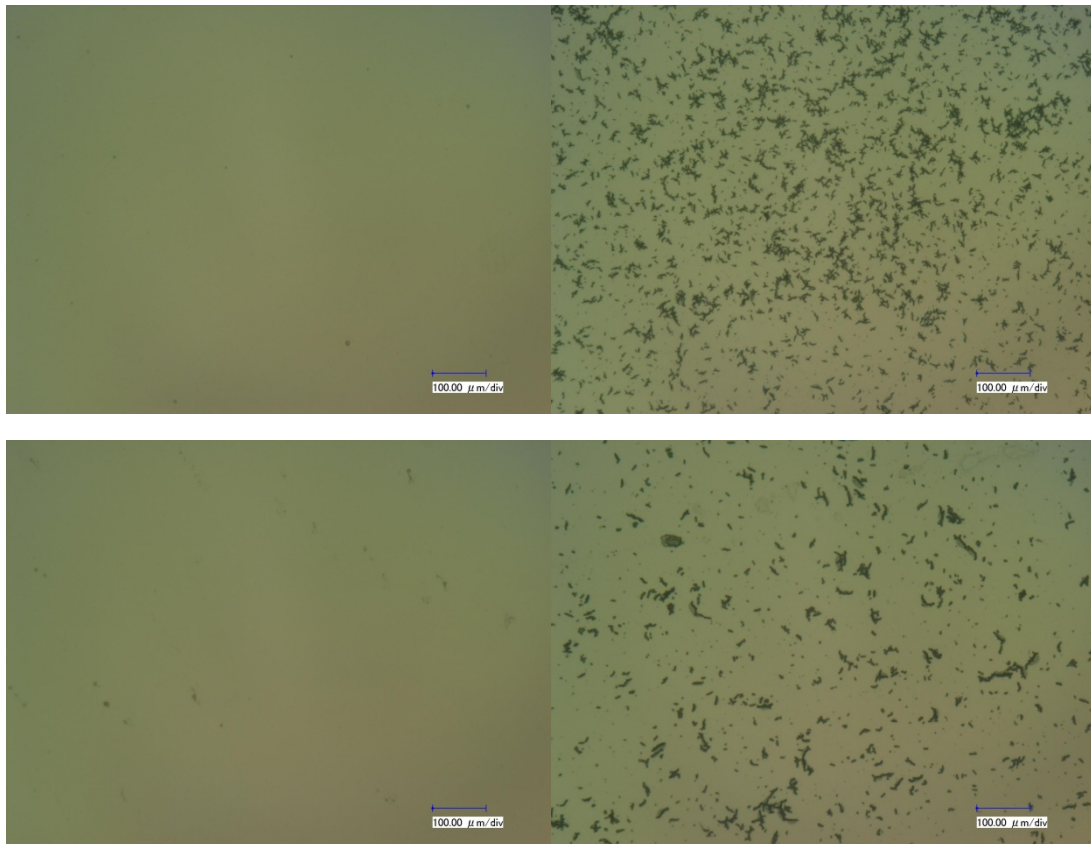
Micro-cracks are inevitably induced in conventional grinding, including fixed-abrasive grinding and loose abrasive grinding. The reason is reckoned to be that the grinding (ductile grinding excluded) proceeds in brittle mode where the material is removed due, to a great degree, to brittle fractures of fused silica. The grinding has been proven to resemble sliding indentation and modeled with a sliding hard indenter against the glass surface. For a sharp indenter, median cracks will occur during the loading of the indenter and unloading can give rise to lateral cracks. One type of cracks can transform to the other, relying on the applied load and the way to load the indenter. The cracks, especially the median cracks, are optically closed. In other words, they cannot be detected with optical or even electron microscopes unless they are enlarged with some methods such as chemical etching, etc. Thus a dangerous but convenient and inexpensive way to observe the cracks is to open the cracks with chemical wet etching first, which is conducive to the inspection with microscopy. For

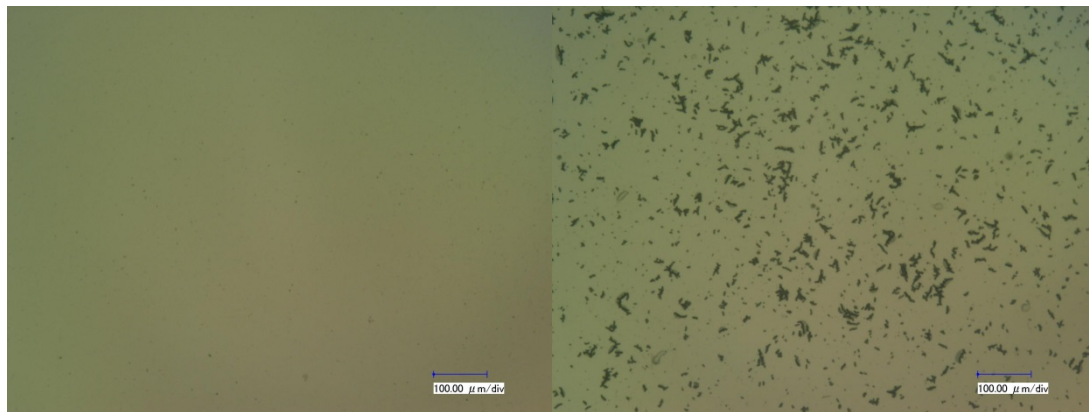
the purpose of verifying machined surface by CMG, some samples from different groups together with a control of pitch polished surfaces were compared.

The surfaces underwent different processing were etched. The etched and un-etched surfaces were recorded with optical microscope at the 300× magnification. It is worth noting that the objective of the etching is just to open/enlarge the cracks in glass. Here we presume that the fused silica glass is homogenous and isotropic and in the meantime the etching progresses evenly in all directions where the etchant remains.

Constant feed grinding with grinding plate

According to the related papers, the fused silica samples were machined under the conditions of dry machining and wet machining with flooding or mist water. The cracks are identified with much ease on the surface after chemical etching. In contrast, the unetched surface does not contain cracks.



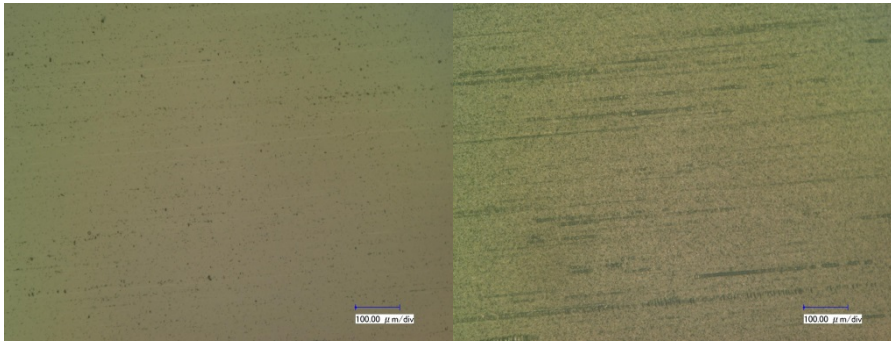
**Unetched****Etched****Fig. 4.1 Samples prior to and following chemical etching**

All the three samples contain brittle cracks. The cracks resemble those induced by grinding with SiC abrasive. The crack distribution in the samples is concentric, just in agreement with the machining path.

Constant feed grinding with grinding wheel

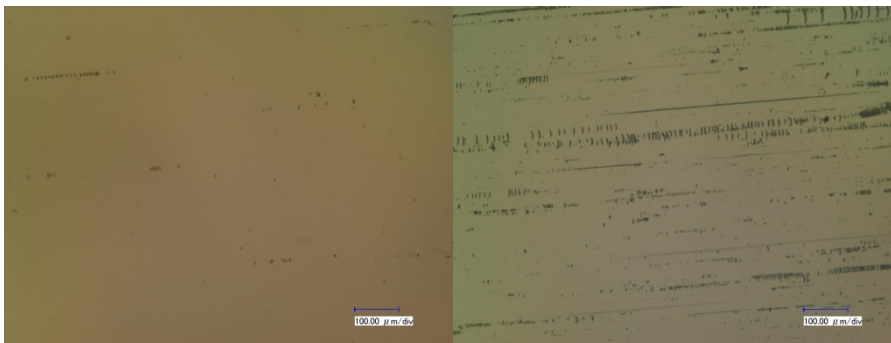
Surfaces finished by different machining technique were etched, too. Once again, cracks/scratches emerge out after etching.

The spark-out and type of pellets are regarded as important issues that might affect the subsurface quality. The spark-out finally takes effect via the force transmitted by the abrasives. The only difference between the two types of pellets exists in whether the pellets contain small pores. The pores may accommodate the debris and dissipate the heat of friction. It is the very pores that serve the sources that may cause adverse effect and mar the surface being machined. Sufficient removed thickness by CMG will guarantee that likely defects, if any, are left behind by CMG process itself rather than preceding grinding. That is, the possible cracks are definitely to be removed and thereafter the CMG is the actual process to generate the final. As the prescribed removal of material ($>5\mu\text{m}$), each sample will take the character of CMG. Thus, the samples were mildly etched (\sim several hundred nanometers) to open latent cracks.



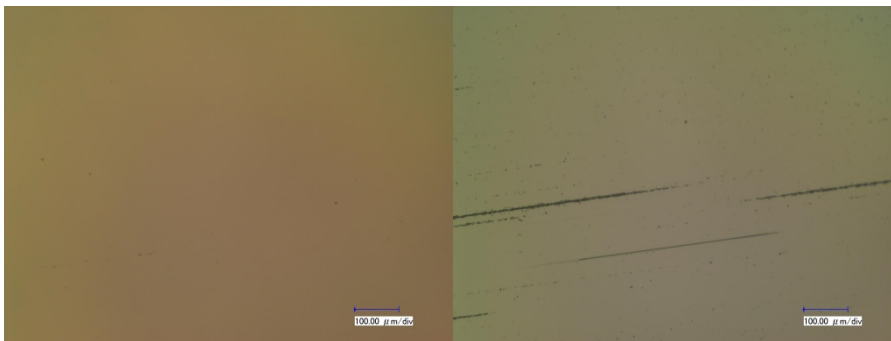
No. 1 Unetched

Etched



No. 2 Unetched

Etched



No. 3 Unetched

Etched



No. 4 Unetched

Etched

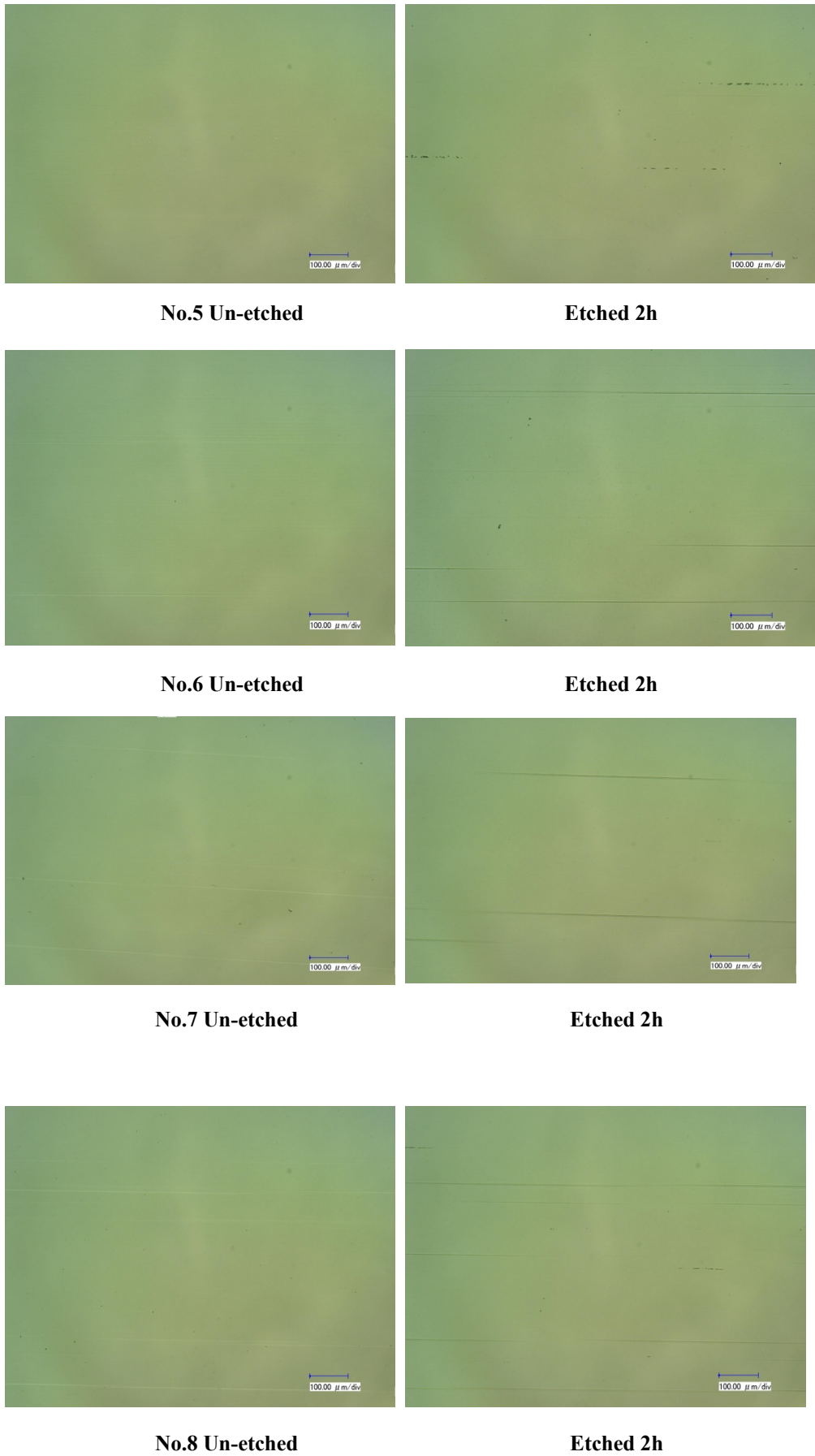


Fig. 4.2 Cracks uncovered by virtue of etching.

All machined surface are covered with scratches and/or cracks. The scratches on samples #4 through #8 appear to be plastic, while on other surfaces both brittle cracks and scratches can be readily discerned (Fig. 4.2). Additional information inferred from the samples is that the hardness of ceria should be no less than that of fused silica glass in that the fused silica surface can be scratched with CMG abrasive ceria. The real hardness of fused silica glass and ceria should be ascertained with hardness tester because the glass hardness differs from manufacturers to manufacturers.

Four samples with pore-free pellet are similar from the viewpoint of the subsurface characteristics, only tiny scratches on the etched surface. The results indicate the processes affect little on subsurface damage, that is to say, whether proc. B or C or D did not alter the subsurface characteristics. The scratches, in my humble opinion, were generated by glass particles that were detached from the bulk. The ceria is comparable to silica in hardness. During the machining, the ceria chemically and/or mechanically bonds and/or scrapes the glass surface being machined. The glass is removed in the form of lump and the lump of glass may score the glass surface if the lump cannot be discharged properly. Our results on ultrasonic vibration, to a greater extent, corroborate the suspicion.

The phenomena can be interpreted by the mechanical abrasion engendered by glass particles. The surface machined with solid pellets is with better quality than pore-containing pellets. Moreover, it can be seen without much difficulty that spark-out potentially influence the subsurface quality. Comparing No. 2 and No. 3, we can find on the surface of No. 2 are many intermittent cracks which constitute scratches, while the scratches are mostly continuous on the No. 3 surface, indicating some great size of particles hard enough were subject great forces during sliding on the surface. I suspect the great particles come from glass. Spark-out can decrease the force applied on the particles, resulting in the decreased scratches. The spark-out speaks more loudly as to the surface machined with CM10000B. Only some trivial scratches lie on the surface. Because in the body of the pellets, there is no room to

lodge glass debris and the probability of scratches occurrence was lowered.

Results are tabulated:

Tag	Type of Pellet	Process	Spark-out	Qualitative assessment
1	CM10000BP	Proc. A	0	Severe
2	CM10000BP	Proc. A	20	Severe
3	CM10000BP	Proc. B	0	Severe
4	CM10000BP	Proc. B	20	Severe
5	CM10000B	Proc. A	0	Appreciably severe
6	CM10000B	Proc. A	20	Slightly severe
7	CM10000B	Proc. B	0	Intermediately severe
8	CM10000B	Proc. B	20	Detectably severe

Based on the above results, machining process does not make big difference to subsurface quality. The subsurface quality is dominated by CMG stone. In accordance with a rule of thumb, the probable thickness of damaged layer for SD2000B grinding wheel is ~7.5microns, and in the meantime, the removal of 6~10microns should remove the majority of cracks. As a consequence, the scratches on each sample should

be incurred by CMG itself. Spark-out has detectable effect on the subsurface quality, which contributes to a better surface. The scratches are not affected by the polishing process and removed thickness. Now we may draw some conclusions that the cracks are induced by glass debris that are hosted between the pellet and glass surface. The pores can be populated by debris and increase the risk of scratching glass surface. Our ultrasonic machining further solidifies the conclusion. The ultrasonic vibration dispels the debris well and secures a better machined surface. Some mathematical and physical model is needed to clarify the process.

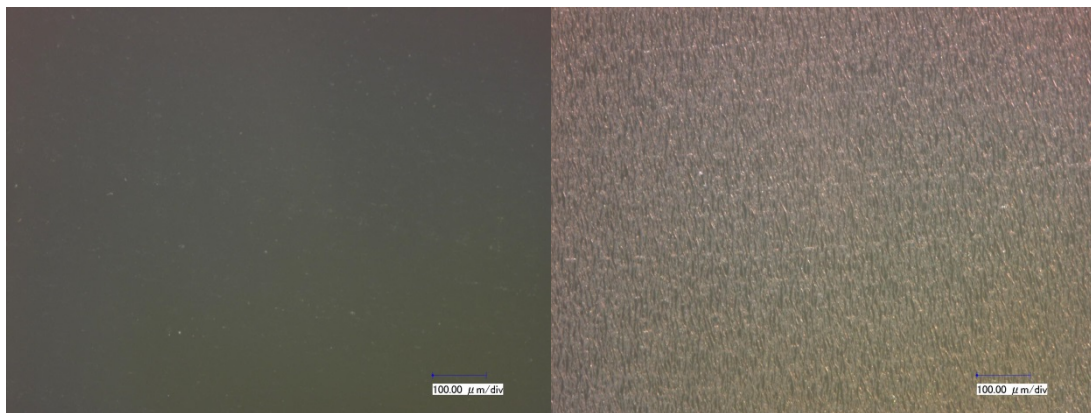
Constant pressure grinding with grinding pellet

Another apparatus machined surfaces, without exception, were pregnant with cracks that line up regularly to form scratches.



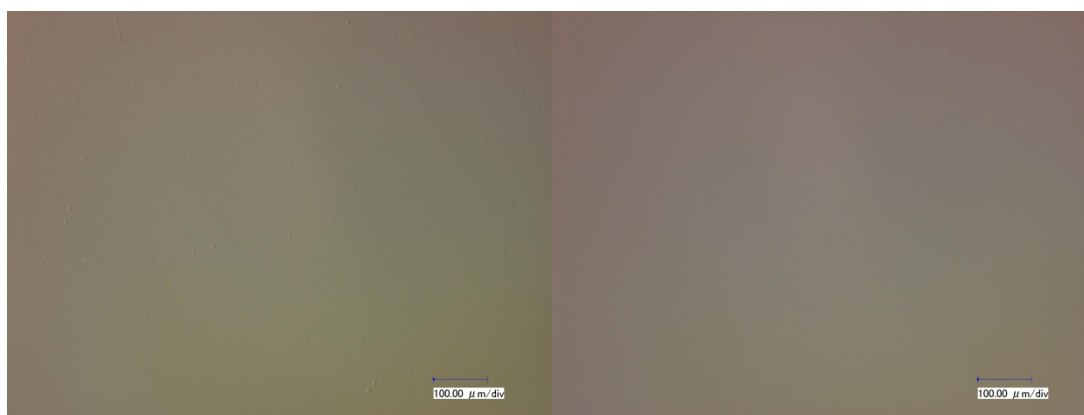
Without UV & unetched

Without UV & etched



With UV & unetched

With UV & etched



Pitch polished & unetched

Pitch polished & etched

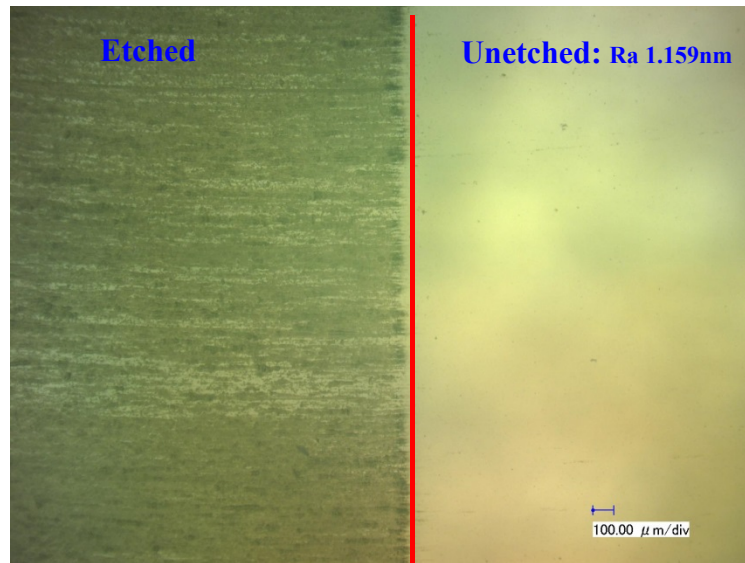
Fig. 4.3 Cracks and scratches unveiled after etching.

The surfaces of the last set that were pre-polished with pith polishing technique. But once again we clearly see that there reside numerous cracks on the machined surface after machining and chemical etching. Furthermore, the number of cracks soars astonishingly. The pitched control samples contain, actual no cracks, irrespective of chemical etching.

From the above results, we can find the fact that no matter what machining process is utilized, cracks are omnipresent and generation of cracks is irrelevant to external machining parameters. Some intrinsic factors related to pellets are responsible for the onset of cracks.

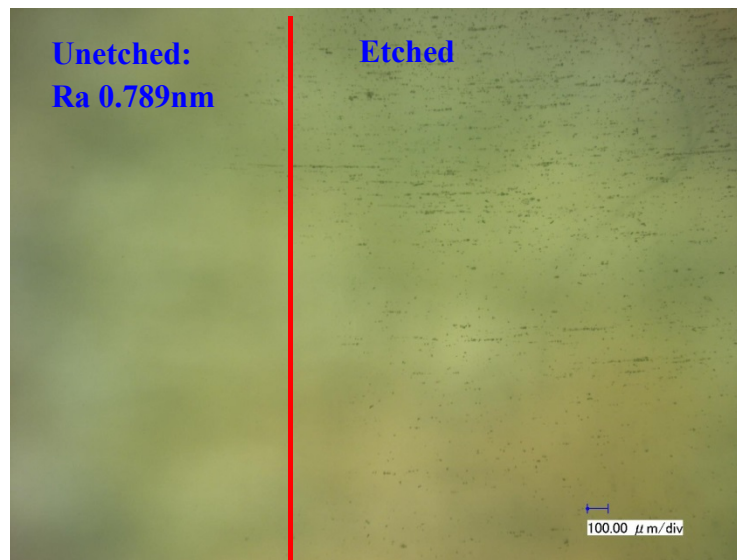
Subsurface quality of glass polished with different pellets

In light of the previous results, we turned to replacing pellet in the hope of finding something new. We experimented pore-containing and pore-free pellets and find that the subsurface seems much better by pore-free pellet than the other in the presence of water (pore-free pellet cannot produce any smooth surface under dry conditions as mentioned before).



CM10000BP polished surface with water

(removed thickness 1.8 microns; etched thickness 1.5microns)



CM10000B polished surface with water

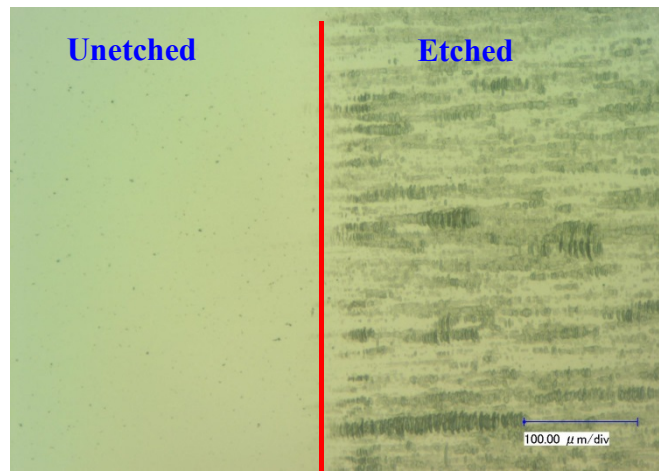
(removed thickness 3.5 microns; etched thickness 2.7microns)

Fig. 4.4 Cracks and scratches unveiled after etching.

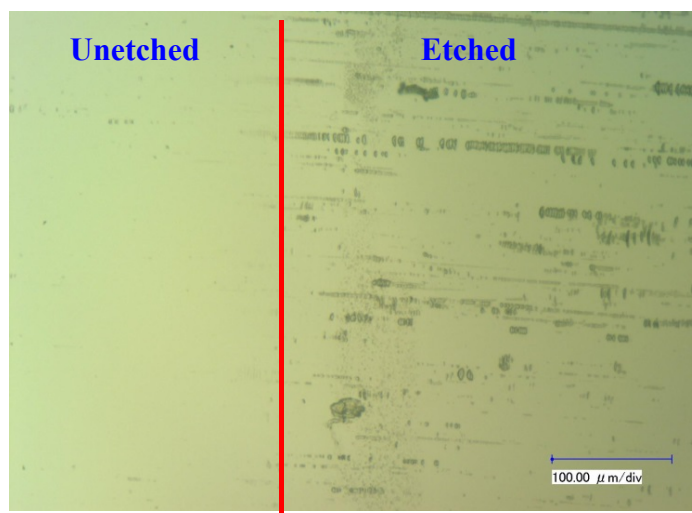
Although both surfaces are free from any defects before polishing and is of similar surface roughness, the CM10000B yield less severe crack (better subsurface) than CM10000BP after etching.

Subsurface quality under dry and wet polishing process (original surface: #1500 abrasive-paper ground, surface roughness Ra ~200nm)

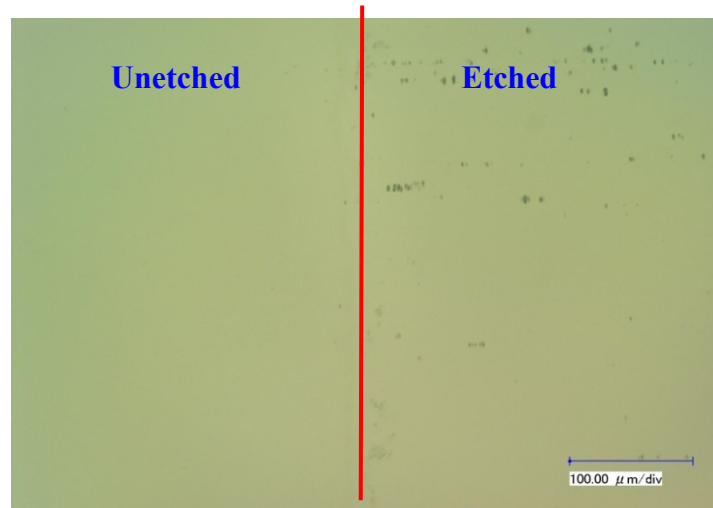
Since water can reduce, to a certain degree, surface roughness, it is very natural to check if the water can take effect in bettering subsurface quality.



CM10000BP dry-polished surface without UV (12~13microns polished out, 1.0micron etched away); Ra=1.3nm (prior to etching), Ra>100nm (following etching)



CM10000BP water-polished surface without UV (5~6microns polished out, 0.8microns etched away); Ra=0.63nm (prior to etching), Ra>57nm (following etching)



CM10000B water-polished surface without UV (4~7microns polished out, 0.8microns etched away); Ra=0.49nm (prior to etching), Ra>1.7nm (following etching)

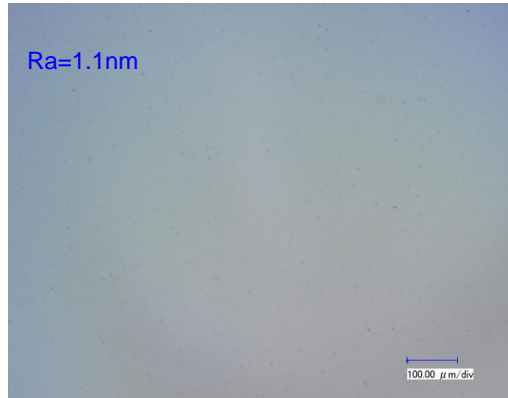
Fig. 4.5 Water effect on subsurface defects

Indeed, the subsurface defects diminish as expected. The results is recurrent that pore-free pellets perform much better.

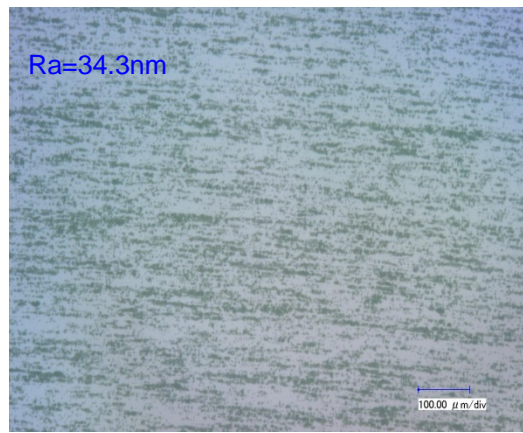
Tag	Aqueous?	Mat. removed	Original Ra	Etched thick.	Ra after etching	Micro-cracks
CM10000BP	dry	12~13 μm (6h)	~1.3nm	1.0 μm	>100nm	heavily
CM10000BP	water	5~6 μm (>10h)	~0.63nm	0.8 μm	>57nm	moderate
CM10000B	water	~7 μm (>10h)	~0.49nm	0.8 μm	>1.7nm	modicum

Effect of ultrasonic vibration on subsurface quality

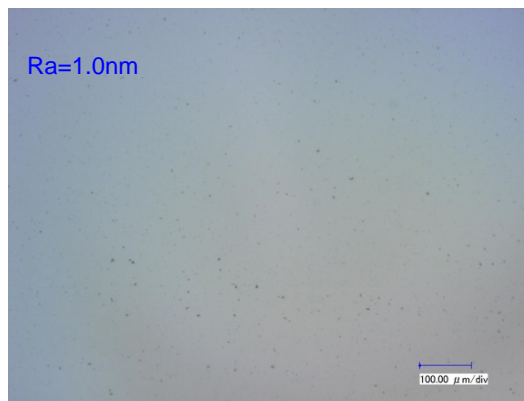
The last task is to examine the ultrasonic vibration on subsurface quality. This time we checked the surface machined by UV under wet conditions.



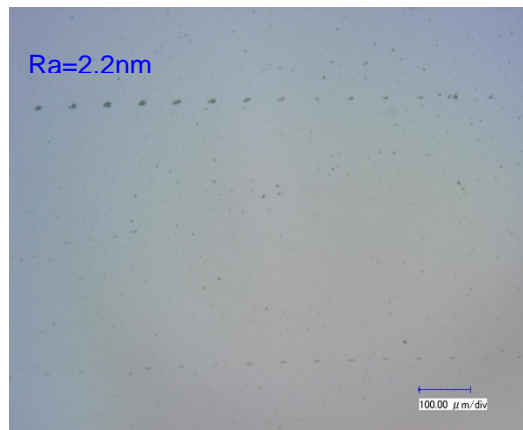
(a) Before etching with pore-free pellet+Non-UV



(b) After etching with pore-free pellet+Non-UV



(c) Before etching with pore-free pellet+ UV



(d) After etching with pore-free pellet+ UV

Fig. 4.6 UV influence on subsurface defects

Before etching, surface roughness is similar for two samples, subsurface is surprisingly different, though. On the UV-machined surface are some scattered point-like defects. By contrast, the surface were marred that were polished with Non-UV process.

To sum up, CM10000BP is applicable to the polishing of fused silica under dry environment, which cannot be accomplished with CM10000B. Water may impact the machining process when CM10000B was adopted. Pellet is the predominant factor to determining the surface roughness and subsurface quality. The machining process, whether it is constant pressure or constant feeding rate, is not much relevant as expected before. Pellet is the most important cause for subsurface cracks. Once scratches are found on the polished surface; there will exist definitely subsurface cracks.

Factors influencing subsurface are summarized:

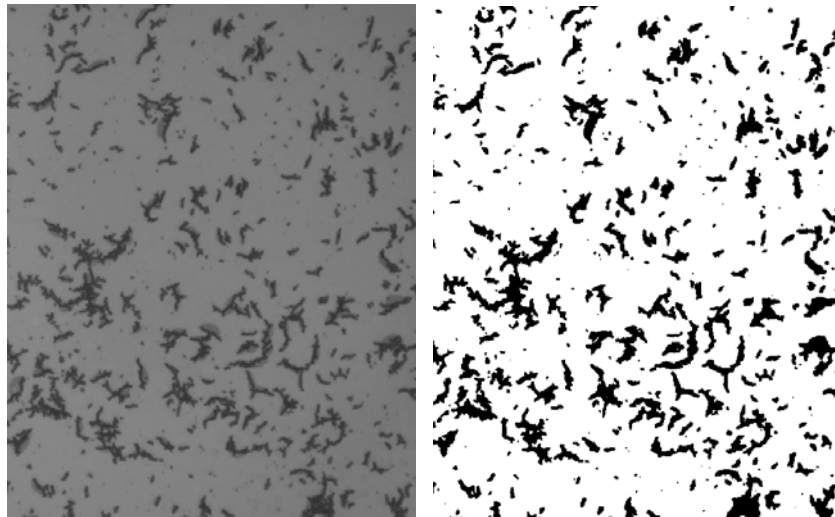
	UV	Water	Pores
Absence	Severe defects	Severe defects	Reduced defects
Presence	Reduced defects	Reduced defects	Severe defects

The beneficial factors have a common nature that in the presence of favorable

factors chips are discharged much more easily. Hence, the scratches are reckoned to be induced by debris, mixture of glass and abrasive, having the same hardness as the glass itself. The removing of debris will be paramount in scratch-free machining. The debris removal can be realized by water-containing fluid.

4.2 Quantifying subsurface defects

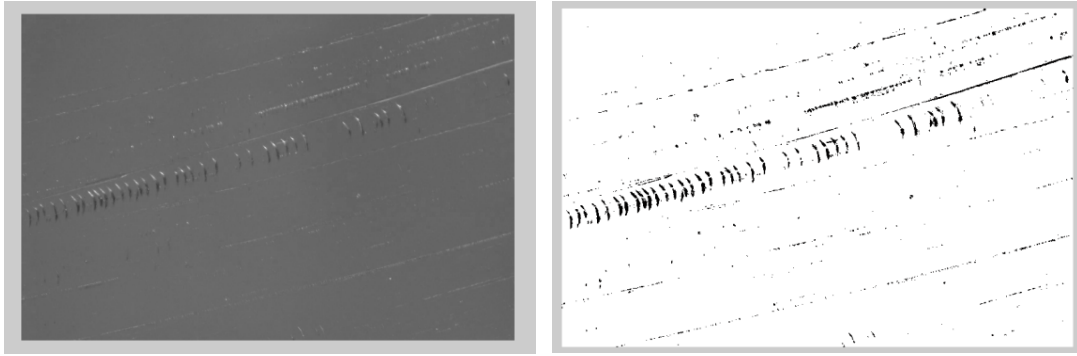
The previous part deals qualitatively with subsurface defects; this portion of the chapter proceeds to process subsurface defects from quantitative at least semi-quantitative view of point. To that end, image processing is utilized. The photograph was filtered, extracted and binarized to calculate the density of the cracks.



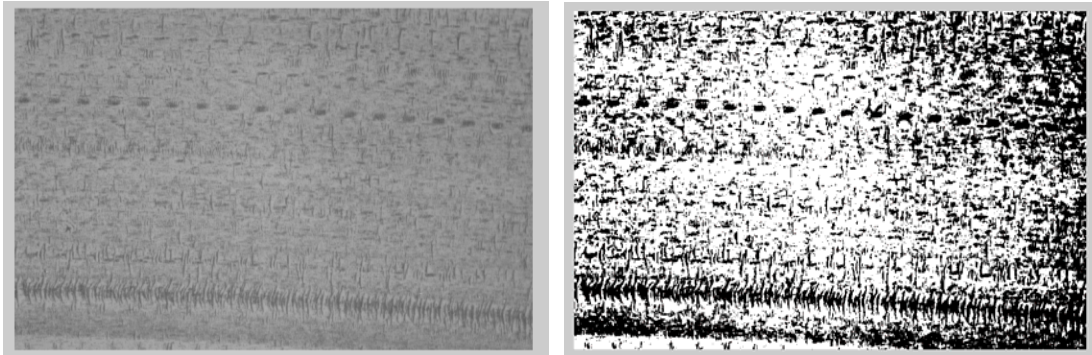
(a) Samples from Ibaraki University density=16.5%



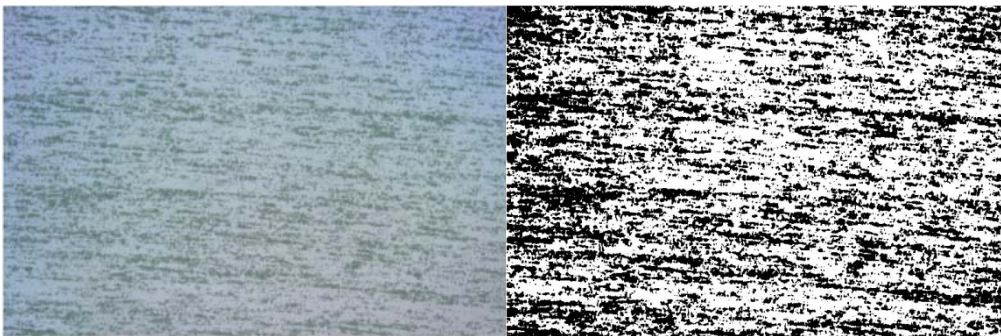
(b) Before etching density=0%



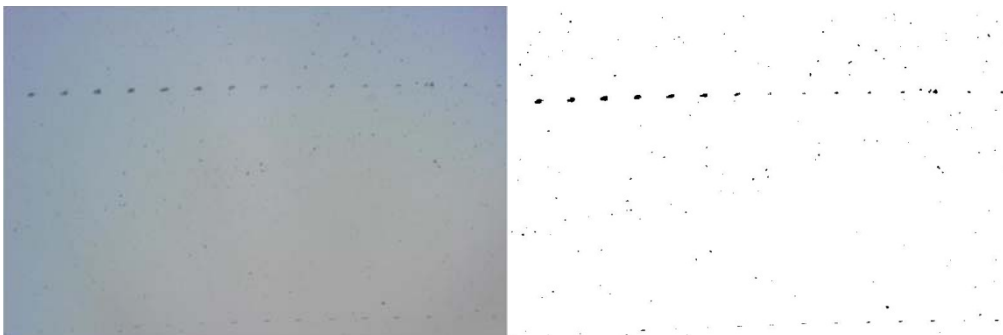
(c) After etching, Non-UV machined density=2 %



(d) After etching, UV machined density>33.19%



(e) After etching without UV, pore-free pellet density=40%



(f) After etching without UV, pore-free pellet density=0.27%

Fig. 4.7 Digitized B&W images

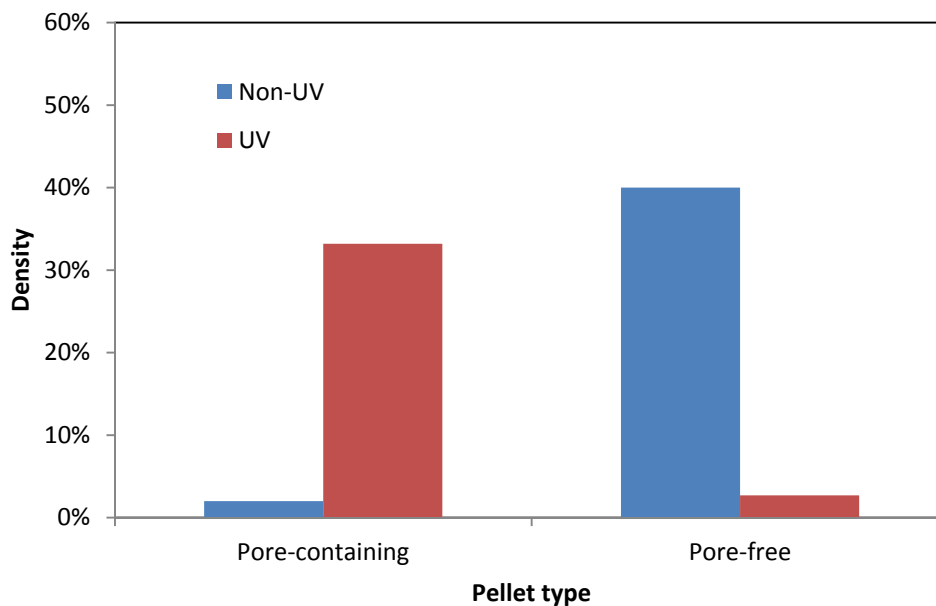


Fig. 4.8 Crack density under varied conditions

It is clear that cracks density depends on pellet type in the present of UV. For the pellet that contains pores, ultrasonic vibration aggravates surface quality whilst the decrement of crack density is contributed to ultrasonic vibration for pore-free pellet.

4.3 Summary

This chapter concentrates on the subsurface attributes of polished glass. The polished glass is plausibly smooth, but after undergoing mild chemical etching various defects were uncovered. The defects are experimentally evidenced to result from chips given rise to in the course of polishing. The chips are presumably composed of abrasive and glass itself, making it open to question that the chip cannot scratch glass surface. Improving the ability to dispel the chips can ameliorate subsurface of polished glass, which is, more or less, corroborated by the water-, UV-, and pore- related experiment results. A micromechanics model is under way in the expectation of elucidating the mechanism of subsurface defect generation and working out an effective method for manufacturing a “really” perfect surface.

References

- [1]. P. E. Miller, T. I. Suratwala, L. L. Wong, M. D. Feit, J. A. Menapace, P. J. Davis, and R. A. Steele, "The Distribution of Subsurface Damage in Fused Silica," Proc. SPIE 5991, 599101 (2005).
- [2]. T. Suratwala, L. Wong, P. Miller, M. D. Feit, J. Menapace, R. Steele, P. Davis, and D. Walmer, "Sub-surface mechanical damage distributions during grinding of fused silica," J. Non-Crystal. Solids 352, 5601-5617 (2006).
- [3]. J. A. Menapace, P. J. Davis, W. A. Steele, L. L. Wong, T. I. Suratwala, and P. E. Miller, "MRF Applications: Measurement of Process-dependent Subsurface Damage in Optical Materials using the MRF Wedge Technique," Proc. SPIE 5991, 599103 (2005).
- [4]. Z. Wang, Y. Wu, Y. Dai, and S. Li, "Subsurface damage distribution in the lapping process," Appl. Opt. 47, 1417-1426 (2008).
- [5]. X. Tonnellier, P. Morantz, P. Shore, A. Baldwin, R. Evans, and D. D. Walker, "Subsurface damage in precision ground ULE[®] and Zerodur[®] surfaces," Opt. Express 15, 12197-12205 (2007).
- [6]. T. Suratwala, R. Steele, M. D. Feit, L. Wong, P. Miller, J. Menapace, and P. Davis, "Effect of rouge particles on the sub-surface damage of fused silica during grinding/polishing," J. Non-Crystal. Solids 354, 2023-2037 (2008).
- [7]. W. Zhang, and J. Zhu, "Controlling subsurface damage in neodymium-doped phosphate glass," Optik 120, 752-757 (2009).
- [8]. J. Shen, S. Liu, K. Yi, H. He, J. Shao, and Z. Fan, "Subsurface damage in optical substrates," Optik 116, 288-294 (2005).
- [9]. D. A. Lucca, E. Brinksmeier and G. Goch, "Progress in Assessing Surface and Subsurface Integrity," Ann. CIRP 47, 669-693 (1998).
- [10]. R. E. Green Jr., "Nondestructive Evaluation of Materials," Annu. Rev. Mater. Sci. 20, 197-217 (1990).

- [11]. E. Brinksmeier, "State-of-the-art of non-destructive measurement of sub-surface material properties and damages," *Prec. Eng.* 11, 211-224 (1989).
- [12]. R. C. Gonzalez, R. E. Woods, S. L. Eddins, *Digital Image Processing Using MATLAB*, 2nd Ed., Gatesmark Publishing, USA, 2009.

This page intentionally left blank.

CHAPTER V

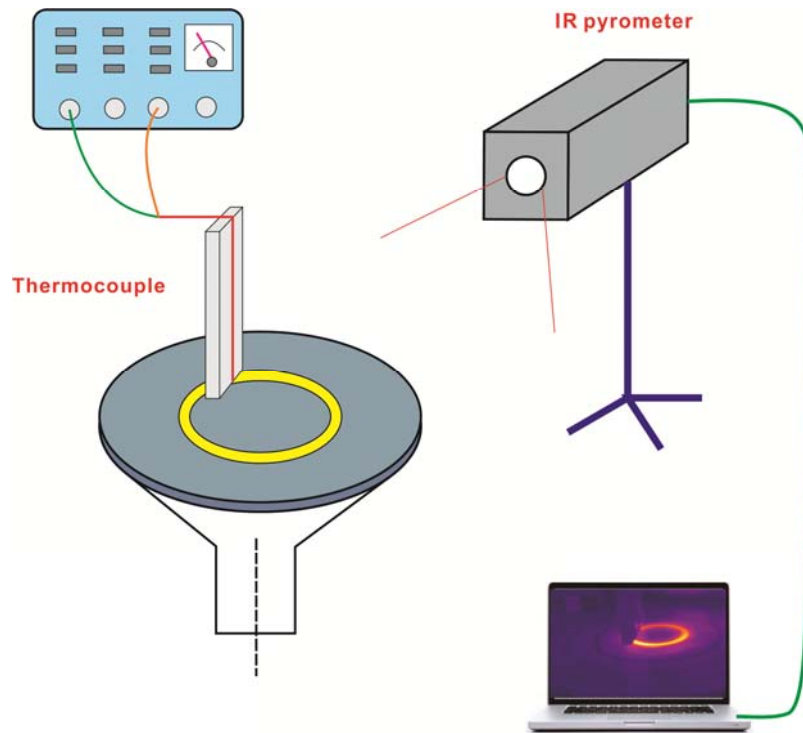
THERMAL ASPECTS IN FIXED-ABRASIVE POLISHING

You never know until you try.

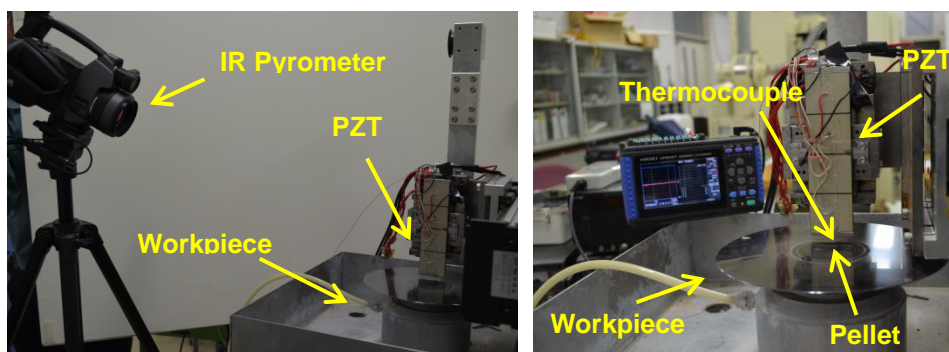
Heat in machining has increasingly been paid attention to by researchers as the status of machined surface can be modified by generated heat in machining process. In particular, the heat is of paramount importance in chemistry-involving process like in chemical mechanical polishing (CMP) and perhaps our fixed-abrasive polishing. Without doubt, it is necessary for us to tentatively evaluate temperature in fixed-abrasive polishing process. We employed *in-situ* infrared camera and thermocouple to test the temperature simultaneously as well as *ex-situ* thermometer. Both methods are effective and the results from two apparatus are similar. Therefore, one can choose any method to measure the temperature dependent upon available experimental apparatus. A model rooted in Fourier heat conduction equation was developed. The modeled temperature is much higher than the tested.

5.1 Temperature measuring system

The real-time testing systems are arranged in line with the follow illustration. The tip of thermocouple was sandwiched between the end face of PZT vibrator and the pellet. An infrared pyrometer meanwhile monitored the vicinity of the interface between the pellet and glass. Admittedly, either the contact (thermocouple) or noncontact method (IR pyrometer) is not capable of measuring the immediate temperature of contacting region, although both ways can be an excellent approximation to the actual temperature. The *ex-situ* measurement with thermometer that contacted the region being tested fully near the final position of pellet was made as soon as an experimental run ended.



(a) Sketch of temperature measuring system



(b) Simultaneously measuring temperature with IR pyrometer and thermocouple

Fig. 5.1 In-situ measurement of temperature

5.2 The temperature in machining silicon and glass

The in-situ temperature in the course of polishing glass and silicon was recorded by means of IR pyrometer and thermocouple, respectively. The temperature increased fast and then reached a plateau in ~ 1 min when the heat generation and dissipation balanced for polishing both silicon and glass. The temperature increases with the increase in rotation rate and downward load irrespective of material to be polished. The steady temperature for glass is greater than silicon; the temperature in the course of polishing silicon achieves stable much faster. The function of vibration can be

differentiated for glass and silicon that applying UV decreases the maximum temperature while increases it in polishing of silicon.

1) Temperature of polishing silicon

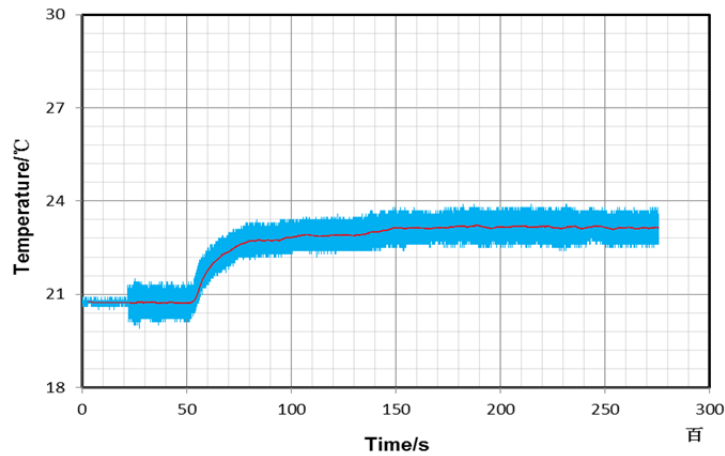


Fig. 5.2 Temperature rise for silicon (600 rpm, 4N)

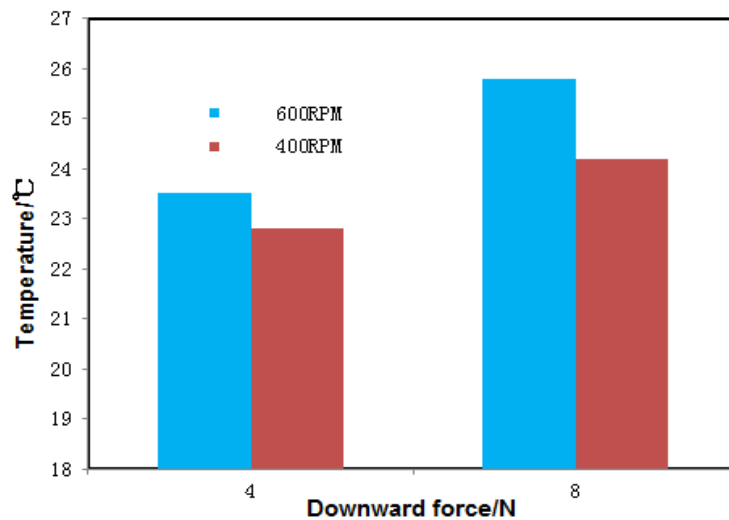


Fig. 5.3 The temperature of silicon polishing versus downward force and rotation rate.

2) Temperature of polishing fused silica

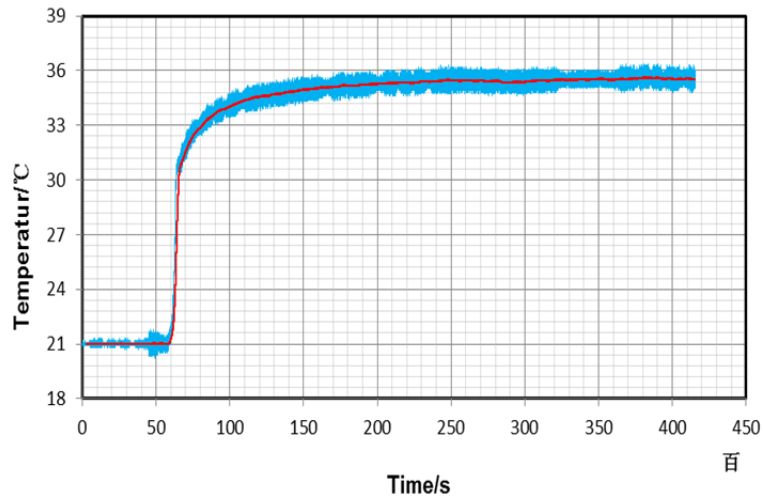


Fig. 5.4 Temperature rise for silicon (600rpm,8N)

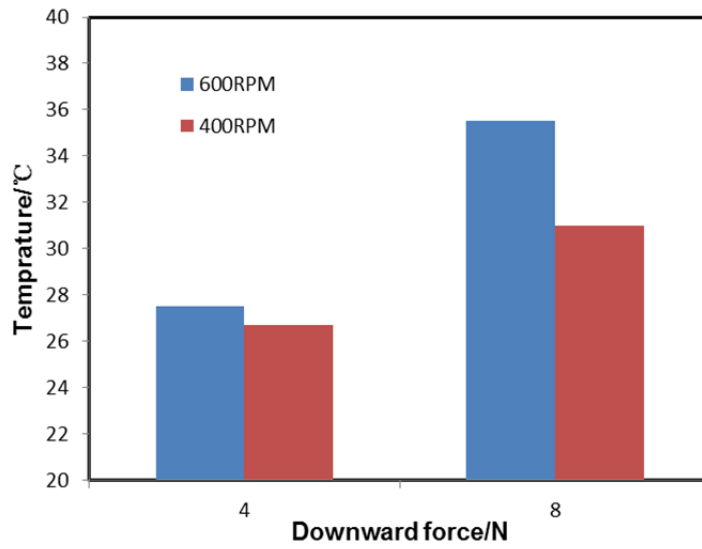
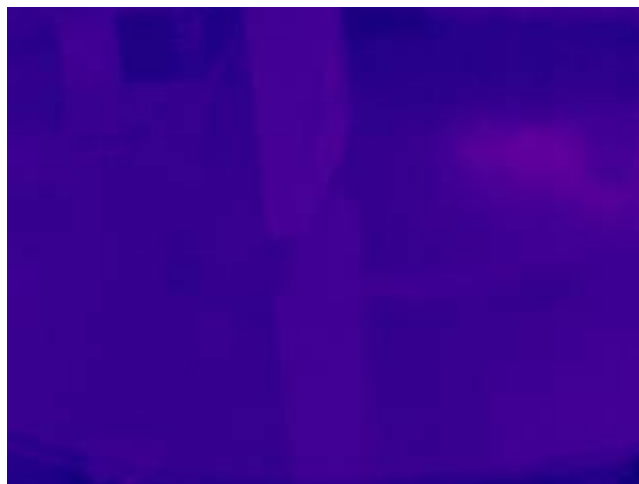
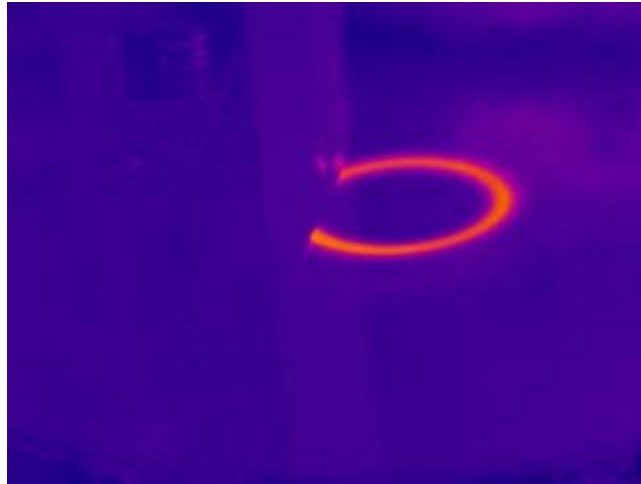


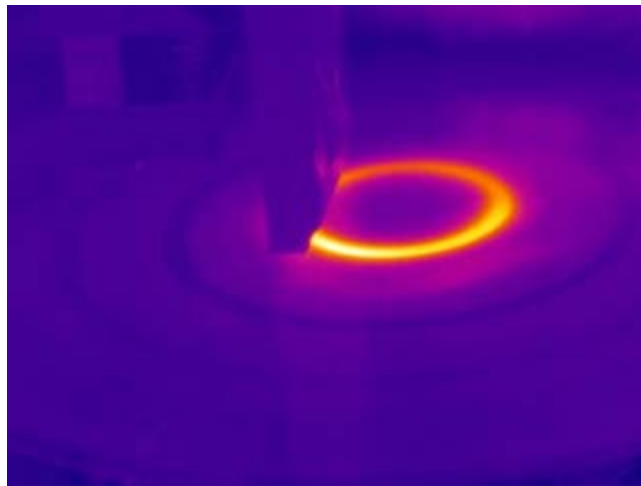
Fig. 5.5 The temperature of fused silica polishing versus downward force and rotation rate.



t=0s



t=20s



t=40s

Fig. 5.6 Thermal image during fused silica polishing at different time instant. The temperature increased with polishing time at first.

3) Temperature of polishing silicon and glass with ultrasonic vibration

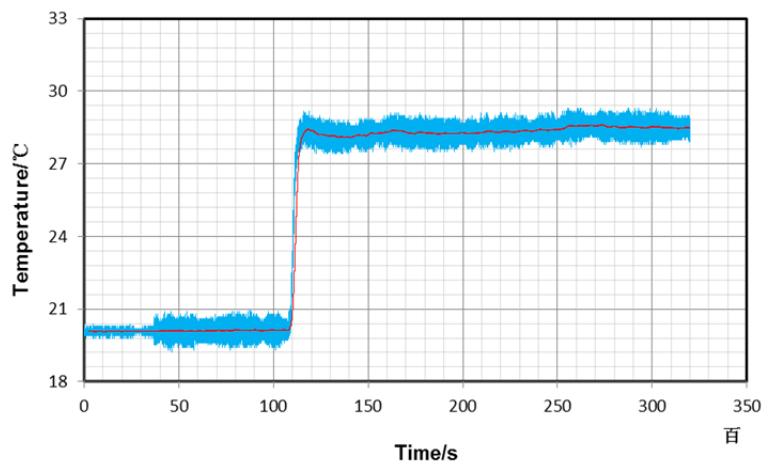


Fig. 5.7 UV polishing of glass (600rpm,4N). The temperature approaches the steady state rapidly.

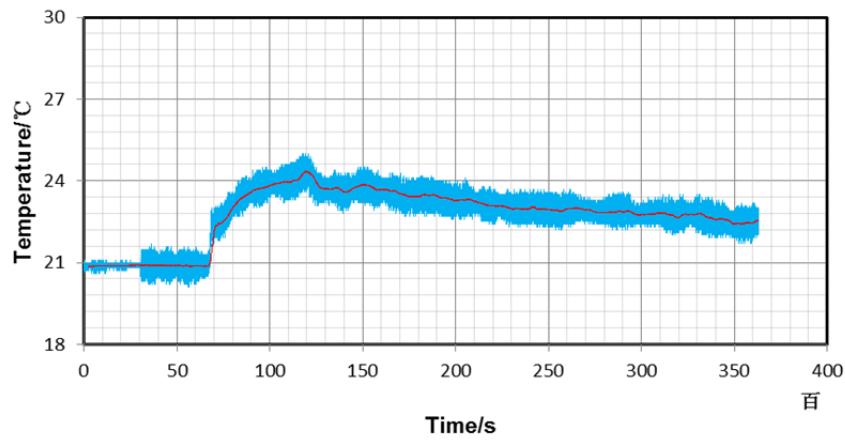


Fig. 5.8 UV polishing of silicon (600rpm,4N). Temperature ascended and then descended, unlike that for non-UV.

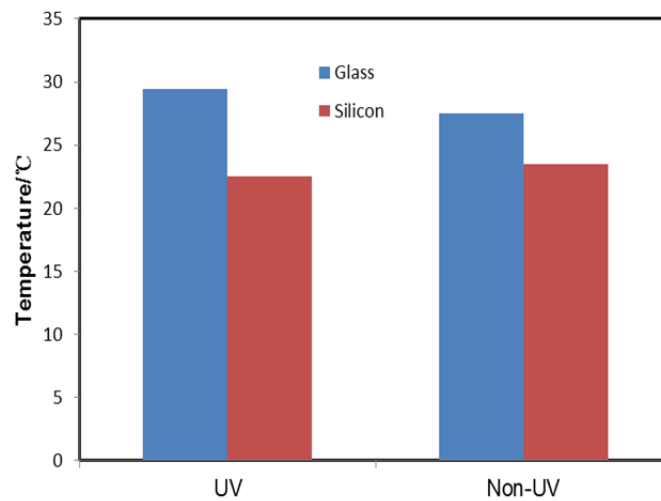


Fig. 5.9 Comparison of temperature in polishing silicon and glass with UV assistance. For silicon, temp. almost similar, but for glass temperature increased in UV polishing, which seems to contradict with the common concept that UV is considered to diminish the machining heat and therefore the temperature.

The temperature for silicon and glass shows that the temperature increases rapidly first and stagnates in several minutes. The temperature strikes a balance between the generated and dissipated heat. Increasing either rotation rate or downward force will

increase the maximum temperature. It is apparent that elevating downward force makes greater difference than rotation rate to temperature. Moreover, for fused silica, the top temperature under the similar conditions is greater than those of silica. The reason is ascribed to the thermal conductivity of which silicon is two orders of magnitude greater than fused silica ($k_{Si} \cong 140\text{W/m} \cdot \text{K}$, $k_{silica} \cong 1.3\text{W/m} \cdot \text{K}$). The generated heat dissipated rapidly over the entire surface ($\Phi=200\text{mm}$). Another cause may be the heat partition between pellet and silica/silicon, which rests on the material property of materials of pellet and that polished. As for ultrasonic vibration, the temperature behaves different slightly for different materials. Vibration appears to increase temperature for silicon polishing while decreases temperature for glass.

Compare IR pyrometer with thermocouple

Although the absolute temperature of IR pyrometer (28 Celsius) is much different from thermal-couple (23 Celsius), the temperature rise (relative temperature) is very similar. Once again the UV may increase slightly the temperature in polishing process. The temperature for glass is much more pronounced than silicon.

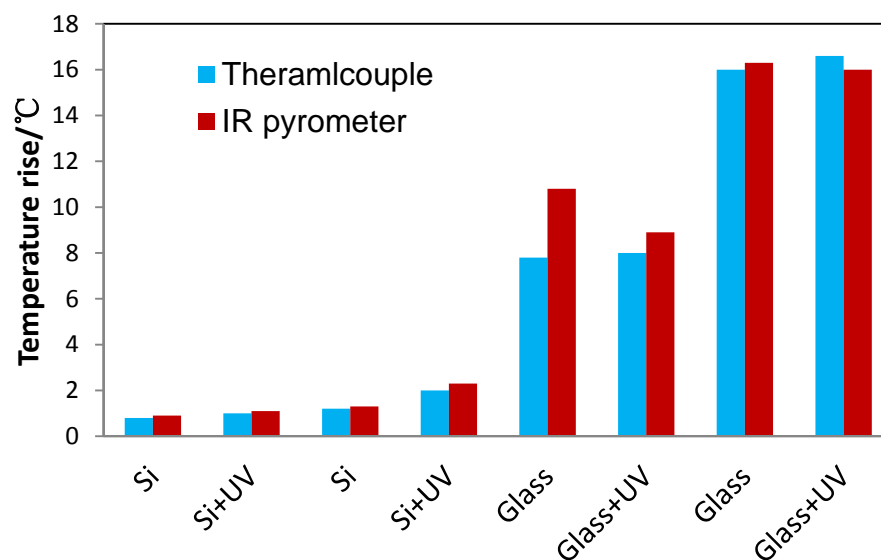


Fig. 5.10 Different temperature apparatus in measuring temperature.

The results from different devices demonstrate that IR thermal camera is sufficient

and reliable for measuring the temperature of polishing process.

5.3 Mathematical model for temperature in dry polishing of fused silica.

The heat Q due to the friction will be diffused into pellet (Q_p) and glass (Q_g).

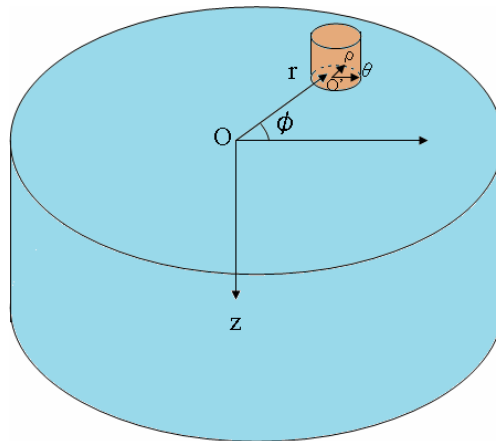
For polishing process,

$$E_w + E_t = W_{\text{thermal}}$$

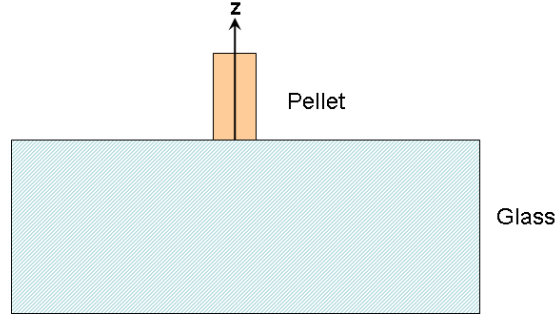
$$W = W_{\text{thermal}} + W_{\text{material}}$$

$$W = \mu Fs = \mu Fvt$$

W_{thermal} is the work transferred to internal energy, W_{material} the work used to removal material. E_w is the energy entering into workpiece and E_t is the part into the polishing tools. The energy partition relies on the properties of workpiece and polishing tools. The process can be viewed as two semi-infinite body of different materials contacting at the interface with same surface temperature and different heat flux. Use the knowledge of heat transfer to analytically and numerically calculate the temperature at the interface.



(a) Configuration of polishing system



(b) Cross-sectional depiction

Fig. 5.11 Modeling the temperature in dry polishing of glass

- A) for pellet, although the pellet moves on the glass, the heat source ($Z=0$ plane) continuously heat the pellet and provide heat. Supposing the heat generation rate per unit time and per unit area is constant. $q_p = Q_p / tA$**

Fourier heat conduction law

$$\vec{q} = -k\nabla T$$

In cylindrical polar coordinate, it will transform into

$$\frac{\partial^2 T}{\partial r^2} + \frac{1}{r^2} \cdot \frac{\partial^2 T}{\partial \phi^2} + \frac{\partial^2 T}{\partial z^2} = \frac{1}{\alpha} \frac{\partial T}{\partial t} \quad (1)$$

Letting the temperature on the surface perpendicular to Z plane is uniform and no heat loss occurs. The equation (1) reduces to one-dimensional problem

$$\frac{\partial^2 T}{\partial z^2} = \frac{1}{\alpha} \frac{\partial T}{\partial t}, \quad \alpha = \frac{\lambda}{\rho c} \quad (2)$$

yielding a linear partial differential equation which can be solved by using separate variables.

Here we let

$$\eta = \frac{z}{\sqrt{4\alpha t}} \quad (3)$$

Differentiating (3),

$$\frac{\partial^2 T}{\partial z^2} = \frac{1}{4\alpha t} \cdot \frac{d^2 T}{d\eta^2} \quad (4)$$

$$\frac{\partial T}{\partial t} = -\frac{z}{2t\sqrt{4\alpha t}} \cdot \frac{dT}{d\eta} \quad (5)$$

Substituting (4) and (5) into (2),

$$\frac{d^2T}{d\eta^2} + 2\eta \frac{dT}{d\eta} = 0 \quad (6)$$

Solving (6),

$$\frac{dT}{d\eta} = C_1 \exp(-\eta^2) \quad (7)$$

$$T = C_1 \int_0^\eta \exp(-x^2) dx + C_2 \quad (8)$$

Initial conditions

$$T(z,0) = T_{atom} \quad (9)$$

Boundary conditions

$$-k \frac{\partial T}{\partial z} \Big|_{z=0} = q_p \quad (10)$$

(9) and (10) determine the integral constant.

Therefore,

$$\frac{\partial T}{\partial z} = \frac{dT}{d\eta} \cdot \frac{\partial \eta}{\partial z} = \frac{1}{\sqrt{4\alpha t}} \frac{dT}{d\eta} = \frac{C_1}{\sqrt{4\alpha t}} \exp(-\eta^2) = -\frac{q_p}{k} \quad (11)$$

$$t = 0, \Rightarrow \eta \rightarrow \infty \Rightarrow \int_0^\eta \exp(-x^2) dx = \frac{2}{\sqrt{\pi}} \quad (12)$$

$$T(z,t) = -\frac{\sqrt{4\alpha t} q_p}{k} \operatorname{erfc}(z/\sqrt{4\alpha t}) + T_{atom} - \frac{4}{\sqrt{\pi}} \frac{\sqrt{\alpha t} q_p}{k} \quad (13)$$

B) for glass, the physical process can be regarded as a moving heat source on a plate with constant heat generation rate $q_g = Q_g / tA$.

$$\frac{1}{r} \frac{\partial}{\partial r} \left(r \frac{\partial T}{\partial r} \right) + \frac{1}{r^2} \frac{\partial^2 T}{\partial \phi^2} + \frac{\partial^2 T}{\partial z^2} = \rho_g c_g \frac{\partial T}{\partial t} \quad (14)$$

$$\varphi = \omega t \Rightarrow \frac{\partial T}{\partial t} = \frac{\partial T}{\partial \phi} \frac{\partial \phi}{\partial t} = \omega \frac{\partial T}{\partial \phi} \quad (15)$$

$$\frac{\partial^2 T}{\partial r^2} + \frac{1}{r} \frac{\partial T}{\partial r} + \frac{1}{r^2} \frac{\partial^2 T}{\partial \theta^2} + \frac{\partial^2 T}{\partial z^2} = \frac{\omega}{\alpha} \frac{\partial T}{\partial \theta} \quad (16)$$

Two order with respect to r, ϕ, z , yields two kinds of initial and boundary conditions

$$\left. \frac{\partial T}{\partial r} \right|_{r=0} = 0, \quad \left. \frac{\partial T}{\partial r} \right|_{r=b} = 0 \quad (17)$$

$$T|_{\theta=0} = T|_{\theta=2\pi}, \quad \left. \frac{\partial T}{\partial \phi} \right|_{\theta=0} = \left. \frac{\partial T}{\partial \phi} \right|_{\theta=2\pi} \quad (18)$$

$$\left. \frac{\partial T}{\partial z} \right|_{z=0} = \begin{cases} -q_g / \lambda (\text{interface}) \\ hT / k (\text{outside interface}) \end{cases}, \quad T|_{z=\infty} = 0 \quad (19)$$

Fourier and Hankel transform must be applied consequentially.

$$\tilde{T} = \int_0^{2\pi} T e^{-in\phi} d\phi (n = 0, 1, 2, 3, \infty) \quad (\text{Fourier transform}) \quad (20)$$

Eq. (16) is converted into (21)

$$\frac{\partial^2 \tilde{T}}{\partial r^2} + \frac{1}{r} \frac{\partial \tilde{T}}{\partial r} - \frac{m^2}{r^2} \tilde{T} + \frac{\partial^2 \tilde{T}}{\partial z^2} = -\frac{im\omega}{\alpha} \tilde{T} \quad (21)$$

$$\tilde{\tilde{T}} = \int_0^{\infty} \tilde{T} J_m(\alpha r) r dr \quad (\text{Hankel tranfrom}) \quad (22)$$

Eq. (21) is reduced to (23)

$$\frac{\partial^2 \tilde{\tilde{T}}}{\partial z^2} - (\beta_n^2 + \frac{im\omega}{\alpha}) \tilde{\tilde{T}} = 0 \quad (23)$$

$$\left. \frac{\partial \tilde{\tilde{T}}}{\partial z} \right|_{z=0} = -\frac{\tilde{q}}{\lambda} + h \cdot \tilde{\tilde{T}}|_{z=0}, \quad \tilde{\tilde{T}}|_{z=\infty} = 0$$

β_n is the solution for $J'_m(\beta_n b) = 0$.

Equation (23) is a two-order linear partial differential equation (ODE) with respect z .

It is much easier to solve Eq. (23). Make inverse Hankel transform and inverse Fourier transform to the solution of Eq. (23) consecutively and the solution to Eq. (16) can be obtained.

$$T = \frac{q}{h} \cdot \left(\frac{a}{b}\right)^2 + 2q \frac{a}{b} \sum_{n=1}^{\infty} \frac{J_1(\beta_n a) J_0(\beta_n e) J_0(\beta_n r)}{(h + \lambda \beta_n) \beta_n b J_0^2(\beta_n b)} \cos(z \beta_n) \exp(-z \beta_n)$$

$$+ 2q \frac{a}{b} \sum_{m=1}^{\infty} \sum_{n=1}^{\infty} \frac{2 \beta_n b J_1(\beta_n a) J_m(\beta_n e) J_m(\beta_n r)}{[(\beta_n b)^2 - m^2] J_m^2(\beta_n b) \delta} \cos[m\theta - \psi - z \eta \cos(\phi)] \exp[-z \eta \cos(\phi)]$$

$$\eta = \sqrt{\beta_n^4 + (m\omega/\alpha)^2} \quad \phi = \frac{\tan^{-1}(m\omega/\alpha\beta_n)}{2} \quad \delta = \sqrt{h^2 + (\lambda\eta)^2 + 2h\lambda\eta \cos(\phi)}$$

$$\psi = \tan^{-1} \left[\frac{\lambda\eta \sin(\phi)}{\lambda\eta \cos(\phi) + h} \right]$$

when β_n approaches infinity, the second and third terms in the above equation approaches 0 because of the exponential term in the equation. In the equation, the first two terms are irrelevant to time. It is the third term that is related to time by means of triangular and exponential terms with respect to rotation rate. Thus the first several terms dictate the final summation of the equation and then we overlook the higher orders of the equation. To a first approximation, we compute the first six terms to stand for the final results as follows:

n	1	2	3	4	5	6
$\beta_n b$	3.83171	7.01559	10.17347	13.32369	16.47063	19.61586

The generated heat enters into pellet and glass, ignoring the dissipation into surroundings. Then

$$q_{total} = q + q_{pellet}$$

The heat is partitioned in terms of heat resistance of pellet and glass, which are

$$R_{pellet} = \sqrt{\frac{a}{2h\lambda}}$$

$$R_{glass} = \frac{a^2}{hb^2}$$

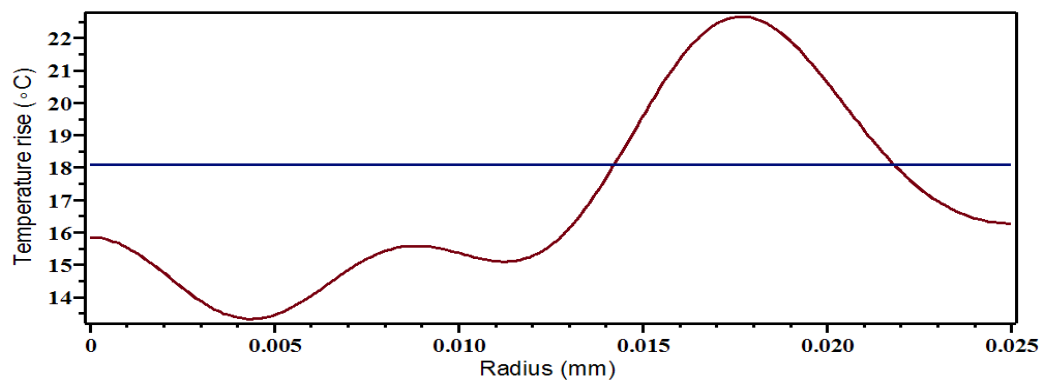
$$\frac{1}{R_{total}} = \frac{1}{R_{pellet}} + \frac{1}{R_{glass}}$$

$$q = q_{total} \cdot \frac{R_{pellet}}{R_{pellet} + R_{glass}}$$

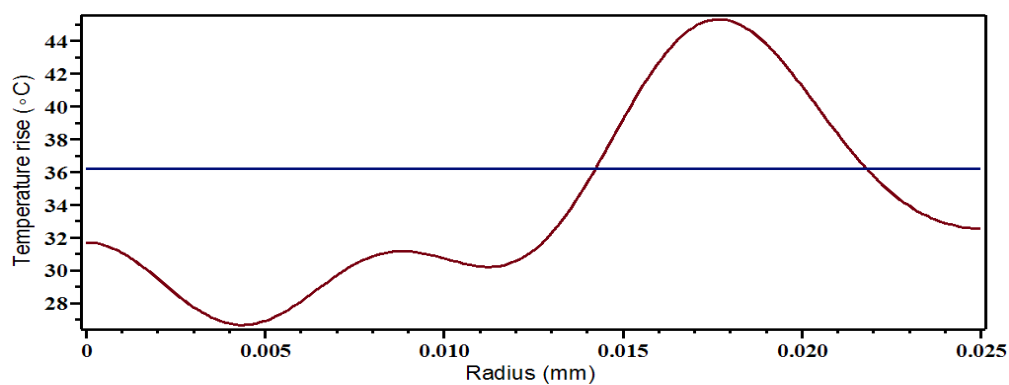
Then the temperature on the surface (i.e. $z=0$) can be modeled along a radius.

1) Temperature distribution of glass

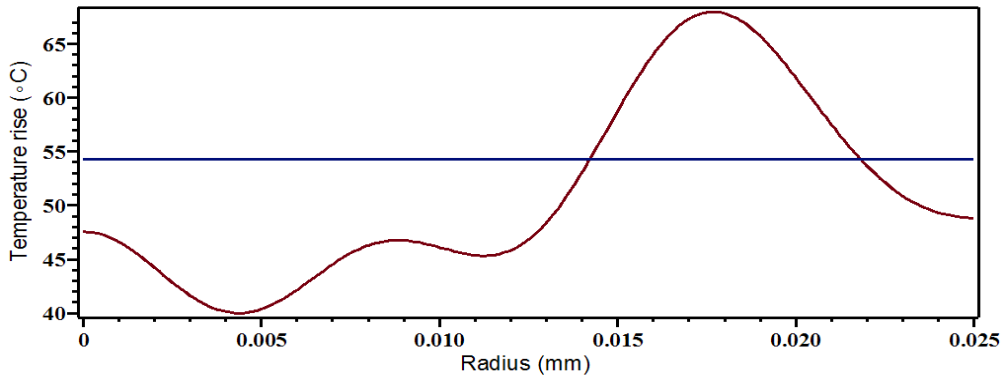
The temperature along the radial direction was listed out as well as maximum temperature.



(a) Maximum temperature rise 22.5°C (load=4N)

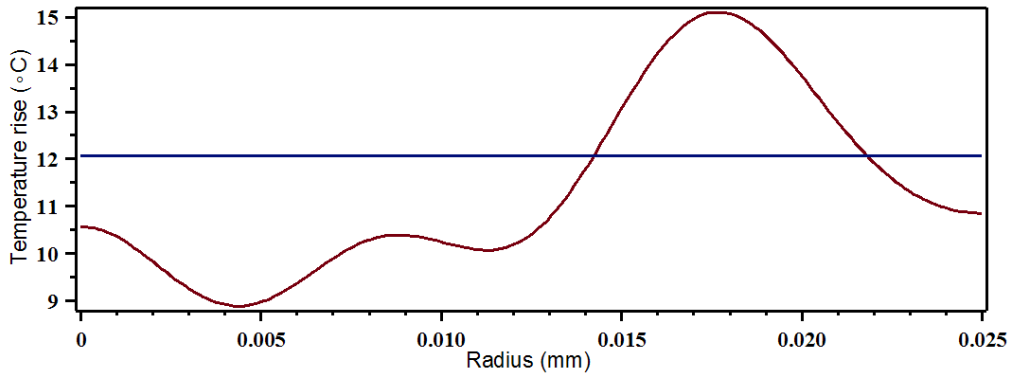


(b) Maximum temperature rise 45°C (load=8N)

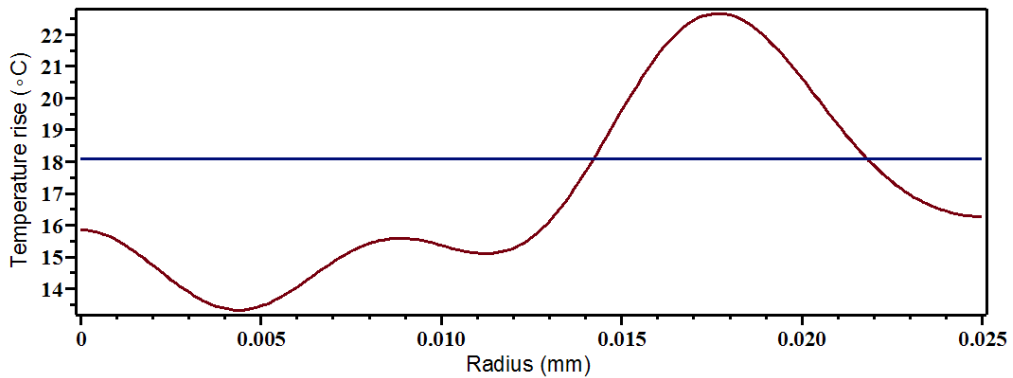


(c) Maximum temperature rise 68°C (load=12N)

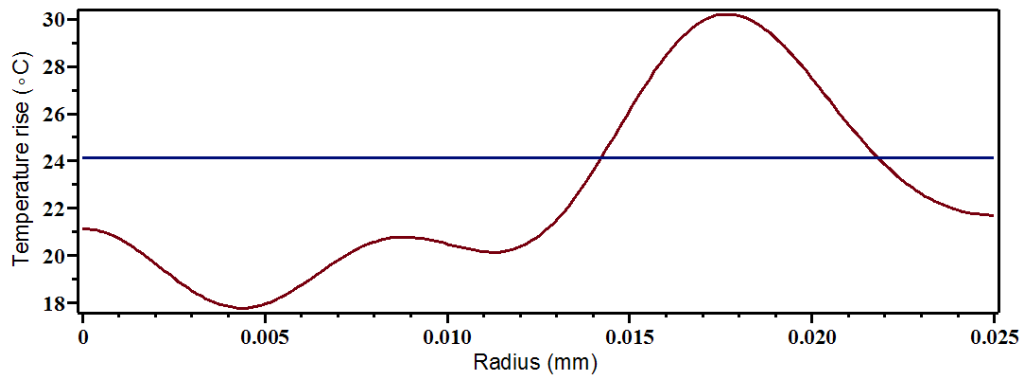
Fig. 5.12 Modeled temperature for glass. The pellet assumes load of 4N, 8N, 12N.



(a) Maximum temperature rise 15°C (load=400rpm)



(b) Maximum temperature rise 23°C (load=600rpm)



(c) Maximum temperature rise 30°C (load=800rpm)

Fig. 5.13 Modeled temperature for glass. The pellet assumes rotation rate of 400rpm, 600rpm, 800rpm.

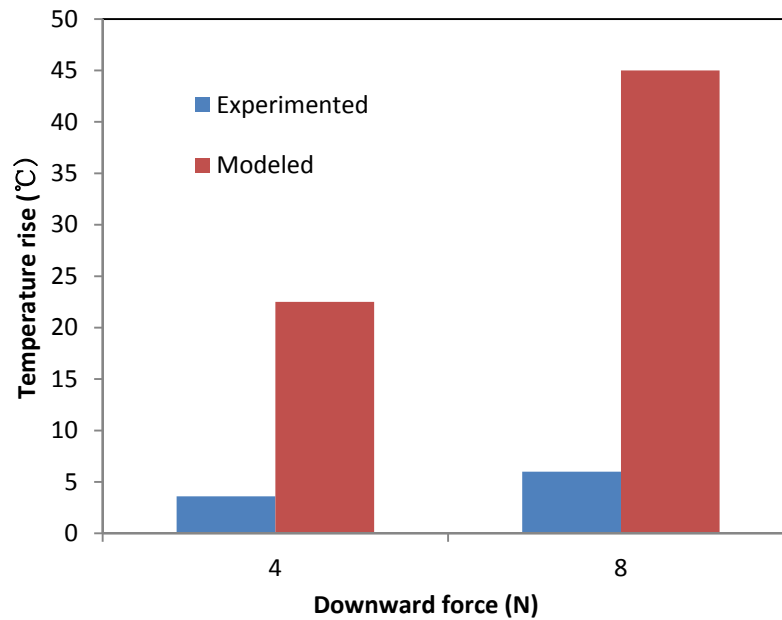


Fig. 5.14 The experimented and modelled temperature rise (rotation rate=600rpm).

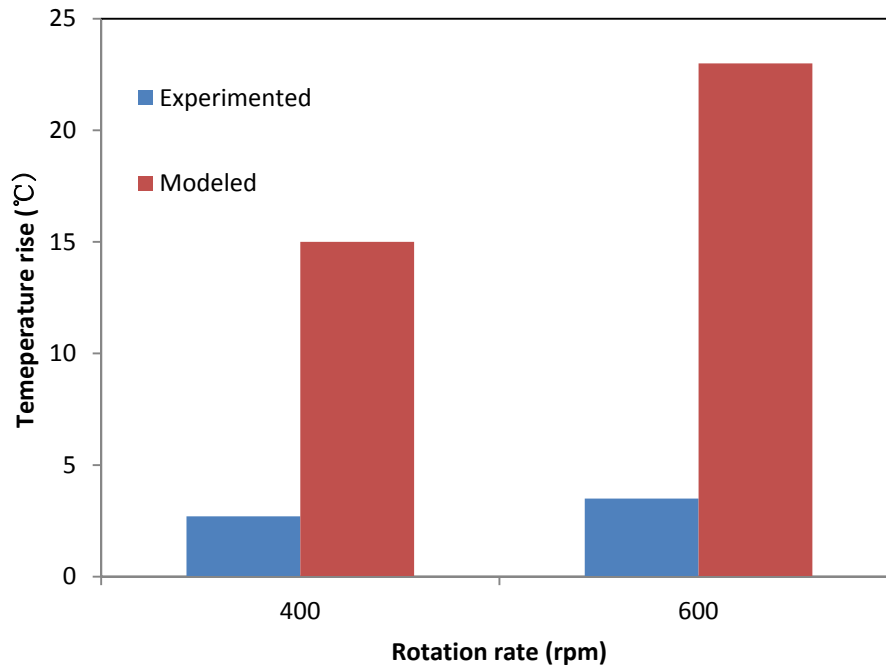
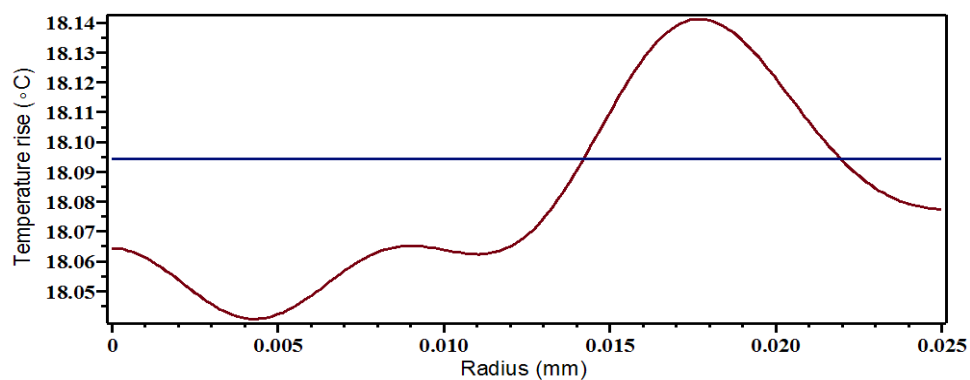


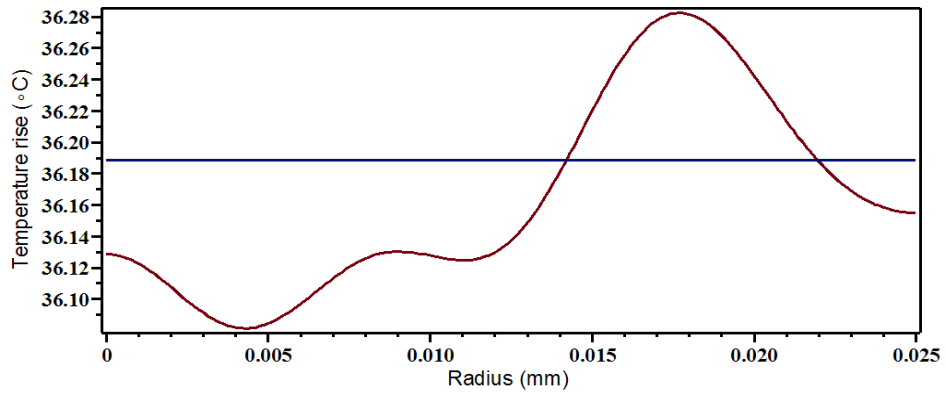
Fig. 5.15 The experimented and modelled temperature rise (load=4N).

The modeled temperature is higher than the experimented, although the trends in are similar that increasing load and rotation rate will increase temperate. Furthermore, the maximum temperature is located in the trace of pellet and load appears to speak more loudly than rotation rate.

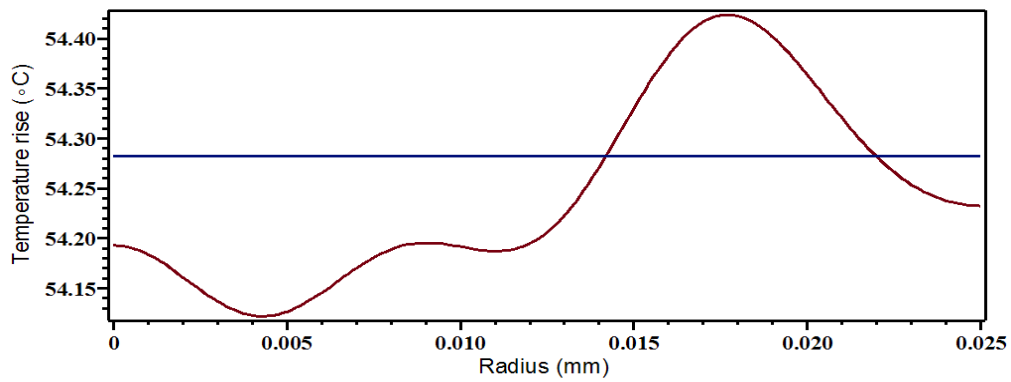
2) Temperature distribution of silicon



(a) Maximum temperature rise 18.14°C (load=4N)

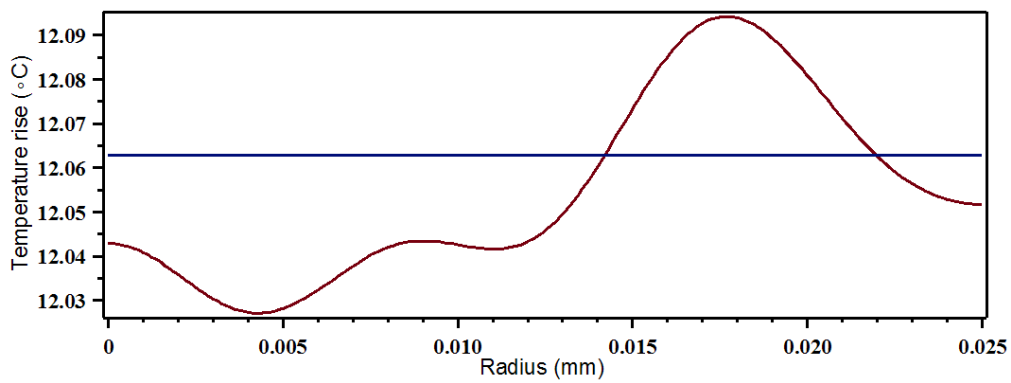


(b) Maximum temperature rise 36.28°C (load=8N)

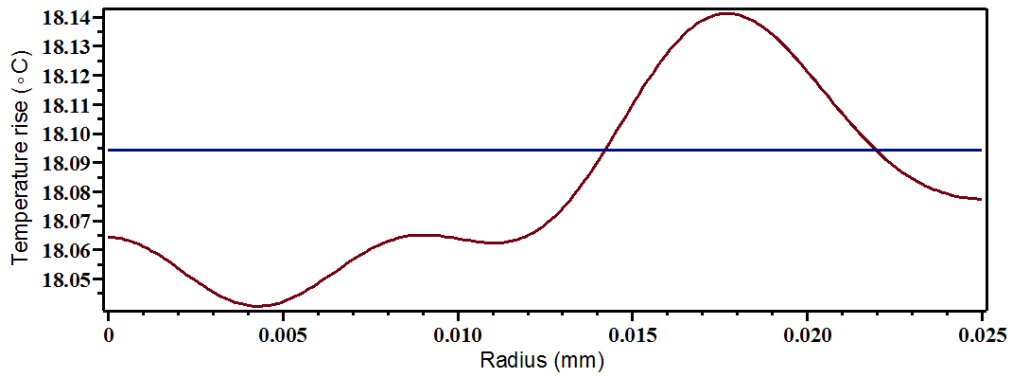


(c) Maximum temperature rise 54.42°C (load=12N)

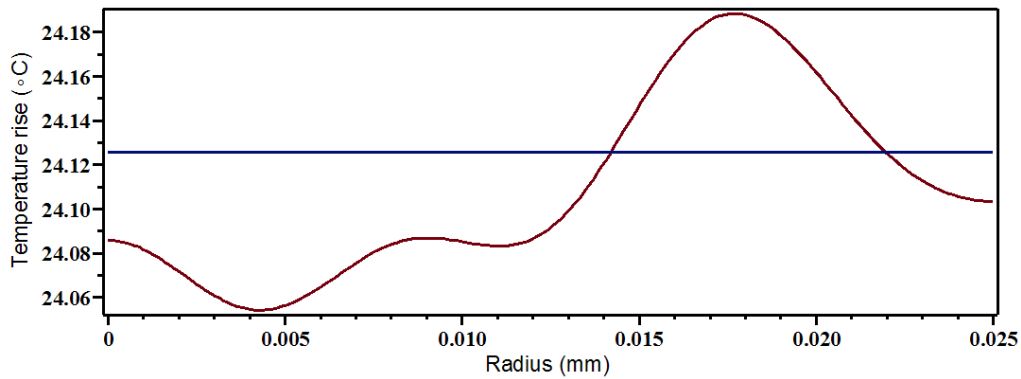
Fig. 5.16 Modeled temperature for silicon. The pellet assumes load of 4N, 8N, 12N.



(a) Maximum temperature rise 12.10°C (load=400rpm)



(b) Maximum temperature rise 18.14°C (load=600rpm)



(c) Maximum temperature rise 24.19°C (load=800rpm)

Fig. 5.17 Modeled temperature for silicon. The pellet assumes rotation rate of 400rpm, 600rpm, 800rpm.

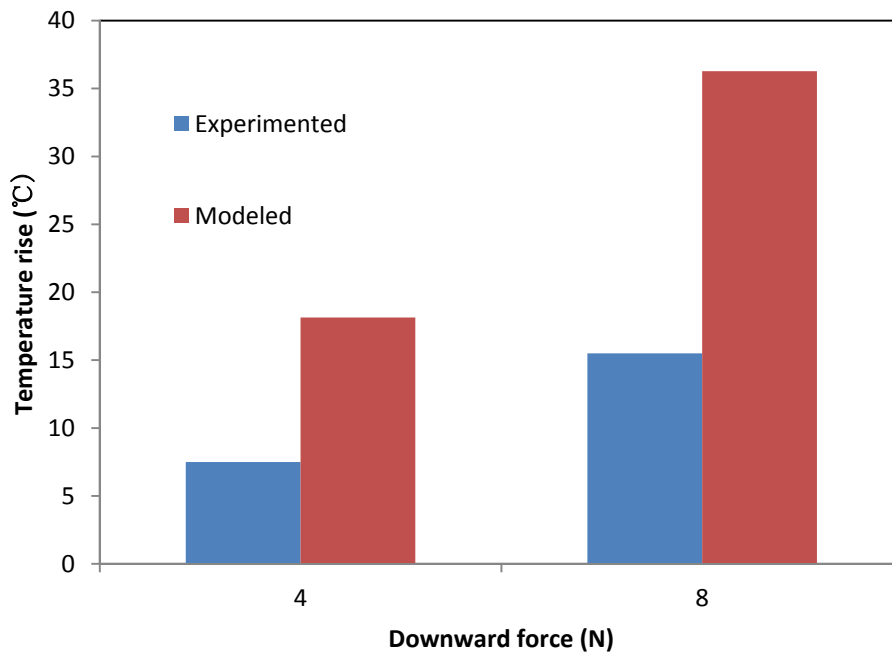


Fig. 5.18 The experimented and modelled temperature rise (rotation

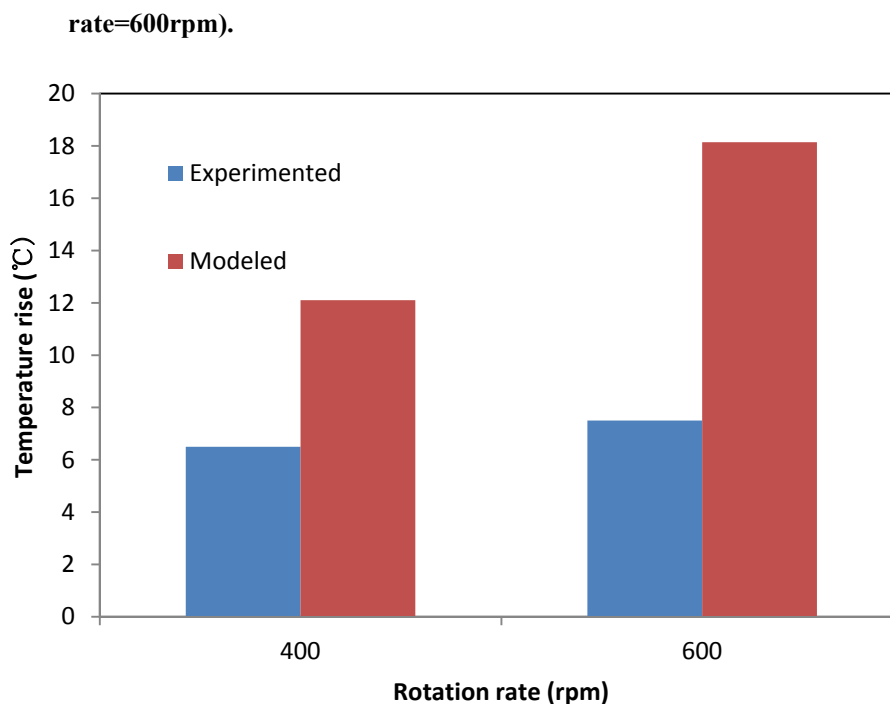


Fig. 5.19 The experimented and modelled temperature rise(load=4N).

The modeled temperature is related to downward load and rotation rate in the same trend as the experiments. Doubling downward load and rotation rate also results in elevated temperature for both silicon and glass. Furthermore, the maximum temperature lies in the trace of pellet. The glass shows higher maximum temperature than silicon. All of the above modeled results are consistent with the experimented.

3) Liquid-affected temperature

The temperature in wet process was contrasted to dry process. The temperature certainly lowered by liquid as thought. The temperature increases after 5 min grinding in both wet (26.2°C to 27.3 °C) and dry grinding (25.5°C to 29.1 °C). The temperature rise is more significant in dry grinding. The temperature increases with increasing the rotational rate. The temperature in the case of 800 rpm+12~13 N is as high as 59.1 °C and the CMG stone was burnt. A layer of black material was generated on the CMG stone surface, as a result of which the material removal is so trifling that the polishing process cannot proceed normally as load=4N.

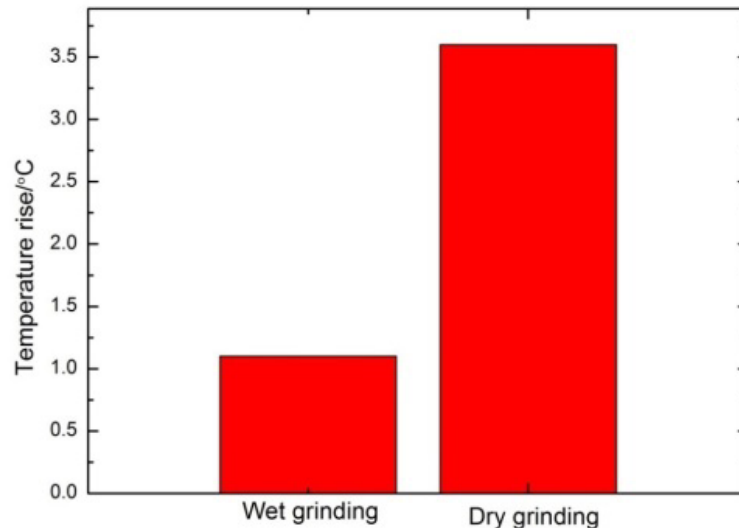


Fig. 5.20 The water absolutely decreases the temperature in the polishing of glass. In our experimnts, the temperature rise is curtailed by a factor of >2.0.

5.4 Summary

This part is dedicated to thermal related issues in fixed abrasive polishing. The temperature was systematically inspected by contact and noncontact thermometers. The results show that the temperature in polishing ranges over $\sim 20^{\circ}\text{C}\sim 60^{\circ}\text{C}$, which, below our expectation, is much lower, comparable to prevailing CMP process where slurry is circulated in the whole process. A mathematical model originating from heat conduction is set up to simulate the temperature. The modeled temperature is a bit higher than the experimented; nonetheless, the influence of external factors is modeled to behave similar to the experiments. At such low temperature, it is difficult for ceria to chemically react with silica. As a consequence, the mechanism of dry polishing might be dissimilar to chemical mechanical polishing process where the water serves as a catalyst for promoting the reaction between ceria and silica.

References

- [1]. Y. Wang and C. M. Rodkiewicz, Temperature maps for pin-on-disk configuration in dry sliding, *Tribology International* 27, 260-267, 1994.
- [2]. H. S. Carslaw, J. C. Jaeger, *Conduction of heat in solids*, 2nd Ed., Oxford University Press, 1959.
- [3]. X. Xu, S. Malkin, Comparison of methods to measure grinding temperatures, *Trans. ASME, J. Manuf. Sci. Eng.* 123, 191-195, 2001.
- [4]. N. Laraqi, N. Alilat, J. M. Garcia de Maria, A. Bairi, Temperature and division of heat in a pin-on-disc frictional device- Exact analytical solution, *Wear* 266, 765-770, 2009.
- [5]. Z. B. Hou, R. Komanduri, General solutions for stationary/moving plane heat source problems in manufacturing and tribology, *Int. J. Heat Mass Transf.* 43, 1679-1698, 2000.
- [6]. I. Lazoglu, Y. Altintas, Prediction of tool and chip temperature in continuous and interrupted machining, *Int. J. Mach. Tool. Manuf.* 42, 1011-1022, 2002.
- [7]. T. L. Bergman, A. S. Lavine, F. P. Incropera, D. P. Dewitt, *Introduction to Heat Transfer*, 6th Ed., John Wiley & Sons, Inc., USA, 2011.

This page intentionally left blank.

CHAPTER VI

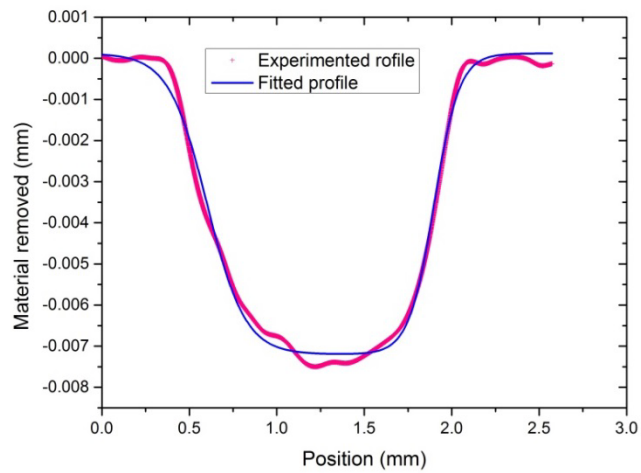
DETERMINISM OF FIXED-ABRASIVE POLISHING

All things in their being are good for something.

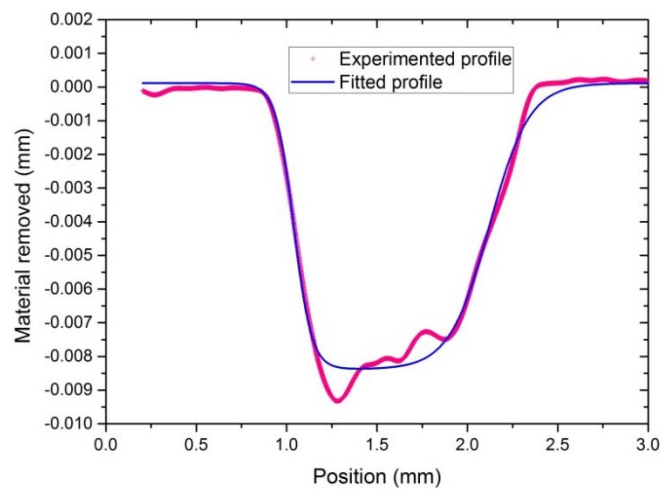
The final goal to develop a technology is to implement it in industrial application. Without exception, our inchoate ultrasonic vibration assisted technology will be extended into actual manufacturing at last. A principal issue in application is the controllability of the technology, which is reflected by the steadiness of material removal. This chapter is aimed at bridging research-oriented laboratory and manufacture-directed shop-floor, at least, providing some insights into the potential application of the technology.

6.1 Profile of material removal of polishing tool

The apparatus was modified so that the influence function of polishing can be easily acquired. In that each polishing tool possesses its own characteristics to be mapped onto the workpiece to be polished, the influence function will differ from tools to tools due to different shape and apparatus. However, the influence functions, speaking generally, obey the Preston's rule regardless of the tool and apparatus. The material removal can, to some extent, be predicted once the influence function ascertained. The apparatus used in our experiment is altered in order that the polishing can rotate with respect to its central axis. The pellets were hollowed out to form a ring-shaped pellet. We tested the possible factors, including external load, rotation rate, and ultrasonic specifications, to find out the possible predominate controlling parameters. The parameters are able to be controlled by CNC once the parameters are steady and predictable.

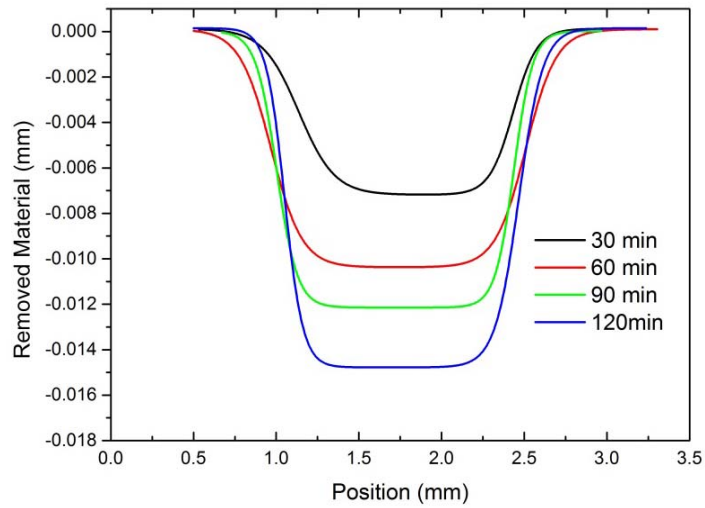


(a) The profile of removed material by a polisher without UV for 30min

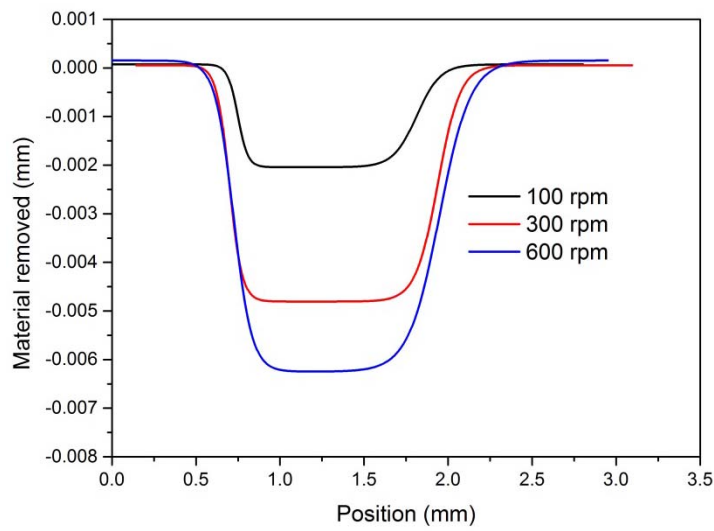


(b) The profile of removed material by the identical polisher with UV for 30min

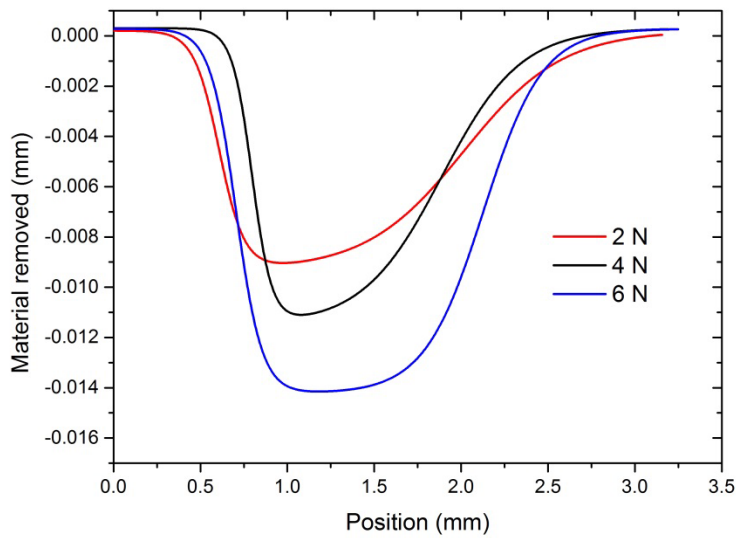
Fig. 6.1 Typical profile of influence function of a ring polisher (Non-UV polishing, 30min) together with fitted profile. The following profile and material removal are based on the fitted profiles unless otherwise specified.



(a) The profile versus polishing time

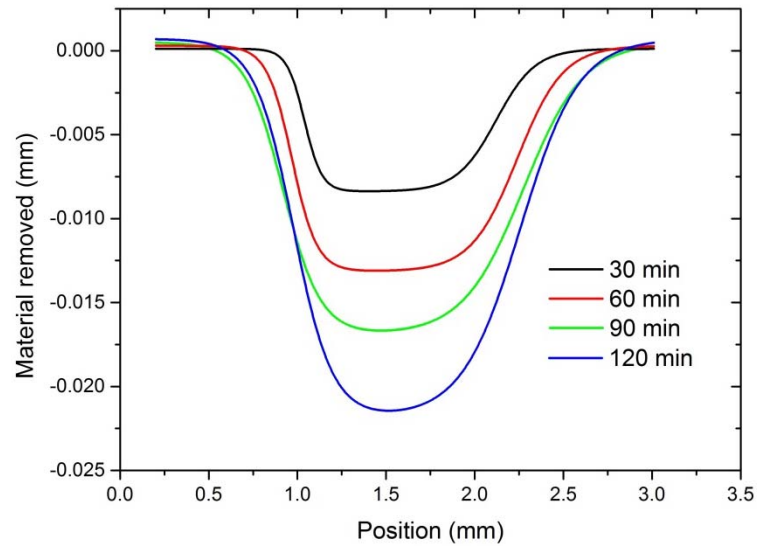


(b) The profile versus rotation rate of polishing tool

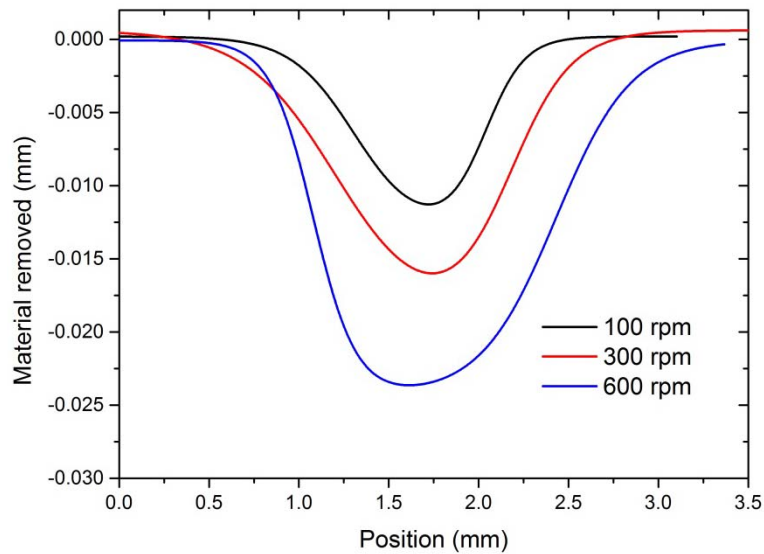


(c) The profile versus load

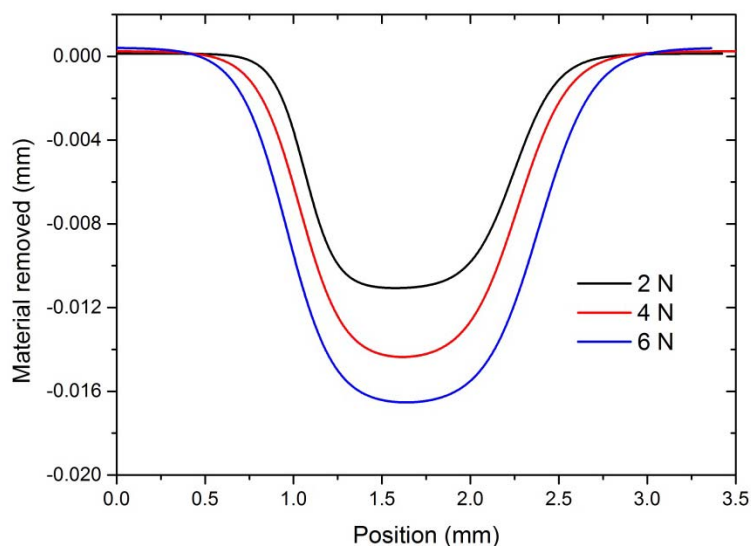
Fig. 6.2 Profile with possible influencing external factors in Non-UV polishing process.



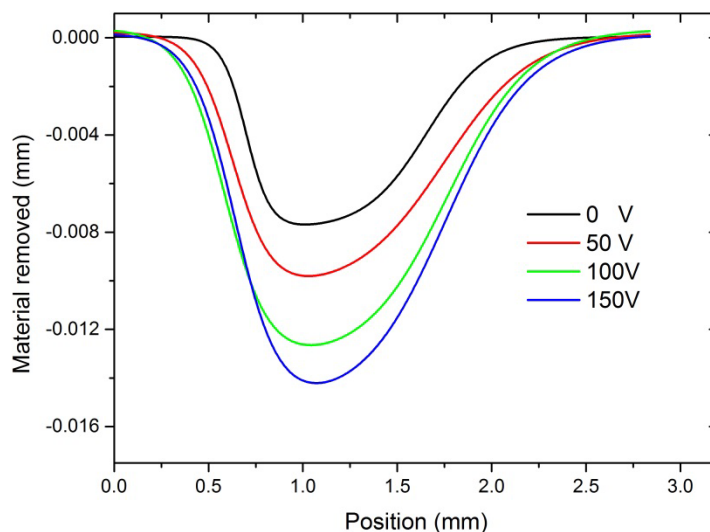
(a) Profiles with different processing time.



(b) Profiles with different rotation rate of polishing tool.



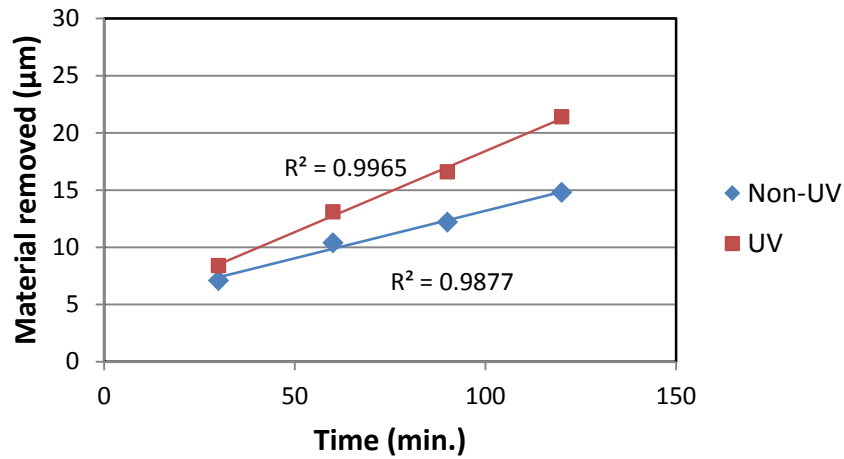
(c) Profiles with different external downward load.



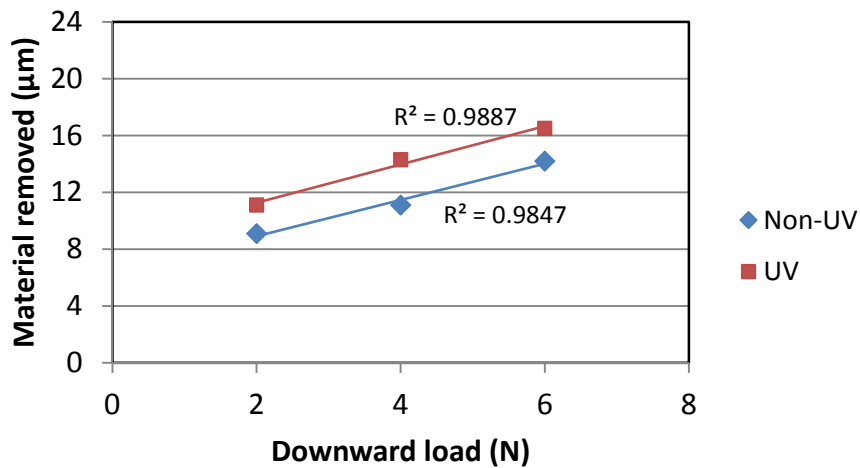
(d) Profiles with respect to various input voltage in UV polishing

Fig. 6.3 Profile with possible influencing external factors in UV polishing process.

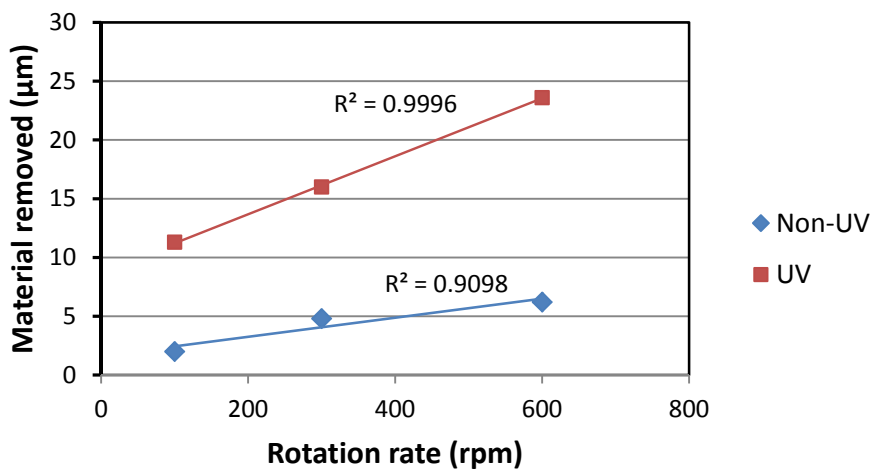
The same family of profiles resembles each other, the greatest material removal is located near the middle of the trench. The depth of the trench develops with processing parameters. The great ability of the polishing process to preserve the shape of profile is definitely a merit for automating the polishing process. Linear dependence of material removal on time, indicating a potentially deterministic polishing process that is helpful for automating CNC polishing process.



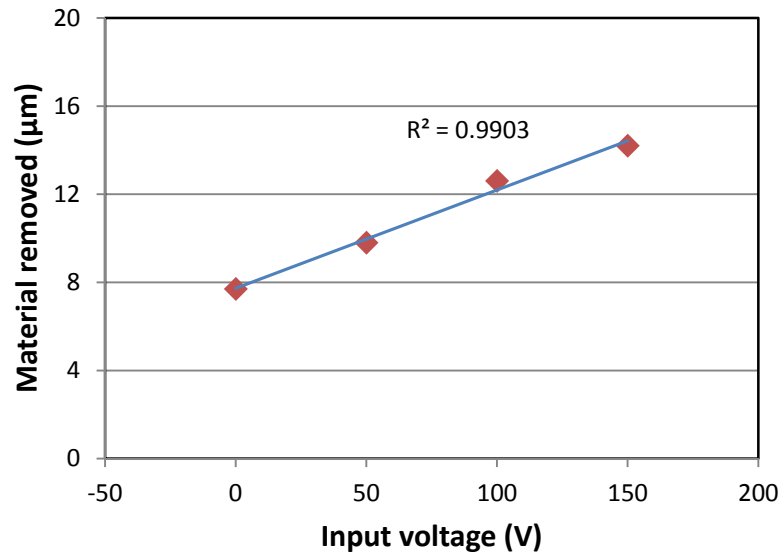
(a) The material removal versus polishing time in UV and Non-UV processes



(b) The material removal versus downward load in UV and Non-UV processes



(c) The material removal versus rotation of polishing tools in UV and Non-UV processes



(d) The material removal versus input voltage in UV polishing

Fig. 6.4 The material removal is correlated linearly with external factors both in UV and Non-UV polishing, demonstrating an outstanding deterministic nature of the processes.

From the previous plots, we can understand that polishing profiles are similar in shape, indicating a satisfying steady status in material removal. The steady profiles are conducive to automated machining by CNC. The material removal is shown to scale linearly quite well with polishing time for both processes. The material removal with regard to rotation rate, downward load and UV specifications exhibits excellent linear scaling. All of the results demonstrate that the material removal is, to a great degree, controllable. The final surface figure in polishing process is dominated both by initial surface figure and dwelling time. The dwelling is further correlated to influence function, which determines how long a specific polishing tool will remain at a local region so that the desired material removal can be removed. This way, the final surface figure can be achieved as designed. Undoubtedly, because of actual wear of polishing tools and measuring errors of influence function, the final surface figure is achieved at last after several iterations.

6.2 Summary

The last part of the work involves the polishing influence function of a specific polishing tool under preset conditions. The shapes of the profiles in fixed abrasive polishing are retained under different polishing conditions, which is conducive to CNC polishing process. Changing external factors will change the material removal accordingly. The removal shows satisfactory linearity with external parameters, indicating the fixed-abrasive processes with and without ultrasonic vibration are deterministic and controllable processes.

References

- [1]. A. V. Oppenheim, *Signals and Systems*, 2nd Ed. (Prentice Hall, USA), 1997.
- [2]. R. A. Jones, Optimization of computer controlled polishing, *Appl. Opt.* 16, 218-224, 1977.
- [3]. C. Shi, J. Yuan, F. Wu, et al., "Ultra-precision figuring using submerged jet polishing, *Chn. Opt. Lett.* 9, 092201, 2011.

This page intentionally left blank.

CHAPTER VII

CONCLUSIONS AND FUTURE SUGGESTIONS

The technology initiated in the work refers to the combination of ultrasonics and fixed-abrasive polishing. Ultrasonics is a flexible technology into which other machining techniques can be integrated to create a hybrid machining method. In the work, ultrasonic vibration is successfully applied to aiding the fixed-abrasive polisher to polish out an optic. The vibration is a 2-D vibration that can be readily tuned to form either 1-D vertical and lateral or 2-D elliptical vibration as needed in actual environment. The creative design of creating 2-D vibration with one PZT realizes a rather controllable vibration by adjusting input voltage and phase difference. The vibration amplitude generally scales linearly with input voltages and the trajectory of the vibrator is susceptible to phase difference.

The two most prominent metrics for a machining technique are material removal rate and micro-surface roughness. The two issues, in general, appear somewhat contradictory. Great material removal rate leads to low surface of quality while high quality surface basically requires low material removal rate. Our UV fixed abrasive polishing absolutely increases material removal rate and meanwhile maintains surface quality. The material removal rate is increased by up to >50% on many occasions. The surface roughness is achieved to as low as <1nm(Ra) without much difficulty. A preliminary mathematical model is put forward to interpret likely causes for increase in material removal rate on the basis of plastic sliding and geometry. The machined surface by UV polishing is featured by a periodic pattern which inherits the period of vibration used. It is the pattern that slightly deteriorates surface roughness compared to polishing without vibration. Chemical analysis was carried out for the purpose of potential reaction. It is inferred from the chemical analysis that the probable mechanism for polishing glass with ceria involves the chemical bonding between

ceria and silica and tearing silica from bulk glass due to stronger bond of Ce-O than Si-O.

Besides of the previous two primary ones, another issue of much concern to us is subsurface attributes beneath the machined surface. A plausibly specular surface of an glass, more often than not, is defaced by mild chemical etching. A principal cause lies on subsurface defect, which has been increasingly paid attention to under stringent applications. It is unfortunate that the same knotty problem besieges us in our polishing. The experiment results demonstrate that subsurface defect incurred is phenomenologically ascribed to chips, the product of polishing process. It is unlikely that glass is damaged by abrasive now that abrasive is less hard than glass in hardness. The chips, a mixture of glass, abrasive and other species, potentially crack the surface during polishing. But we are consoled with the fact that although it seems impossible to eradicate subsurface defect in polishing process, the subsurface defect can be reduced with different pellet plus vibration. A rudimentary mechanic model is in progress in an attempt to elucidate the results.

The heat plays a pivotal part in machining process, which dominate the process in certain cases, in particular chemical reaction-involved process. Against our expectations, the temperature was inspected to be so trivial that chemical reaction is impossible to be intrigued for ceria and silica in ambient surroundings. The temperature for glass is more pronounced than silicon under similar conditions. Either increasing downward load or rotation rate results in elevated temperature. The maximum temperature experimented was $\sim 40^{\circ}\text{C}$ for glass. The modeled temperature shows that greatest temperature can reach $\sim 70^{\circ}\text{C}$, almost a double of the experimented.

The last part concerns the prospective application of the technique to industry, which aims to verify the feasibility of the technique in practice. The stable influence function of polishing tool justifies that it is rational and practical to automate the polishing process in industry. Both UV and Non-UV polishing possess exceptional

linearity with polishing time, external load and so forth. All of the consistency with Preston rules renders fixed-abrasive polishing as a mechanical-dominant process, which is instrumental in implementing the process in a CNC machine.

The preliminary results on the fixed polishing process have validated that combining UV with fixed-abrasive polishing will yield good results in some respect. However, there are still many issues needing further investigation. For instance, how the subsurface damage is induced on earth? If the chips are suspect, subsurface damage is intrinsic and then the most manifest way is to remove the chips as soon as they are given rise to. Overall, the state-of-the-art technique is superior over traditional loose abrasive polishing from the abrasive-use and deterministic point of view.

This page intentionally left blank.

ACKNOWLEDGEMENTS

The three years in Japan has enriched my experience and will impress me forever. Countless benevolent people must be gratefully thanked in the course of pursuing doctoral degree. Without their kindhearted help and full-hearted support, the work would, by no means, have been finished.

First of all, thanks must go to my advisor, Prof. Yongbo Wu. Prof. Wu is more a considerate friend than a supervisor. I am fortunate to have such a precious opportunity to study under his guidance. His erudition on precision manufacturing has left a long-lasting impression on me. His prudent and rigorous attitude towards scientific research will definitely spur me to go on with scientific research with meticulous attitude throughout the rest of my scientific career.

I am grateful to Prof. Libo Zhou of Ibaraki University for his invaluable advice and suggestions on my work and for severing as a member of oral defense committee. I would like to acknowledge the willingness of Prof. Jianhui Qiu, Prof. Hiroyuki Taniuchi, Prof. Mitsuyoshi Nomura to assume advisory committee.

I am deeply indebted to Prof. Masakazu Fujimoto and Mr. Seiichi Kimura for their kind help and assistance in my work. I turned to you without hesitation each time I was confronted with some cumbersome problems. I could not imagine my life here without you.

I must express my gratitude towards Ms. Aki Asada for her continuing support during my stay in Japan and Ms. Minako Saito for helping me with the application of travel grant.

Thanks are due to, including but not limited to, the following people for sharing indelible experiences in Japan: Dr. Weixing Xu, Mr. Jianguo Cao, Mrs. Huiru Guo, Mr. Youliang Wang, Mr. Tailin Zhu, Prof. Li Jiao, Prof. Wenqing Song, Prof. Jingti Niu, Prof. Weiping Yang, Prof. Dong Lu, Mr. Shoichi Sasaki, Mr. Ryutairou Mori, Mrs. Natsuko Kato, Miss Cynthia Li, Mr. Minoru Shikata, Mrs. Yayoi Hoshino, Mr.

Kiyoshi Yokomori, Miss Karen Toyota.....The above list is in no way complete owing to limited space.

The support of several private foundations to finance my living in Japan and travelling outside Japan for international academic conferences is acknowledged as well.

Lastly, I extend my immense gratitude to my former employers, supervisors and colleagues for their long-distance and enduring support and generous help over three years.

Thank you all. Wish you all the best.

ACCOMPLISHMENTS

Monograph

1. Y. Wu, Y. Li, J. Cao, and Z. Liang, "Chapter 4: Ultrasonic assisted fixed abrasive machining of hard-brittle materials" in *Ultrasonics: Theory, Techniques and Practical Applications*, H. Ayabito and M. Katsukawa ed., ISBN 978-1-62257-685-2, Nova Publishers, USA, 2012.

Papers

1. Y. Li, Y. Wu, L. Zhou, and M. Fujimoto, "Vibration-assisted dry polishing of fused silica using a fixed-abrasive polisher," *International Journal of Machine Tools & Manufacture*, Vol. 77, No. 1, 93~102, 2014.
2. Y. Li, Y. Wu, L. Zhou, M. Fujimoto, J. Wang, Q. Xu, S. Sasaki, M. Kemmochi, "Chemo-Mechanical Manufacturing of Fused Silica by Combining Ultrasonic Vibration with Fixed-Abrasive Pellets," *International Journal of Precision Engineering and Manufacturing*, Vol. 13, No. 12, 2163~2172, 2012.
3. Y. Li, Y. Wu, J. Wang, W. Yang, Y. Guo, and Q. Xu, "Tentative investigation towards precision polishing of optical components with ultrasonically vibrating bound-abrasive pellets," *Optics Express*, Vol. 20, No. 1, 568~575, 2012.
4. Y. Li, Y. Wu, L. Zhou, H. Guo, J. Cao, M. Fujimoto, and M. Kemmochi, "Investigation into chemo-mechanical fixed abrasive polishing of fused silica with the assistance of ultrasonic vibration," *Key Engineering Materials*, Vol. 523-524, 155~160, 2012.

Academic Conferences

1. Y. Li, Y. Wu, L. Zhou, H. Guo, J. Cao, M. Fujimoto, and M. Kemmochi, "Investigation into chemo-mechanical fixed abrasive polishing of fused silica with the assistance of ultrasonic vibration," the 14th International Conference on Precision Engineering (ICPE2012), Hyogo, Japan, Nov. 8-10, 2012.
2. 李亜国, 吳勇波, 藤本正和, 周立波, "超音波援用固定砥粒加工による石英ガラスのポリシング," 第9回生産加工、工作機械部門講演会, 秋田県由利本荘市, 2012.10.27-2012.10.28.
3. Y. Li and Y. Wu, "Hybrid polishing of fused silica glass with bound-abrasive polishers in

conjunction with vibration,” the SPIE Optics + Photonics 2012: Optical Engineering + Applications, San Diego, U.S.A., Aug. 12-16, 2012.

4. Y. Li, Y. Wu, M. Fujimoto, and L. Zhou, “Polishing fused silica glass by incorporating ultrasonic vibration into fixed abrasive polishers,” the euspen 12th International Conference and Exhibition, Stockholm, Sweden, Jun. 04-08, 2012.
5. Y. Li, Y. Wu, J. Wang, Q. Xu, W. Yang, and Y. Guo, “Precision manufacturing of fused silica glass by combining bound-abrasive polishing with ultrasonic vibration,” the 6th International Symposium on Advanced Optical Manufacturing and Testing Technologies, Xiamen, China, Apr. 26-29, 2012.
6. 李亜国, 吳勇波, 曹建国, 郭会茹, 藤本正和, 周立波, “石英ガラスの超音波援用化学的機械複合研削,” 2012 年度日本精密工学会春季大会, 首都大学東京, 東京, 2012.03.14-2012.03.16.
7. 李亜国, 吳勇波, 曹建国, 郭会茹, 藤本正和, “超音波を援用した光学ガラスの化学機械複合研削,” 2011 日本精密工学会東北支部講演会, 仙台, 2011.10.21.

Awards & Travel Grants

1. euspen-Heidenhain Scholar for the euspen 12th International Conference, Stockholm, Sweden, 2012.
2. 工作機械技術振興財団助成, 三豊科学技術振興協会助成, 本荘由利産業科学技術振興財団助成, 2012.